NASA CR-134534
BCAC D6-41513

727 AIRPLANE CENTER DUCT INLET LOW-SPEED PERFORMANCE CONFIRMATION MODEL TEST FOR REFANNED JT8D ENGINES

PHASE II

by G. Kaldschmidt
B. E. Syltebo
C. T. Ting

BOEING COMMERCIAL AIRPLANE COMPANY
A DIVISION OF
THE BOEING COMPANY

Prepared for

NATIONAL AERONAUTICS AND SPACE ADMINISTRATION

NASA Lewis Research Center

Contract NAS3-17842

1. Report No. NASA CR-134534	2. Government Accession No.	3. Recipient's Catalog No.
4. Title and Subtitle 727 Airplane Center Duct Inlet Low-Speed Performance Confirmation Model Test for Refanned JT8D Engines - Phase II		5. Report Date NOVEMBER 1973
		6. Performing Organization Code
7. Author(s) G. Kaldschmidt, B.E. Syltebo, C. T. Ting		8. Performing Organization Report No. D6-41513
		10. Work Unit No.
9. Performing Organization Name and Address Boeing Commercial Airplane Company, P.O. Box 3707, Seattle, Washington 98124		11. Contract or Grant No. NAS3-17842
		13. Type of Report and Period Covered Contractor Report
12. Sponsoring Agency Name and Address National Aeronautics and Space Administration, Washington, D.C. 20546		14. Sponsoring Agency Code

15. Supplementary Notes

Project Manager, Arthur Medeiros, V/STOL and Noise Division
NASA Lewis Research Center, Cleveland, Ohio

16. Abstract

This report presents the results from testing of a 0.3 scale model center duct inlet ("S" duct) for the Pratt & Whitney Aircraft JT8D-100 engines. The objective of this test was to demonstrate that the required airflow of the JT8D-100 engine (480 lb/sec as compared to 334 lb/sec for JT8D-15) can be achieved with minimum modifications to the existing 727 airplane structure at acceptable levels of total pressure recovery and distortion. Steady-state pressure recovery, steady-state pressure distortion, and dynamic pressure measurements were taken at the engine face station. Surface static pressure measurements were taken along the duct.

Test results indicated that the required airflow was achieved with acceptable pressure recovery (comparable to the current 727-200 "S" duct). Inlet inflow angle variation within the 727 airplane operating regime (-5 to 5 degrees) had no effect on the inlet performance. Pressure distortion at static and forward speed at takeoff airflow conditions are within P&WA limits for the Phase II duct when equipped with vortex generators. Static crosswind operation between 10 knots and 25 knots appears feasible at full takeoff power.

17. Key Words (Suggested by Author(s)) 727 Airplane; "S" duct; Inlet Pressure Recovery and Distortion; Co-rotating Vortex Generators; Counter-rotating Vortex Generators	18. Distribution Statement Unclassified - Unlimited

19. Security Classif. (of this report)	20. Security Classif. (of this page)	21. No. of Pages	22. Price*
UNCLASSIFIED	UNCLASSIFIED	132	

* For sale by the National Technical Information Service, Springfield, Virginia 22151

PRECEDING PAGE BLANK NOT FILMED

FOREWORD

The low-speed wind tunnel tests described in this report were performed by the Propulsion Technology Staff of the Boeing Commercial Airplane Company, A Division of The Boeing Company, Seattle, Washington. The work, sponsored by NASA Lewis Research Center and reported herein, was performed between July and November 1973.

This report has been reviewed and is approved by:

L. J. Winslow — Date 31 JAN 1974

L. J. Winslow, Group Engineer
Propulsion Technology Staff

G. J. Schott — Date 31 Jan 1974

G. J. Schott
Chief, Staff Technology
JT8D Refan Program

K. P. Rice — Date 2/1/74

K. P. Rice
Program Manager
JT8D Refan Program

PRECEDING PAGE BLANK NOT FILMED

PRECEDING PAGE BLANK NOT FILMED

TABLE OF CONTENTS

TABLE OF CONTENTS Continued

1.0 SUMMARY

Phase I testing of a 0.3 scale model 727 inlet and "S" duct in the Boeing 9' x 9' Low-Speed Wind Tunnel demonstrated the design feasibility of the 727 inlet and "S" duct for the JT8D-100 series engines. Phase I test results indicated improvement in the "S" duct distortion was required. In addition, during Phase I studies, certain structural design problems were exposed. To resolve these design problems, a new 0.3 scale inlet and "S" duct, referred to as the Phase II duct, was designed and tested in the Boeing 9' x 9' Low-Speed Wind Tunnel.

The duct was designed for a nominal MCR (maximum cruise) corrected airflow of 480 lb/sec (compared to 334 lb/sec for the existing JT8D-15* engine on the 727-200) with minimum modification to the existing 727 airplane structure. Steady-state pressure recovery, steady-state pressure distortion, and dynamic pressure measurements were taken at the engine face station. Surface static pressure measurements were taken along the duct. The presence of the engine was simulated by screens installed at the JT8D-100 fan station behind the rotating rake assembly.

Test measurements and flow visualization indicated a strong secondary flow at the first bend which produced a low total pressure region in the lower part of the annulus at the compressor face. At the upper wall a flow separation region just in front of the compressor face was indicated. Installation of the vortex generators along the duct wall improved the steady state radial and circumferential pressure distortions. Vortex generator configuration 12 was the flow control device selected for the full scope of testing.

* For performance comparisons in this document, the current production 727-200 with the highest engine rating (JT8D-15) is compared to the JT8D-100 engine series which all have the same design airflow requirements.

Co-rotating type vortex generators were used on the lower wall of the "S" duct. In this configuration, on each side of the duct, the vanes were set at the same angle with respect to the local streamline to produce a set of co-rotating vortices. Each side was a mirror image of the other. The main advantage of co-rotating type vortex generators over counter-rotating vortex generators is their downstream effectiveness, i.e., the induced vortices will remain closer to the wall. This type of vortex generator has a few special advantages over the counter-rotating type vortex generator when applied on the lower wall of the "S" duct: (1) the induced vortices will remain close to the wall; consequently, a cleaner core (primary) region will be obtained,(2) the induced cross flows at the walls tend to counteract the tendency of the secondary flow to deposit and accumulate low energy air at the 6 o'clock position. The improvement in pressure recovery is most pronounced at the 6 o'clock position as can be seen in Figure S1.

Pressure recovery versus corrected airflow is shown in Figure S2 for the bare duct and in Figure S3 for the duct with vortex generators (flow control configuration 12). A recovery penalty of 0.1 percent at cruise was associated with the installation of vortex generators. Inlet inflow angle variation within the 727 airplane operating regime (-5 to 5 degrees) had no effect on the inlet pressure recovery as shown in Figure S4.

Several inlet lip configurations were tested in the static crosswind environment. A steady-state pressure distortion comparison of the selected 30-percent inlet lip and a 34-percent lip is shown on Figures S5 and S6. No discernible advantage is evident for either lip at the 10-knot crosswind condition with both possibly meeting P&WA limits. At the 25-knot condition neither configuration will meet P&WA radial distortion criteria, both lips showing comparable performance. However, utilizing the selected 30-percent inlet lip configuration, it is seen that with the normal rolling-takeoff procedure, the pressure distortion effect is minimal, Figure S7, for a 29-knot crosswind upon attaining the takeoff thrust-setting speed of 67 knots.

The "S" duct (Figure S8) was designed using a Boeing two-dimensional compressible potential flow/boundary layer computer program. Predicted surface Mach number distributions, obtained by transforming the three-dimensional duct into an equivalent two-dimensional duct, were found to be in good agreement with the test results as shown in Figure S8.

Pressure recovery and distortion, $(P_{T_{AVG}} - P_{T_{MIN}})/P_{T_{AVG}}$, comparisons of the Phase II and 727-200 production ducts are shown in Figures S3 and S9, respectively. The results indicate comparable duct performance. Steady-state radial and circumferential pressure distortion comparisons of the Phase II and 727-200 production ducts are shown in Figures S10 and S11, respectively. In the core region (primary), which is very critical for engine/inlet compatibility as evidenced by the low distortion limit imposed by P&WA, the Phase II duct has a lower distortion. In the tip region, which is relatively less important for engine/inlet compatibility, the Phase II duct has a higher radial distortion.

Steady-state (P_T/P_{T_∞}) and dynamic (RMS/P_{T_∞}) compressor-face total pressure contour maps at 160 knots and MCR airflow are shown in Figures S12 and S13, respectively. It is seen that a good correlation (i.e., higher dynamic activity in regions of large steady-state total-pressure gradients) between steady-state and RMS/P_{T_∞} contours is obtained.

Conclusions drawn by The Boeing Company are:

- The required airflow was achieved with acceptable pressure recovery (comparable to the current 727-200 duct).

- o Pressure recovery for the Phase II center duct inlet is 0.1 percent better than that of the Phase I duct at 160 knots, takeoff airflow condition (with best vortex generator installed for both Phase I and Phase II ducts).

- o Installation of co-rotating type vortex generators on the lower wall improved pressure distortion in the core region when compared to the 727-200 or Phase I ducts. Therefore, the Phase II center duct should provide improved engine/inlet compatibility.

- o Pressure distortion at static and forward speed, takeoff airflow conditions is within P&WA limits for the Phase II duct when equipped with vortex generator configuration 12. (P&WA is independently assessing the results of the test program to determine if the model test results indicate that the engine and "S" duct are compatible. Findings have not yet been received).

- o Static crosswind operation up to 10 knots appears feasible at full takeoff power. Somewhere between 10 knots and 25 knots, a thrust setting procedure involving rolling takeoff would be required. This rolling-takeoff procedure is the prescribed method shown in the 727 Boeing Operations Manual for all takeoff conditions.

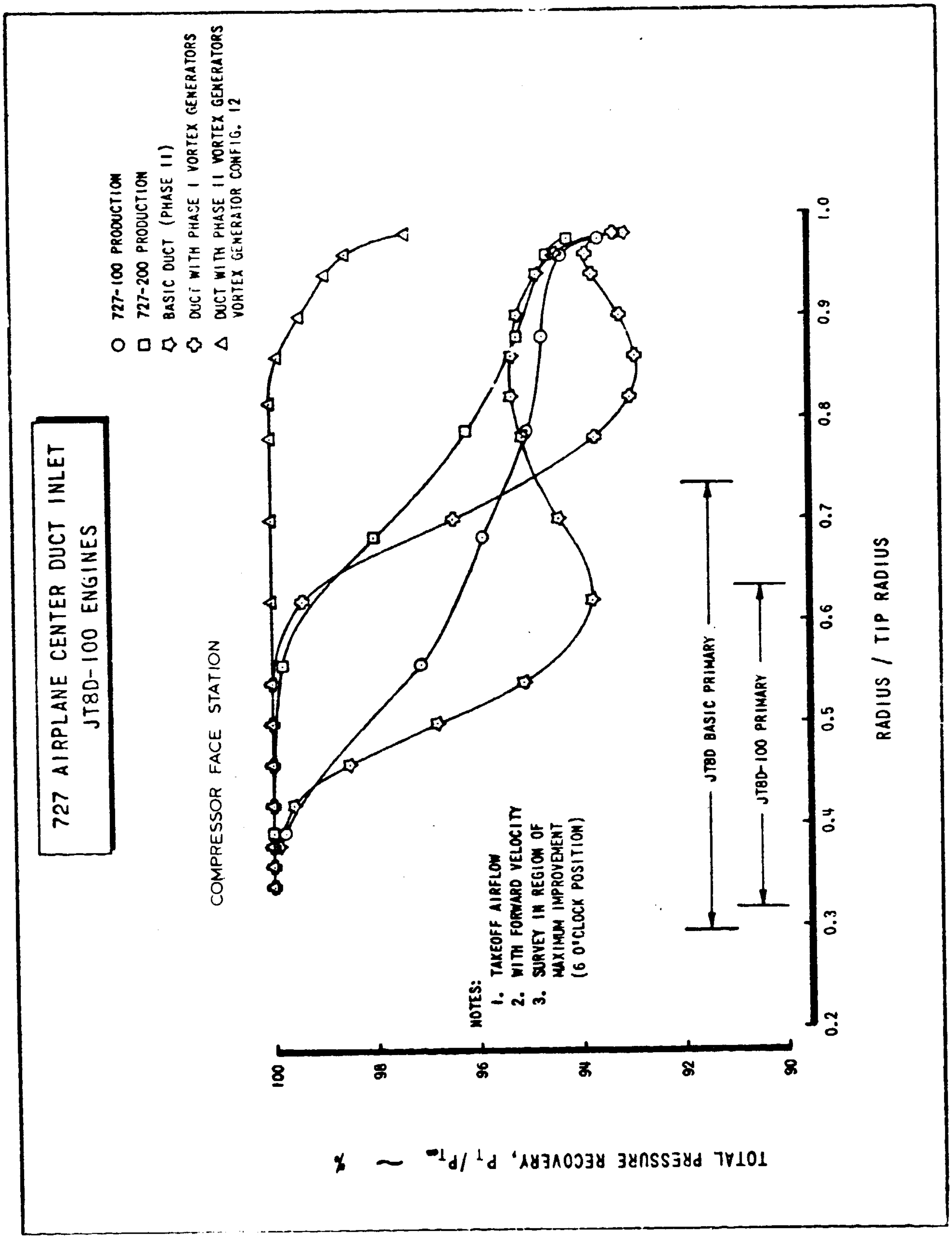

FIGURE S1. - PRESSURE RECOVERY PROFILES 727-100, -200, PHASE I AND II AREA OF MAXIMUM IMPROVEMENT (6 O'CLOCK)

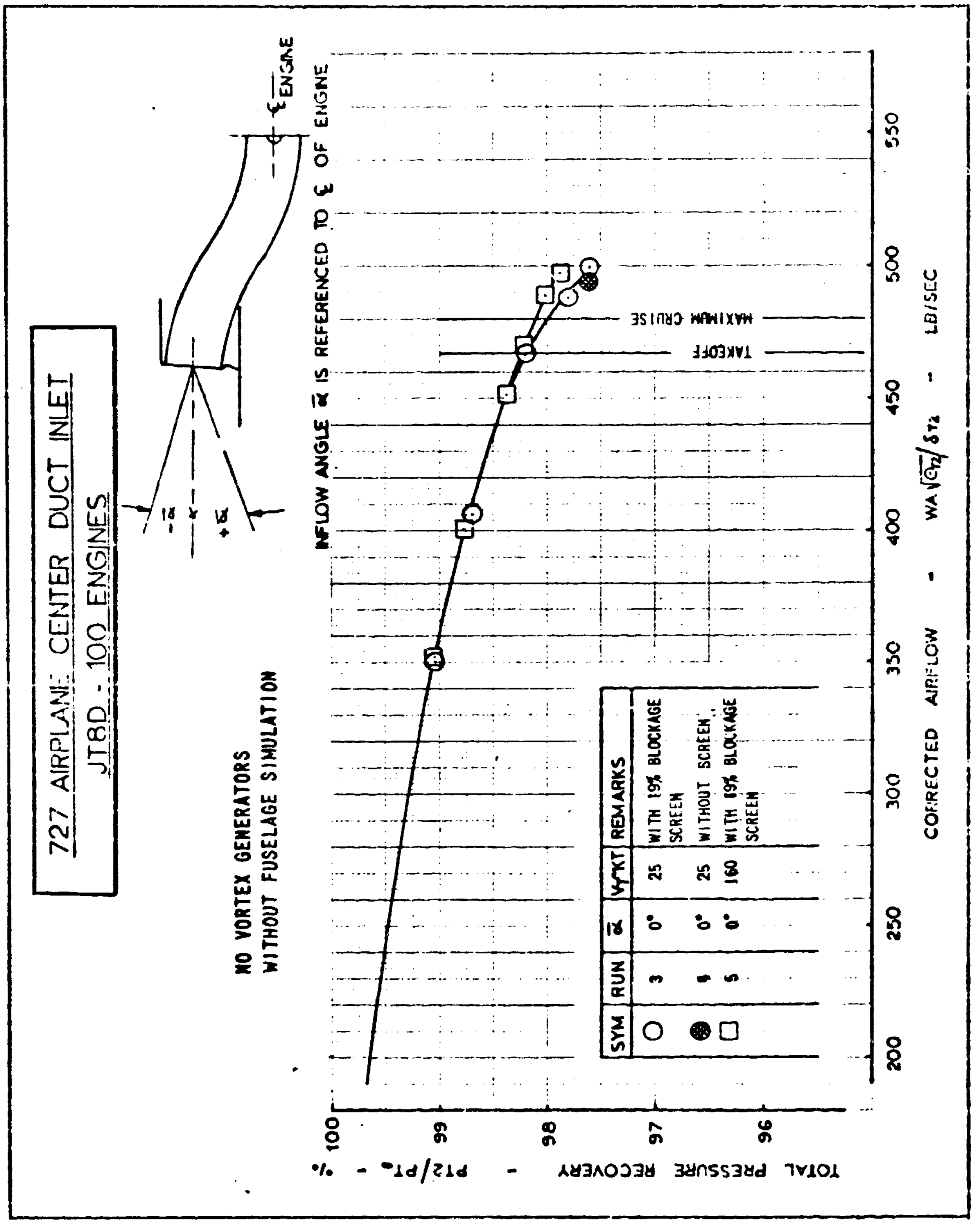

FIG. S2. - PRESSURE RECOVERY VS. AIRFLOW AT α = 0° WITH FORWARD SPEED (WITHOUT FLOW CONTROL DEVICES)

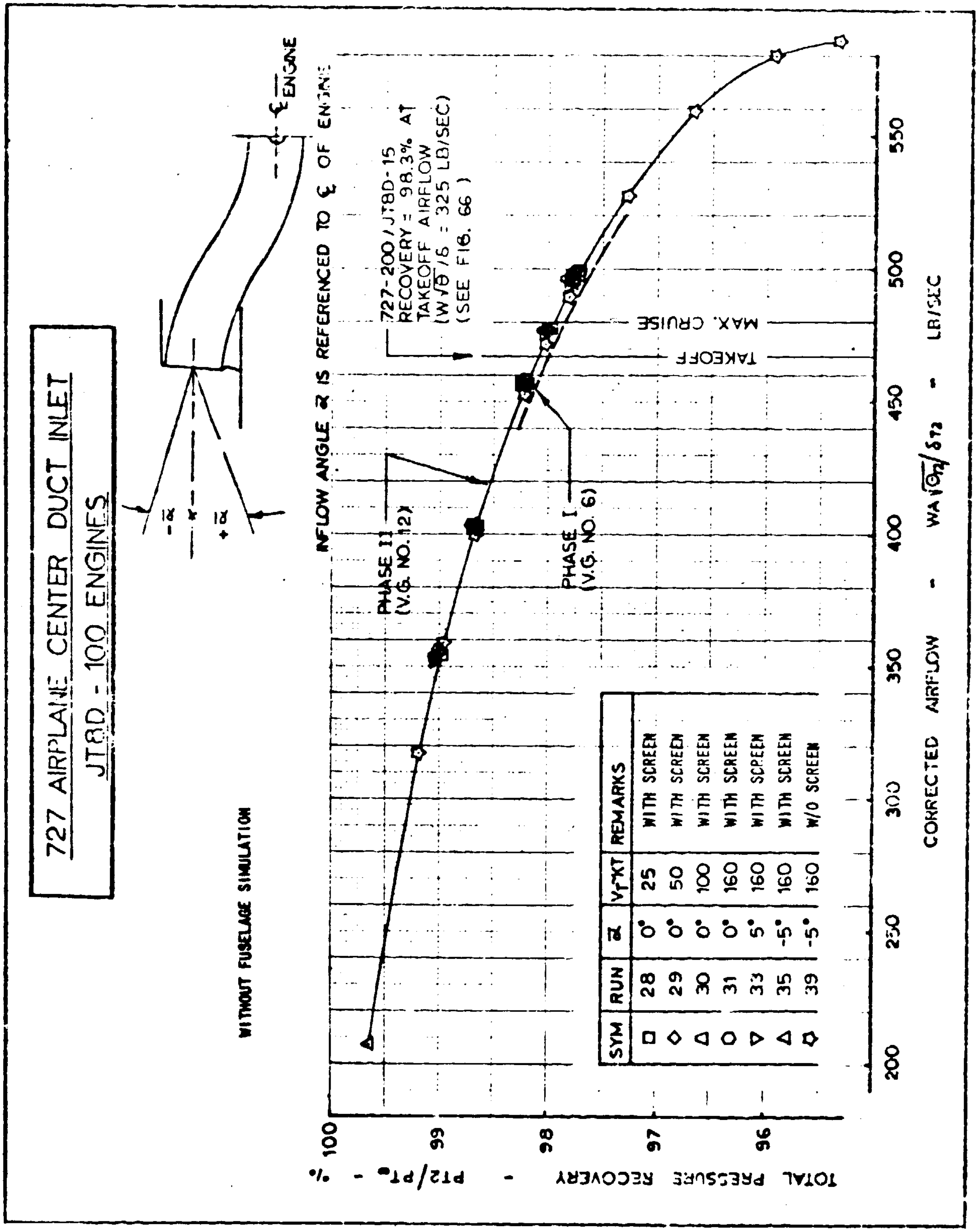

FIGURE S3. - TOTAL PRESSURE RECOVERY
COMPARISON OF PHASE I, II AND 727-200

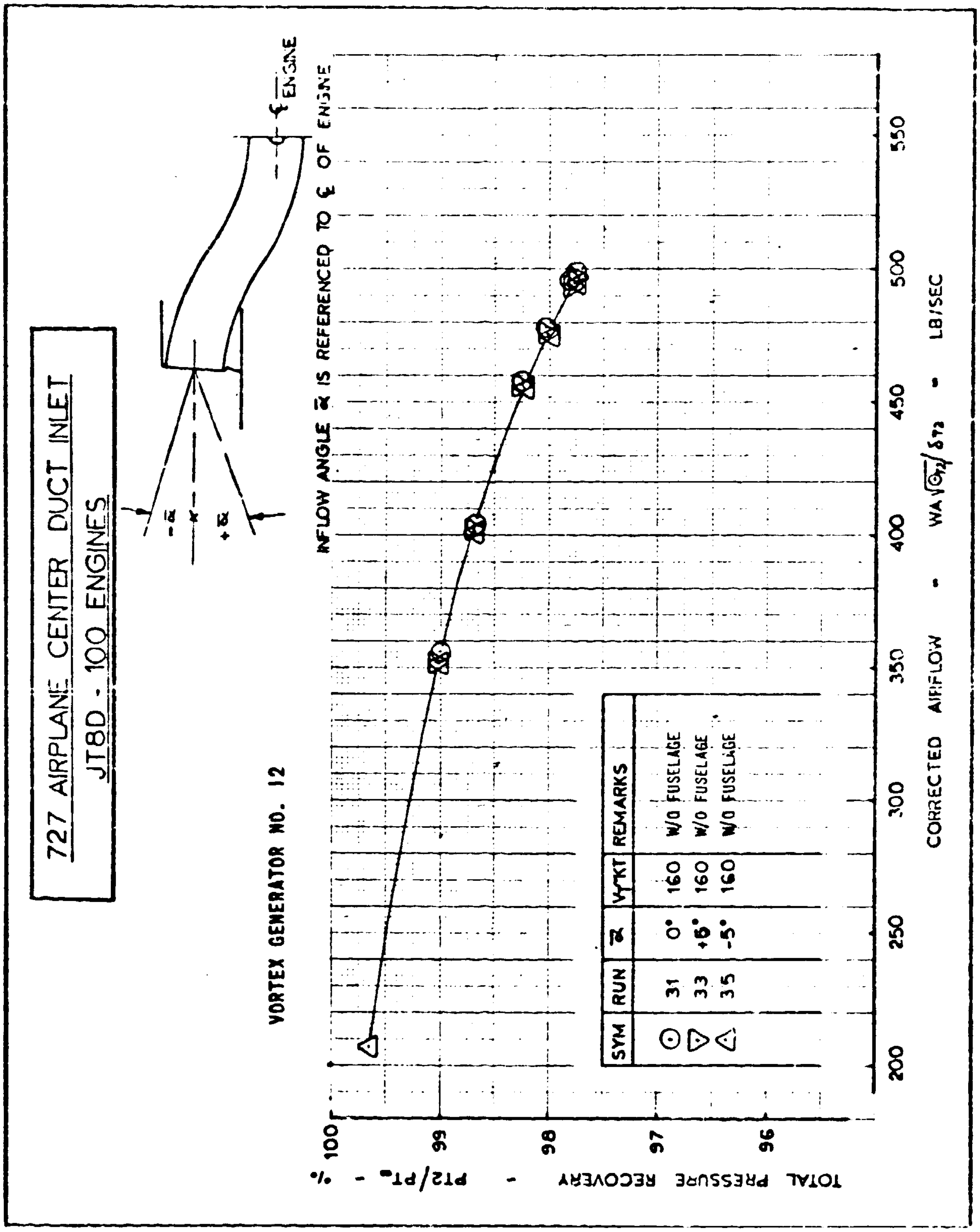

FIGURE S4. - TOTAL PRESSURE RECOVERY
EFFECT OF INLET INFLOW ANGLE

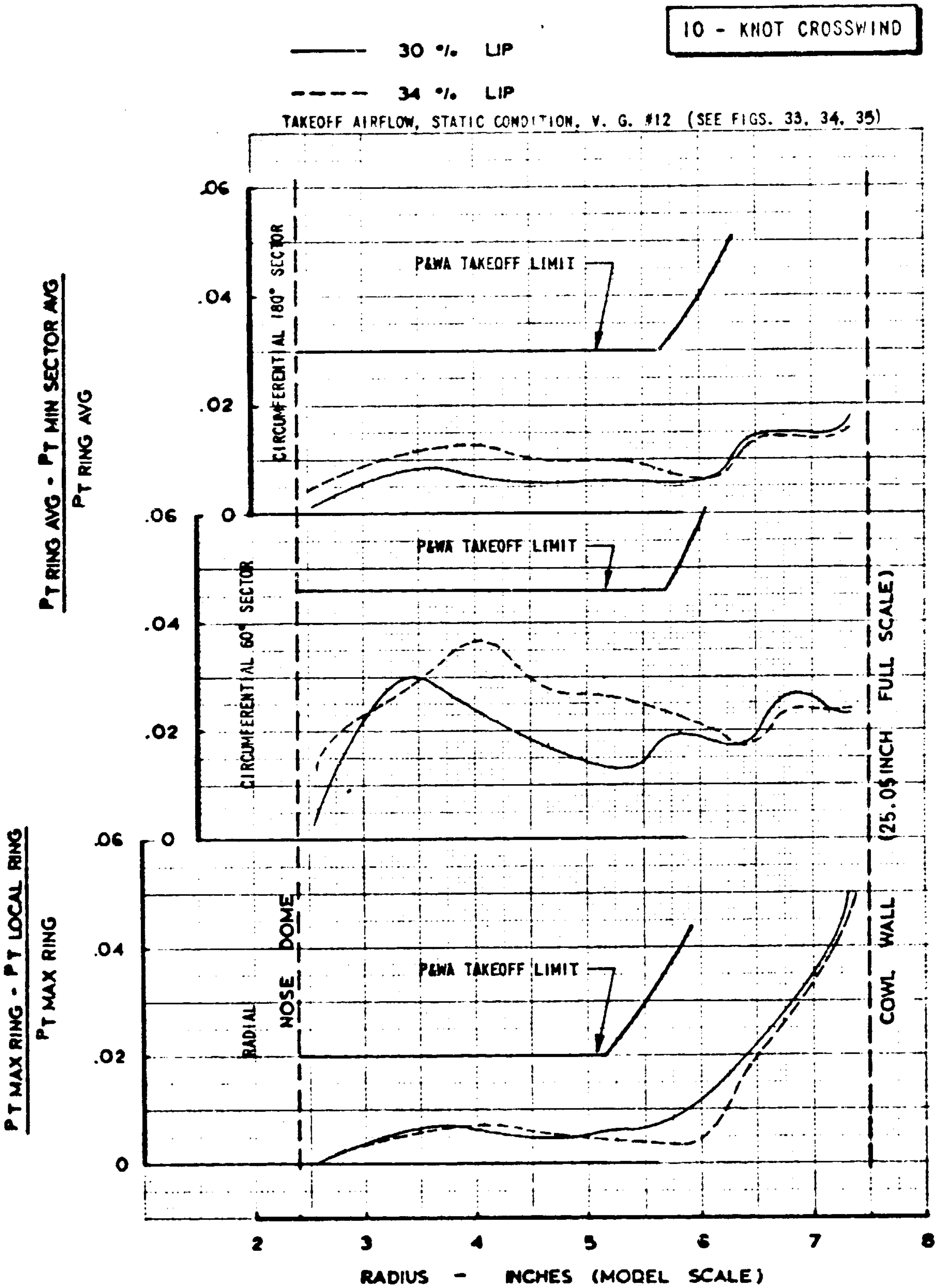

FIGURE S5. - STEADY - STATE PRESSURE DISTORTION - 10 KNOT CROSSWIND

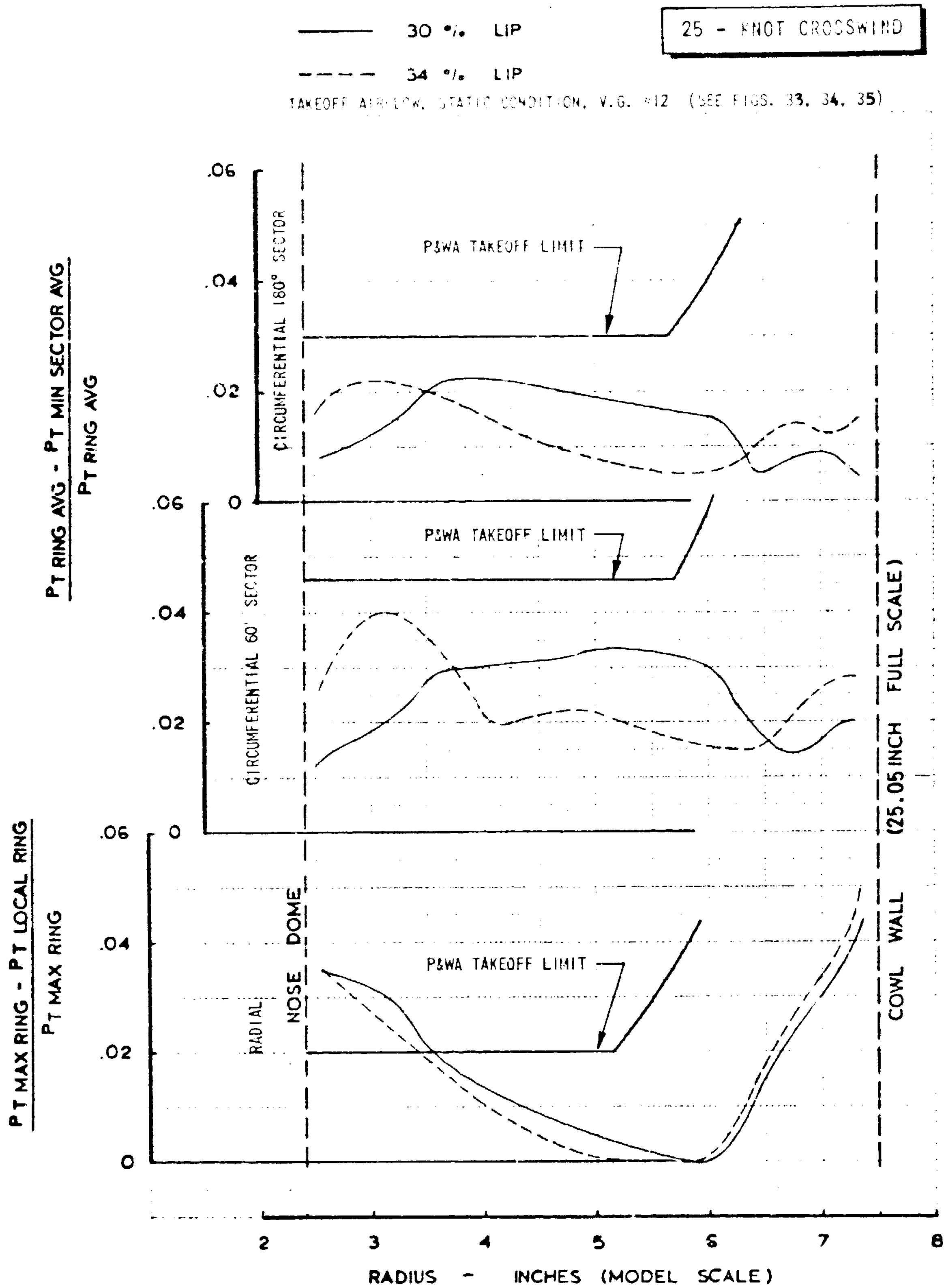

FIGURE S6. - STEADY - STATE PRESSURE DISTORTION - 25 KNOT CROSSWIND

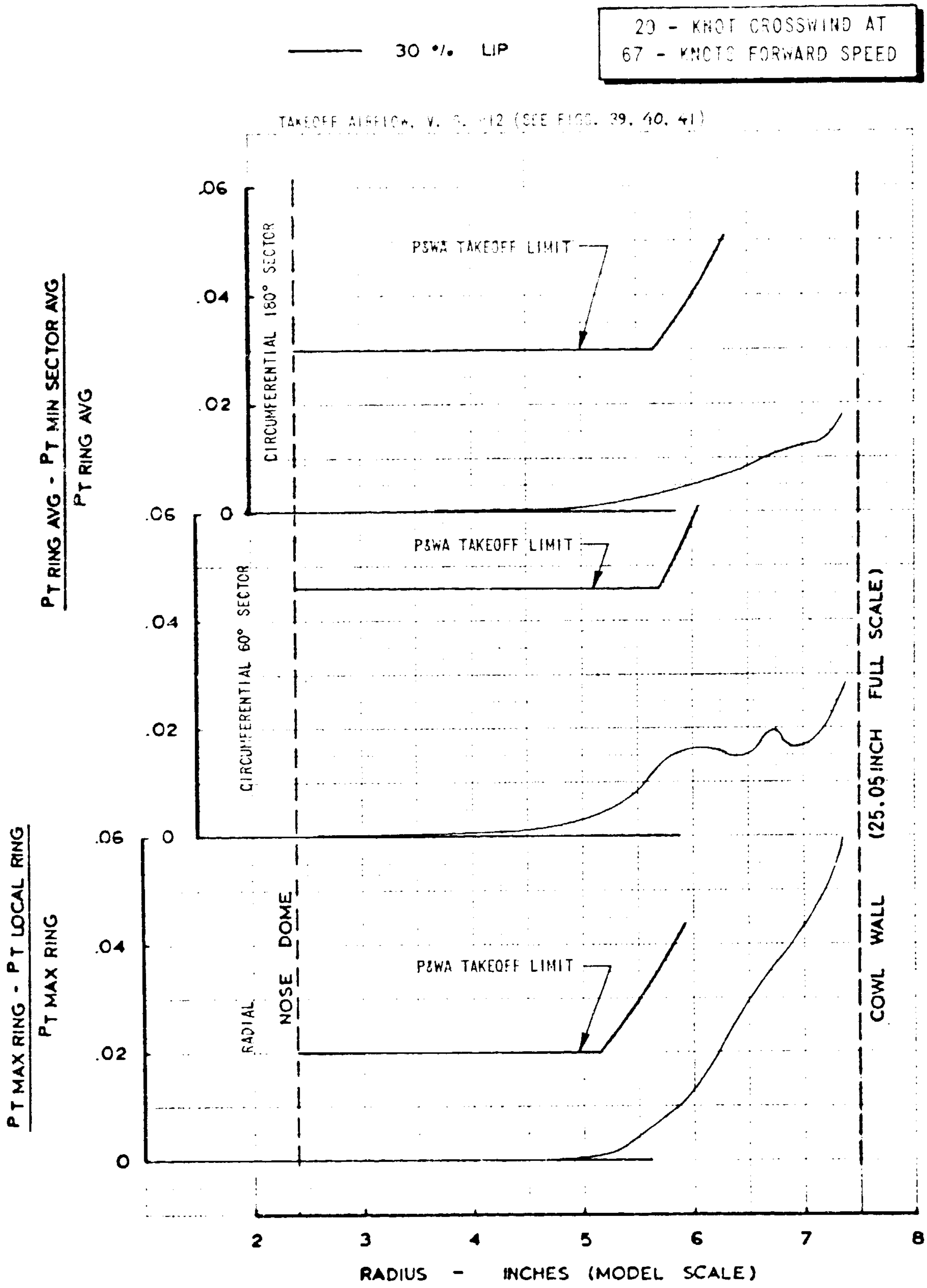

FIGURE 57. - STEADY - STATE PRESSURE DISTORTION -
29 KNOT CROSSWIND AT 67 KNOTS FORWARD SPEED

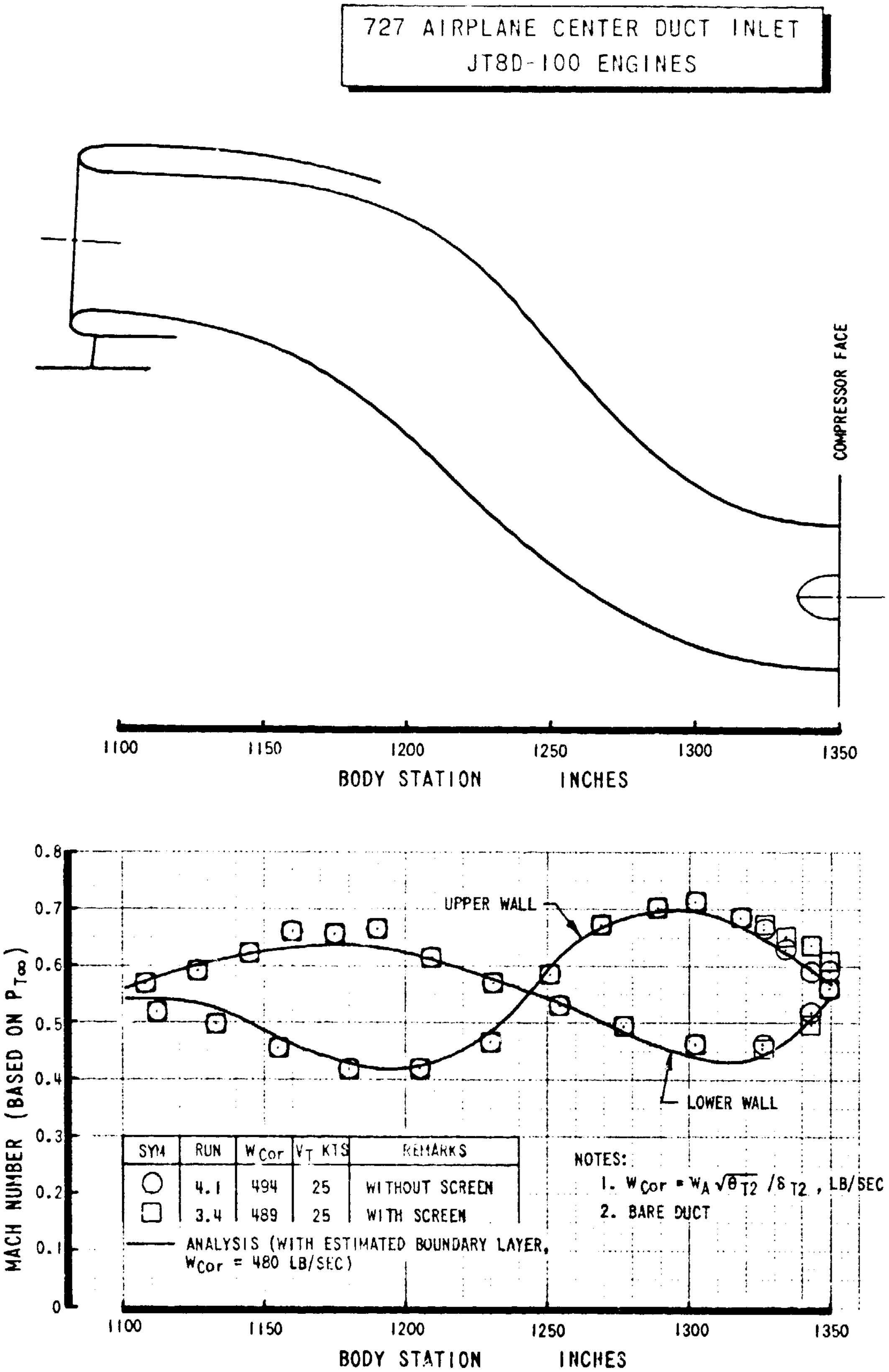

FIGURE S8. - DUCT WALL MACH NUMBER DISTRIBUTION
EFFECT OF 19% BLOCKAGE SCREEN AT FAN STA.

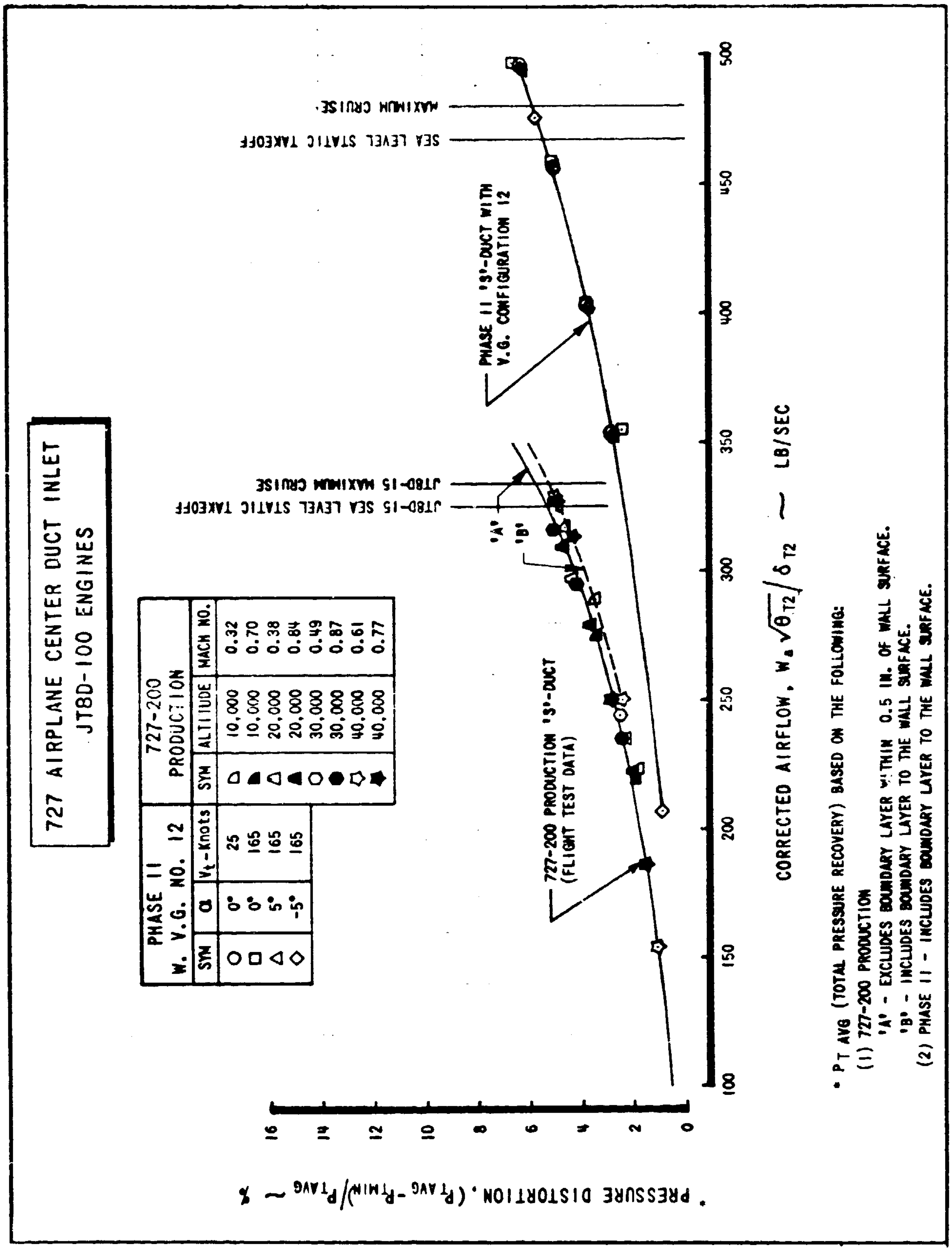

FIGURE S9. - STEADY-STATE PRESSURE DISTORTION VS. AIRFLOW AT FORWARD SPEEDS FOR 727-200 AND PHASE II DUCT WITH VORTEX GENERATOR CONFIG. 12.

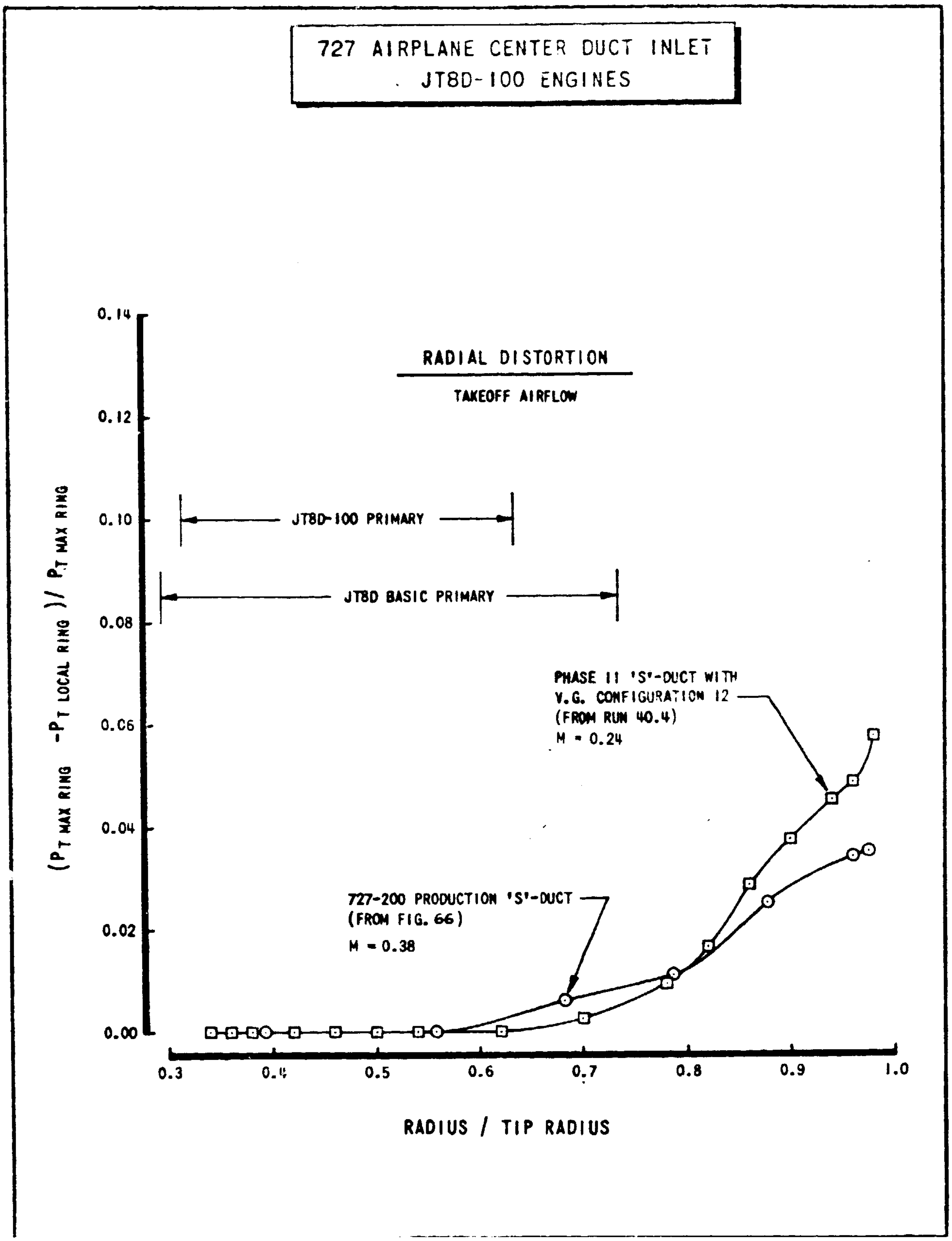

FIGURE S10. - STEADY-STATE RADIAL PRESSURE DISTORTIONS FOR 727-200
AND PHASE II DUCT WITH VORTEX GENERATORS CONFIG. 12

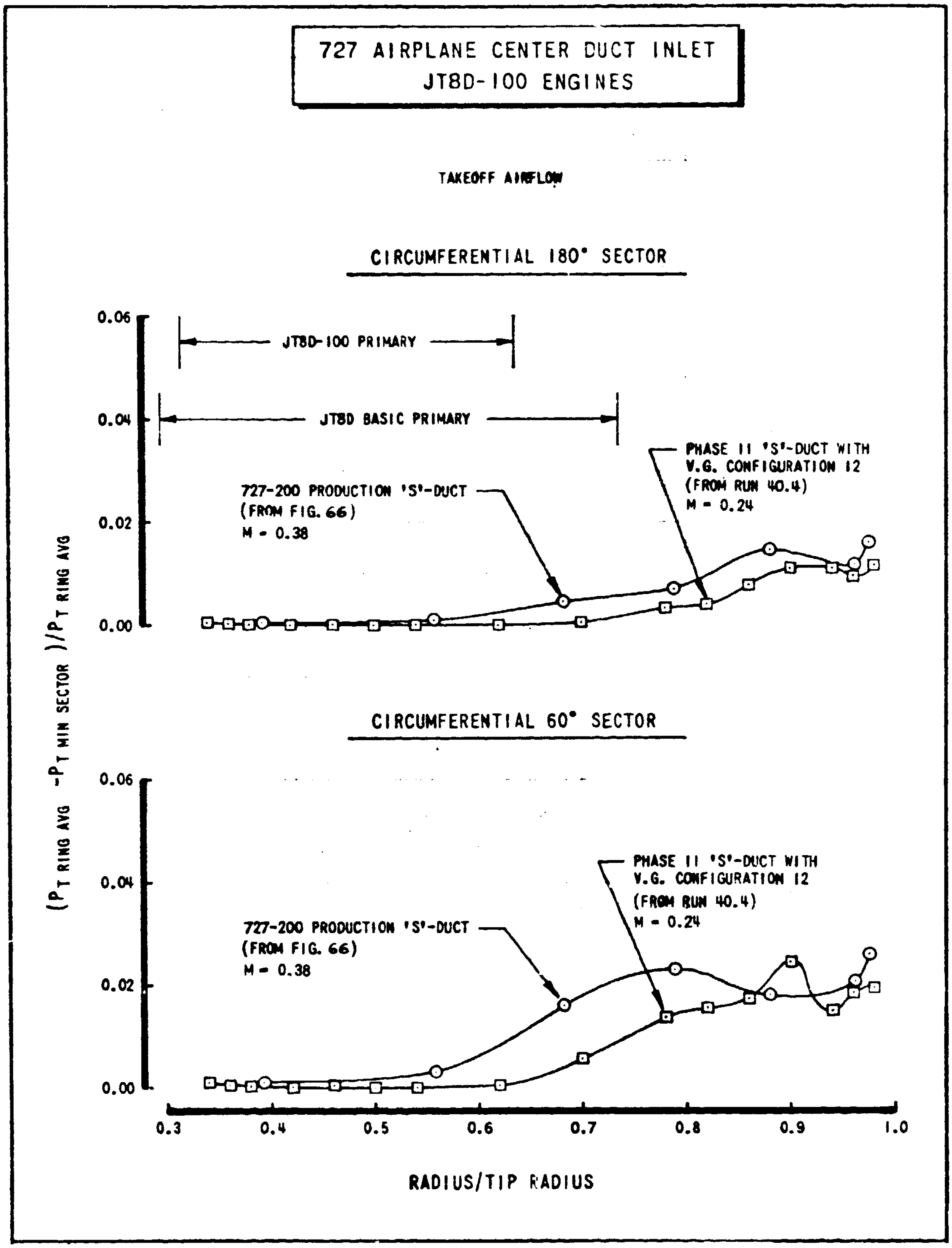

FIGURE S11. - STEADY-STATE CIRCUMFERENTIAL PRESSURE DISTORTIONS FOR 727-200 AND PHASE II DUCT WITH VORTEX GENERATOR CONFIG. 12

727 CENTER ENGINE DUCT AND INLET TEST - JT8D-109
TUNNEL VELOCITY = 160 KNOTS   ANGLE OF ATTACK = 0 DEG.
VORTEX GENERATOR CONFIG NO. 12

	P_T/P_{T_∞}		P_T/P_{T_∞}
1	.995	6	.920
2	.990	7	.900
3	.980	8	.880
4	.960	9	.840
5	.940	0	.800

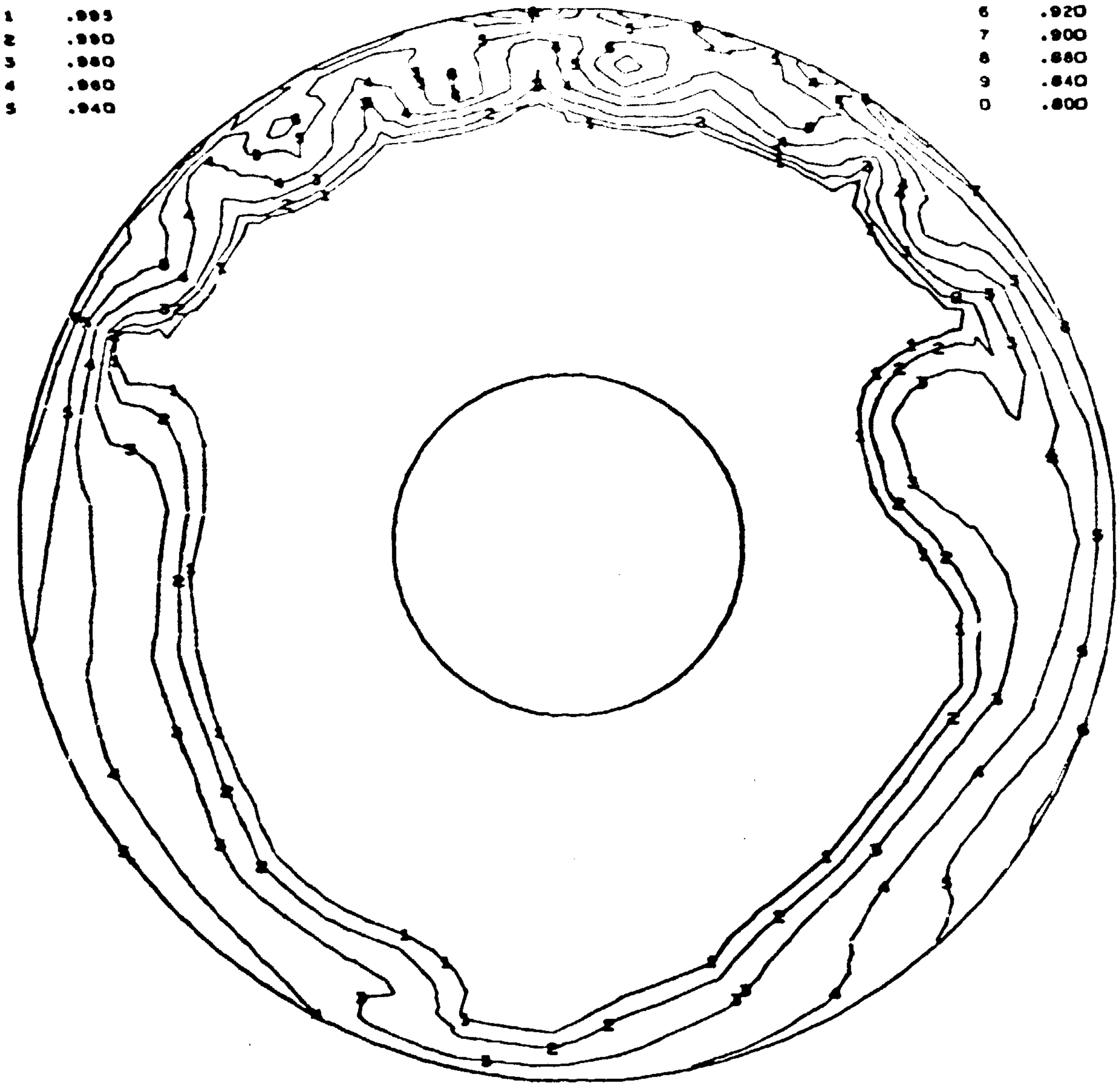

TEST NO.	2370	TEST DATE	8/ 3/73	CALC. DATE	10/03/73
RUN NO.	22	RECOVERY	.9805	PRI RECOVERY	1.0000
COND. NO.	1.0000	WCFS2	476.038 LB/SEC	FAN RECOVERY	.9699

FIGURE S12. - 160-KNOT STEADY-STATE COMPRESSOR FACE PRESSURE RECOVERY MAP WITH VORTEX GENERATOR CONFIG. 12

727 CENTER ENGINE DUCT AND INLET TEST JT8D-109

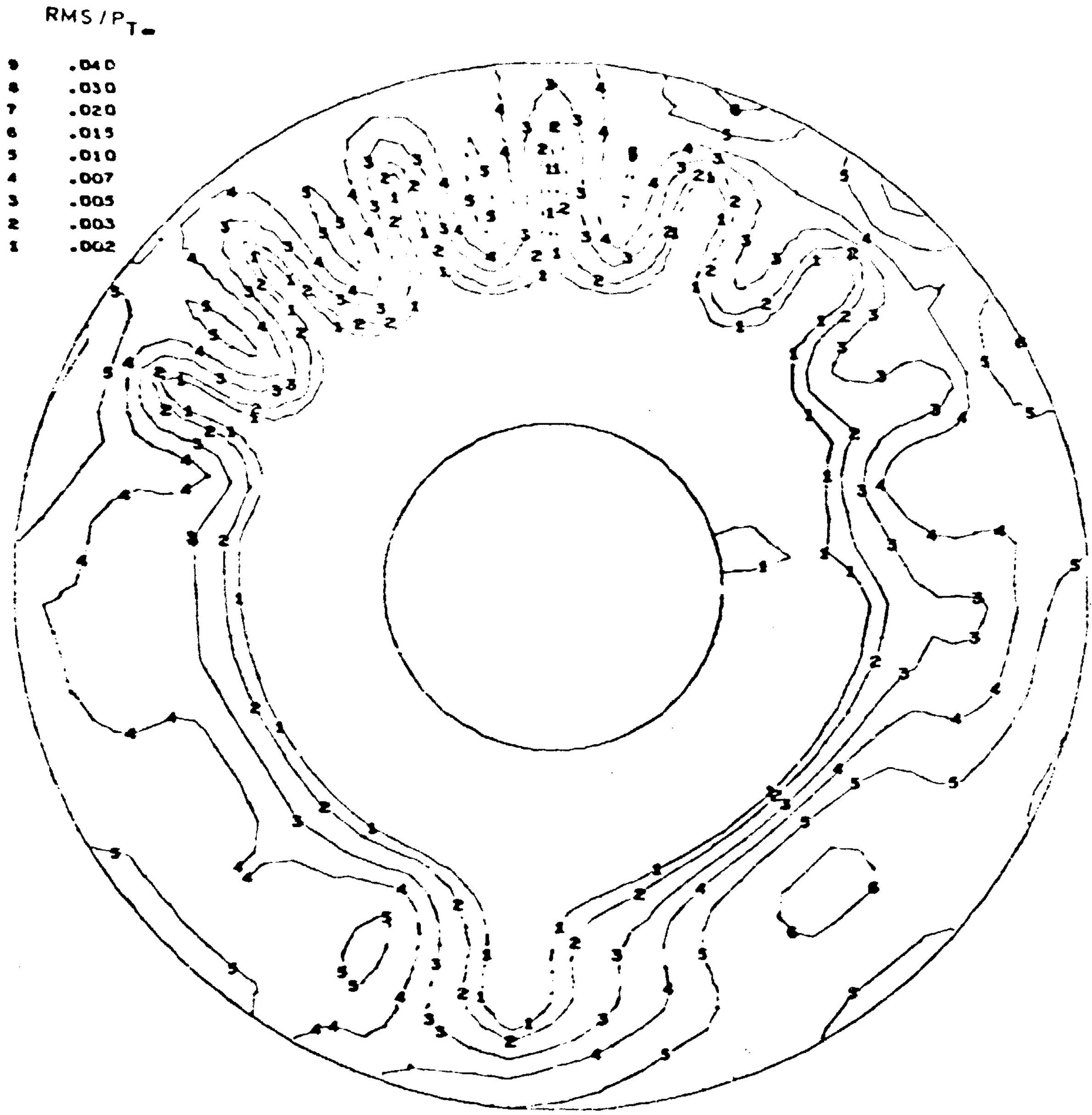

TEST NO.	2370	CALC. DATE	11/05/73
RUN NO.	22	RECOVERY	.9805
COND. NO.	1.0000	WCFS2	475.000 LB/SEC

FIGURE S13. - 160-KNOT DYNAMIC (RMS/$P_{T\infty}$)
COMPRESSOR FACE CONTOUR MAP WITH VORTEX GENERATOR CONFIG. 12

PRECEDING PAGE BLANK NOT FILMED

2.0 INTRODUCTION

2.1 BACKGROUND

The Pratt & Whitney Aircraft JT8D-100 engine is a derivative of the basic JT8D turbofan engine, modified to incorporate a new, larger diameter, single-stage fan with a bypass ratio of 2.03 and two supercharging low-pressure compressor stages. The modification lowers jet noise, increases takeoff and cruise thrust, and lowers specific fuel consumption. The use of the JT8D-100 series engines on the Boeing 727 airplane requires a larger center duct inlet ("S" duct), referred to as the NASA Refan Configuration.

Previous center duct inlet studies and Phase I testing reported in Reference 1 indicated that, without modification to the vertical fin front spar or other major structural changes, the increased airflow demands of the refanned JT8D engine were feasible and the predicted "S" duct performance was attainable.

This Phase II model inlet low-speed performance test is a second stage in the center duct inlet development program and has the objectives of (1) resolving design problems exposed in Phase I model tests and, (2) providing confirmation for the design configuration to be selected for the full-scale ground test program. It should be recognized that further testing at full scale is required to demonstrate engine/inlet compatibility. This will include ground testing of the engine with (1) simulated inlet distortion patterns and (2) the full-scale "S" duct. In addition to the Phase II testing, 727 airplane flight testing will be required for final substantiation.

This test was performed under authorization of NASA Contract NAS3-17842, Phase II Program on Ground Test of Refanned JT8D Engines and Nacelles for the 727 Airplane to support the development of a new 727 center engine inlet.

2.2 INLET AND "S" DUCT DESIGN

2.2.1 Design Constraints

The following restrictions were imposed on the design to enable the "S" duct to clear airplane structure:

- o Center line of inlet throat at Body Station (BS) 1091.85 Body Water Line (BWL) 350.20: Slope 3°40' horizontal.

- o Pressure bulkhead notch: Lower flow surface at BS 1183.00, BWL 297.50.

- o Front spar forging: Lower flow surface at BS 1196.72, BWL 286.50.

- o Front spar forging: Upper flow surface at BS 1247.33, BWL 316.54.

- o Rear spar bulkhead: Centerline of duct horizontal at BS 1342.40, BWL 228.00.

2.2.2 Design Goals

The following design goals were set:

- o Airflow requirements

  Corrected design airflows as follows:

  (1) 467 lb/sec at takeoff, sea level static condition, Std. day.

  (2) 480 lb/sec at MCR, 0.8M, 30,000 ft., Std. day (duct design condition).

  (3) 501 lb/sec at MCT, 0.6M, 35,000 ft., Std. day.

The maximum JT8D-100 engine cold-day airflow at both sea level and 10,000 feet, -60°F ambient temperature, is 516 lb/sec. Applying a ±3 percent production engine airflow tolerance results in a 531.5 lb/sec maximum airflow requirement.

- o Inlet inflow angle requirement

  The normal inlet inflow angle requirement for the 727 airplane during low speed operation falls within a positive 5 degrees and negative 5 degrees with respect to the body water lines. The maximum inlet inflow angle is experienced during airplane stall and is approximately a negative 15 degrees, Reference 2.

- o Crosswind capability

  Equivalent to Boeing production airplane fixed lip inlets.

- o Pressure distortion

  Equivalent to 727-200 center inlet.

2.2.3 Center Duct Inlet Geometry - Lip Sizing

The lip geometry was selected based on the following aspects:

Lip Loading

Lip loading is defined as the corrected airflow per unit highlight area ($W_A\sqrt{\theta_{T1}}/\delta_{T1}A_{HI}$). For fixed lip inlets with contraction ratios of about 1.25 to 1.35, the recommended lip loading is approximately 30 lb/sec/ft^2. This value, which was selected for the center duct inlet, represents a compromise between internal performance (inlet pressure recovery and distortion) and external drag (cowl drag, pressure drag, interference, etc.).

Contraction Ratio

Contraction ratio is defined as the ratio of highlight area to throat area, A_{HI}/A_{TH}. Generally, it is desirable to employ high contraction ratios around 1.30 to 1.35 for better static and crosswind performance. For forward speed, at MCR conditions, a contraction ratio below 1.30 would be more favorable from the drag standpoint when considering a specific inlet throat area. For the center duct inlet lip the ratio A_{HI}/A_{TH} = 1.30 was selected as the best compromise. A blunter lip (A_{HI}/A_{TH} = 1.34) was also tested for crosswind conditions.

Lip Contour

For any given contraction ratio A_{HI}/A_{TH} an infinite variety of lip contours can be generated. A gentle curvature distribution between highlight and throat favors static and crosswind behavior. A sharp lip (rapid change of curvature close to the highlight) improves the inlet inflow-angle capability. Three lip contours were tested in Phase II (Figure 1). A "super ellipse" $\left[\left(\frac{X}{a}\right)^{2.2}+\left(\frac{y}{b}\right)^{2.2} = 1.0\right]$ was chosen for the inlet configuration to undergo the full range of test conditions.

Throat Mach Number

The inlet was sized to produce an average throat Mach number of $M_{TH} \approx 0.53$, design airflow.

2.2.4 Center Duct Inlet Geometry - Duct Design

The selection of the center duct contours was based upon analytical results obtained from a two-dimensional potential flow/boundary layer analysis computer program. The method of application of this analysis was previously proven by the good agreement of Phase I "S" duct test data with the predictions (Reference 1). The criterion used in the selection of the final duct contours was a low analytically predicted peak shape factor (H).

$$H = \frac{\delta^*}{\theta}$$

where $$\delta^* = \int_0^\delta \left(1 - \frac{\rho u}{\rho_e U}\right) dy \quad \text{(Displacement Thickness)}$$

and $$\theta = \int_0^\delta \frac{\rho u}{\rho_e U}\left(1 - \frac{u}{U}\right) dy \quad \text{(Momentum Thickness)}$$

In the analyses of a number of "S" ducts it was found that a low shape factor at the lower wall usually results in a high shape factor at the upper wall and vice-versa. The duct, with the minimum combination of peak shape factors at both upper and lower walls was chosen as the wind tunnel test model.

It is realized that the flow field calculated based on the modified two-dimensional potential flow/boundary layer program will be different from that of the actual three-dimensional flow in the duct. Also, the secondary flow effect is not accounted for; consequently, the absolute values of the shape factors will be different from those of real flow conditions. The trend of shape factors, however, is believed to be similar between two-dimensional and three-dimensional analyses. The criteria used in the selection of the upper and lower contours (12 and 6 o'clock) of the "S" duct were based on comparison of the relative values of shape factors only and therefore should be valid.

The side wall contours (3 and 9 o'clock position) were splined with maximum wall diffusion half angles not exceeding 3 degrees.

Duct contours, Mach number and shape factor distributions for both lower and upper walls, and one-dimensional flow area and Mach number distributions for the design are shown in Figure 2.

PRECEDING PAGE BLANK NOT FILMED

3.0 MODEL AND TEST DESCRIPTION

3.1 MODEL DESCRIPTION AND MODEL INSTRUMENTATION

A 0.2994 scale fiberglass "S" duct model was constructed. Figure 3 shows the contours of the upper and lower walls. Also shown is a comparison of the Phase II duct lines with the Phase I and the production 727-200 duct. All model surfaces were of the hardwall type (i.e. without acoustic lining). The model was made in two halves such that it could be opened up for the purpose of observing and photographing oil flow patterns. A 727 fuselage section was simulated under the "S" duct inlet section during crosswind testing. Figures 4 and 5 show photos of the model installed in the wind tunnel facility for forward-speed and crosswind testing, respectively.

The model "S" duct surface was instrumented with 59 static pressure ports, which were positioned over the length of the duct on lines at angles of 0 (12 o'clock), 90, 180 and 270 degrees. The centerbody and duct wall were instrumented with 8 static pressure ports at the engine face at 45 degree intervals.

Flow properties at the engine face station were measured using a 15-inch diameter rotating rake section. The rake consisted of four equally spaced arms containing 16 steady state and 5 dynamic total pressure probes each. The instrumentation was set up to measure compressor face total pressures at angular increments of 10 degrees. The rotating rake section also had two traversing probes located 180 degrees apart. Each traversing probe contained a total pressure port and a dynamic transducer for measuring the steady-state and dynamic total pressures across the annulus. These traversing probes were kept available as back-up instrumentation in case the regular dynamic instrumentation on the rotating rake failed. Figure 6 shows a sketch of the rotating rake and the traversing probes.

3.2 FLOW CONTROL CONFIGURATION

During the test program the "S" duct was tested with and without flow control devices. A total of 17 flow control configurations were investigated. The flow control devices were positioned on the upper and lower surfaces of the "S" duct in the vicinity of convex curvature. Table I lists the flow control devices tested. The flow control devices tested can be divided into three categories: (1) Vortex generators (configurations 1 through 12), (2) Boundary layer fences (configurations 13 and 14) and (3) Turning vanes (configurations 15 through 17). For vortex generator configurations both co-rotating and counter-rotating types were tested. The co-rotating type vortex generators have the vanes set at the same angle while the counter-rotating type vortex generators have the vanes set alternately at positive and negative angles.

3.3 TEST FACILITY AND FACILITY INSTRUMENTATION

The test was conducted in the Boeing 9 foot by 9 foot Low Speed Wind Tunnel "B" (LSWT). The wind tunnel, located at the North Boeing Field site of the Propulsion Mechanical Engineering Laboratories, is an open circuit type wind tunnel drawing air in through a bellmouth from the atmosphere. An Allison model 501-D13 gas turbine is used as a prime mover. A variable pitch propeller is used to vary airspeed in the tunnel from 0 to approximately 165 knots. Engine airflow simulation is obtained by utilizing a General Electric J-47 turbojet engine. Air was drawn in through the test model, down through flow straighteners, a venturi meter and into the engine. Variations in inlet airflow were obtained by varying the engine RPM. The presence of the engine was simulated by the installation of screens at the JT8D-100 fan station behind the rotating rake assembly. A 19-percent blockage screen configuration consisting of 0.41 inch mesh with 0.041 inch diameter wire was used.

Tunnel total and static pressure, tunnel total temperature and venturi temperatures and pressures were recorded for each test condition.

TABLE I

FLOW CONTROL CONFIG. NUMBER	12 O'CLOCK SECOND BEND	6 O'CLOCK FIRST BEND	3 AND 9 O'CLOCK FIRST BEND	COMMENTS
1	Single-row V.G., Sta. 1300 105° sector, counter rotating	Single-row V.G., Sta. 1180 120° sector, corotating	None	
2	Single-row V.G., Sta. 1300 120° sector, counter rotating	Same as config. number 1	None	
3	Single-row V.G., Sta. 1300 90° sector, corotating	Same as config. number 1	None	
4	Same as config. number 3	Same as config. number 1	Single row V.G., Sta. 1120 90° Sector, Corotating	
5	None	None	Same as config. number 4	
6	None	Single-row V.G., Sta. 1180 155° sector, corotating	None	Oil flow study only
7	Single-row V.G., Sta. 1269 109° sector, corotating	Same as config. number 6	None	
8	Single-row V.G., Sta. 1269 82° sector, counter rotating	Same as config. number 6	None	
9	Single-row V.G., Sta. 1269 105° sector counter rotating	Same as config. number 6	None	Counter-rotating pairs alternating in direction forward and backward
10	Single-row V.G., Sta. 1300 104° sector counter rotating	Single-row V.G., Sta. 1180 187° sector, corotating	None	Counter-rotating pairs have triangular shape
11	Single-row V.G., Sta. 1300 104° sector counter rotating	Same as config. number 10	None	Counter-rotating pairs have chamfered leading edge

TABLE I (CONTINUED)

FLOW CONTROL CONFIG. NUMBER	12 O'CLOCK SECOND BEND	6 O'CLOCK FIRST BEND	3 AND 9 O'CLOCK FIRST BEND	COMMENTS
12	Same as config. number 2	Same as config. number 10	None	
13	Same as config. number 2	Same as config number 10	Boundary layer fence	
14	Same as config. number 2	None	Boundary layer fence	
15	Same as config. number 2	Turning vanes 3 successive pairs	None	Oil flow only
16	Turning vanes 3 successive pairs	Turning vanes 3 successive pairs	None	
17	Turning vanes 2 successive pairs	Turning vanes 2 successive pairs	None	

This steady-state data along with the model steady-state data were recorded on the standard 9' X 9' LSWT data acquisition system. This system, a Hewlett-Packard Dymec 2010D, is a trap and scan scannivalve system with output on punched paper tape. The capability of monitoring on-line engine RPM and a selected number of static pressures was available for setting test conditions.

Dynamic data were recorded at the compressor face for a selected number of conditions. The dynamic signal, measured using the Kulite transducers located as shown in Figure 6, was passed through a bandpass filter prior to recording. The frequency range was set at 5 to 1200 Hz (the lower limit set by the recording system and the high limit based on an input from P&WA concerning the frequency sensitivity range of the JT8D-100 engine).

Dynamic data were recorded as a permanent record on magnetic tape.

3.4 TEST PROCEDURES AND TEST CONDITIONS

The following test procedure was followed throughout the test program:

1. Each day inspect instrumentation lines and blow out for 1/2 minute with industrial nitrogen (a complete leak check was made after each model installation or major configuration change).

2. Inspect model and facility.

3. Zero check instrumentation.

4. Start J-47 turbojet and warm up (inlet airflow).

5. Start Allison 501 and warm up (if tunnel velocity is required).

6. Establish desired tunnel velocity and inlet airflow and stabilize at least 30 seconds prior to obtaining data.

7. Close cut-off valves.

8. Activate scannivalves and record data.

9. After scan, open cut-off valves.

10. Rotate rake and repeat steps 7 through 10.

11 Repeat steps 6-10 at other desired airflow conditions.

12. Change model attitude or configuration, and repeat steps 2 through 11.

Data were taken for static, crosswind, forward speed and angle of attack conditions. Steady state and dynamic data could be taken simultaneously during a run. Oil flow studies required a separate run. Table II gives a summary of the "S" duct test runs. Runs 1 through 9 define bare-duct performance; Runs 10 through 27 were used to select the flow control configuration; and Runs 28 through 56 demonstrate performance of the selected configuration for the full scope of testing including crosswind.

3.5 DATA REDUCTION AND DATA PRESENTATION

During the test program steady-state data were reduced using a standard Boeing data reduction program for inlet tests. Data were reduced using a quick-look and final reduction version of the program.

Quick-look data were obtained by processing the punched paper tape through the Boeing Mechanical Laboratories SDS 92 computer. The tabular output consisted of total and static pressure measurements, surface Mach number distributions, inlet recovery, inlet airflow, and the commonly used steady-state distortion parameters defined as:

$$\frac{P_{T\ MAX} - P_{T\ MIN}}{P_{T\ AVG}} \quad \text{and} \quad \frac{P_{T\ AVG} - P_{T\ MIN}}{P_{T\ AVG}}$$

Additional quick-look data were obtained from the test facility's own PDP8 computer in form of tabulations of radial and circumferential distortion parameters defined by Pratt & Whitney Aircraft (see Section 4.6.3).

D1 4100 7740 ORIG.3/71 J18-.4

TABLE II

RUN NO.	INLET INFLOW ANGLE, DEGREES	TUNNEL VELOCITY, KNOTS	INLET AIRFLOW, LB / SEC	VORTEX GENERATOR	STEADY STATE PRESSURE DATA	DYNAMIC DATA	19% BLOCKAGE SCREEN IN	SIMULATED FUSELAGE	COMMENTS
1	0	25	350-400	NONE					INITIAL CHECK OUT RUNS,
2	0	25	350-400	NONE					DATA NOT VALID
3	0	25	350-499	NONE	X	(1)(2)	X		30% Lip, a/b=2.5, (7)
4	0	25	494	NONE	X				
5	0	160	180-498	NONE	X	(1)	X		
6	0	160	470	NONE			X		TRAVERSE AT LOWER WALL STA. 1160.4
7	0	160	470	NONE			X		TRAVERSE AT LOWER WALL STA. 1209.1
8	0	160	470	NONE			X		TRAVERSE AT LOWER WALL STA. 1277.4
9	0	160	470	NONE			X		OIL FLOW STUDY
10	0	160	477-495	# 1	X	(1)(2)T12	X		FLOW CONTROL STUDY (8)
11	0	160	478-498	# 2	X	(1)(2)	X		
12	0	160	477-496	# 3	X	T6, T12	X		
13	0	160	477-496	# 4	X		X		
14	0	160	477	# 5	X	(1)	X		
15	0	160	470	# 6			X		OIL FLOW STUDY
16	0	160	477-494	# 7	X	(1)(2)	X		
17	0	160	477-496	# 8	X	(1)	X		
18	0	0	475	# 8	X		X		
19	0	160	477-494	# 9	X		X		
20	0	160	477-495	#10	X	(1)	X		
21	0	160	477-495	#11	X		X		
22	0	160	476-495	#12	X	(1)	X		

(1) DYNAMIC DATA AT TAKEOFF AIRFLOW (~470 LB/SEC)
(2) DYNAMIC DATA AT MAX AIRFLOW (~ 495 LB/SEC)
T6 DYNAMIC DATA TRAVERSING PROBE AT 6:00 O'CLOCK POSITION
T12 DYNAMIC DATA TRAVERSING PROBE AT 12:00 O'CLOCK POSITION

(7) 30% LIP, a/b = 2.5 AT RUN NO'S 3 THROUGH 44 AND RUN NO'S 54 THROUGH 56
(8) FLOW CONTROL STUDY RUN NO'S 10 THROUGH 27

D1 4100 7740 ORIG.3/71

J18-047

TABLE II (CONTINUED)

RUN NO.	INLET INFLOW ANGLE, DEGREES	TUNNEL VELOCITY, KNOTS	INLET AIRFLOW, LB / SEC	VORTEX GENERATOR	STEADY STATE PRESSURE DATA	DYNAMIC DATA	19 % BLOCKAGE SCREEN IN	SIMULATED FUSELAGE	COMMENTS
23	0	160	477-495	# 13	X		X		(#13 = #12 + B/L FENCE)
24	0	160	477-496	# 14	X		X		B/L FENCE
25	0	160	470	# 15			X		OIL FLOW STUDY
26	0	160	479	# 16	X		X		
27	0	160	478	# 17	X		X		
28	0	25	354-499	# 12	X	(1)	X		SELECTED FLOW CONTROL CONFIG. (9)
29	0	50	355-499	# 12	X	(1)	X		
30	0	100	354-499	# 12	X	(1)	X		
31	0	160	356-499	# 12	X	(1)	X		
32	+5	100	352-499	# 12	X	(1)	X		
33	+5	160	352-497	# 12	X	(1)	X		
34	-5	100	345-500	# 12	X	(1)	X		
35	-5	160	207-498	# 12	X	(1)	X		
36	-5	160	470	# 12			X		OIL FLOW STUDY
37	-5	160	470	# 12			X		TRAVERSE AT LOWER WALL STA 1209.1
38	-5	160	470	# 12			X		TRAVERSE AT LOWER WALL STA 1277.4
39	-5	160	317-585	# 12	X	(1)(3)			SCREEN REMOVED
40	-5	160	354-496	# 12	X	(1)	X		7.5 IN (LONG) NOSE DOME
41	90 (10)	10	306-475	# 12	X	(1)(4)(5)	X	X	30% Lip, a/b=2.5
42	90	0	306-473	# 12	X	(1)(4)(5)	X	X	
43	90	25	306-471	# 12	X	(1)(4)(5)	X	X	
44	90	35	306-476	# 12	X	(1)(4)(5)	X	X	

(1) DYNAMIC DATA AT TAKEOFF AIRFLOW (~ 470 LB/SEC)
(2) DYNAMIC DATA AT MAX AIRFLOW (~ 495 LB/SEC)
(3) DYNAMIC DATA AT 527 LB/SEC (W/) SCREENS ONLY)
(4) DYNAMIC DATA AT 306 LB/SEC
(5) DYNAMIC DATA AT 400 LB/SEC
(9) SELECTED FLOW CONTROL CONFIGURATION RUN NO'S 28 THROUGH 56
(10) CROSSWIND TESTING RUN NO'S 41 THROUGH 53

D1 4100 7740 ORIG.3/71 J15-347

TABLE II (CONTINUED)

RUN NO.	INLET INFLOW ANGLE, DEGREES	TUNNEL VELOCITY, KNOTS	INLET AIRFLOW, LB/SEC	VORTEX GENERATOR	STEADY STATE PRESSURE DATA	DYNAMIC DATA	19 % BLOCKAGE SCREEN IN	SIMULATED FUSELAGE	COMMENTS
45	90	10	304-472	# 12	X	(1)(4)(5)	X	X	34% Lip, a/b=2.5, (11)
46	90	25	307-475	# 12	X	(1)(4)(5)	X	X	
47	90	25	475	# 12	X	(1)	X	X	RERUN OF 46.3
48	90	35	309-477	# 12	X	(1)(4)(5)	X	X	
49	90	0	304-474	# 12	X	(1)(4)(5)	X	X	
50	90	0	305-475	# 12	X	(1)(4)(5)	X	X	30% Lip, a/b=2.0, (12)
51	90	10	307-474	# 12	X	(1)(4)(5)	X	X	
52	90	25	307-477	# 12	X	(1)(4)(5)	X	X	
53	90	35	308-479	# 12	X	(1)(4)(5)	X	X	
54	23 (13)	76	449-492	# 12	X	(1)(2)(6)	X		30% Lip, a/b=2.5,
55	23	74	472-492	# 12	X	(1)(2)	X		WITH STRUTS
56	23	50	472-492	# 12	X	(1)(2)	X		WITH STRUTS

(1) DYNAMIC DATA AT TAKEOFF AIRFLOW (≈ 470 LB/SEC)
(2) DYNAMIC DATA AT MAX AIRFLOW (≈ 495 LB/SEC)
(3) DYNAMIC DATA AT 527 LB/SEC (W/O SCREENS ONLY)
(4) DYNAMIC DATA AT 306 LB/SEC
(5) DYNAMIC DATA AT 400 LB/SEC
(6) DYNAMIC DATA AT 449 LB/SEC
(11) 34% LIP, a/b = 2.5, RUN NO'S 45 THROUGH 49
(12) 30% LIP, a/b = 2.0, RUN NO'S 50 THROUGH 53
(13) 29 KT CROSSWIND AT APPROX. 67 KT SPEED

Final data were obtained by generating a magnetic tape from the paper tape for processing through the Boeing CDC 6600 computer. The final data consisted of tabular information similar to that obtained from the quick-look data.

All airflow data shown in this report have been converted from 0.2994 model scale to full scale values.

The recovery measurements ($P_{T2}/P_{T\infty}$) presented in this document are computed on an area-averaged basis. The wall region is handled by taking the average of the wall static measurement and the closest total probe multiplied by the annular area segment between the two. Other regions are handled by multiplying the annular area segment between any two probes by the average of their total pressures.

Computer plots were also generated on the CDC 6600. These plots consisted of:

1. Compressor face steady-state pressure recovery maps
2. Local Mach number vs. location in "S" duct
3. Compressor face maps of the RMS level of the dynamic pressure data.

Final dynamic data consisted of RMS pressure data to be evaluated by P&WA.

Dynamic pressure as used in this report is defined as the time varying portion of the total pressure. The term instantaneous pressure is taken as the sum of the steady-state total pressure plus the dynamic total pressure at a given instant.

The statistical term RMS pressure as used in this report is usually called the standard deviation (frequency response between 5 and 1200 Hertz).

Steady-state tabulated and machine plotted data are permanently stored on microfilm.

4.0 RESULTS AND DISCUSSION

4.1 FLOW VISUALIZATION STUDIES

Oil flow studies were conducted for selected conditions. Figure 7 shows the flow pattern inside the duct at takeoff airflow and 160-knot speed. Examination of wall streamline patterns indicated that strong secondary flows existed. The flow was curving from both sides toward the lower wall at the first bend. The co-rotating vortex generators at the lower wall counteract that flow at the same time they re-energize the lower wall boundary layer. At the second bend flow was curving from both sides toward the upper wall. Vortex generators at the upper wall re-distribute the secondary flow and re-energize the upper wall boundary layer. The secondary flow is explained in more detail in Section 4.4.2.

4.2 SURFACE MACH NUMBER DISTRIBUTION

Surface Mach number distributions at the lower and upper walls at MCR airflow for the JT8D-100 engine are shown in Figure 8 for the 25-knot condition. Analytically predicted surface Mach number distributions are superimposed and found to be in good agreement with the test results.

4.3 FAN SIMULATION-SCREEN TECHNIQUE

As a result of joint program planning with P&WA, it was agreed that the effect of fan simulation was desirable during the inlet testing. The feasibility of simulating the engine in inlet test with respect to both steady-state and dynamic interactions has been examined previously, Reference 3. Properly sized screens at the fan station of an inlet model can be employed for the simulation of the engine. A 19-percent blockage screen configuration consisting of 0.41 inch mesh with 0.041 inch diameter wire was installed at the simulated rotor plane. This screen was sufficiently dense that the flow was choked at the screen minimum area for a full-scale flow of 500 lb/sec. The screen was selected to provide a pressure ratio/

flow characteristic similar to that predicted by P&WA for the JT8D-100 fan at the design speed. Inspection of the duct wall Mach number distribution indicates a slightly improved surface pressure gradient at the 12 o'clock duct orientation, Figure 8. Figures 9 and 10 verify this improvement showing less total pressure loss in the boundary layer at the same position.

4.4 CONFIGURATION SELECTION

4.4.1 External Flow Field Consideration

The external flow field around the inlet highlight plane was investigated and reported in Reference 2. It was indicated that at cruise conditions, flow direction is downward and is approximately 1 degree with respect to the body water line. At airplane rotation, an upward flow angle of approximately 1 degree was measured. Downflow angles of 11 to 14 degrees can be experienced at wing stall. The "S" duct was essentially insensitive to angular variations over this range of inflow angles based on Phase I testing; therefore, the investigation of these large inflow angles was not repeated in Phase II.

It is advantageous to slant the inlet highlight plane (an upward tilt of the inlet centerline) to reduce the curvature of the first bend. The slanted inlet results in a slightly higher inflow angle at airplane rotation. The final inlet highlight plane was slanted 3°40' as shown in Figure 3.

4.4.2 Flow Control Devices

The center inlet has two bends between the inlet highlight and compressor face and is commonly called the "S" duct. Because of the bends the pressure recovery at the compressor face is highly distorted. A compressor face pressure recovery map (bare duct) for 25 knots at the takeoff airflow condition is shown in Figure 11. A localized, highly depressed region at the upper wall is evident. A low pressure region symmetrical about a vertical plane is noticeable at the lower wall. The upper wall pressure depression resulted from deterioration of flow quality at the second bend. The low pressure region at the lower wall is attributed to the effects of secondary flow. At the first bend of the duct, the particles near the flow axis which have a higher velocity, dictate the normal pressure gradient. The slower particles near the wall cannot balance this gradient. This leads to the emergence of a secondary flow which is directed outwards in the center and inwards (i.e., towards the center of curvature of the bend) near the wall as shown in the following sketch.

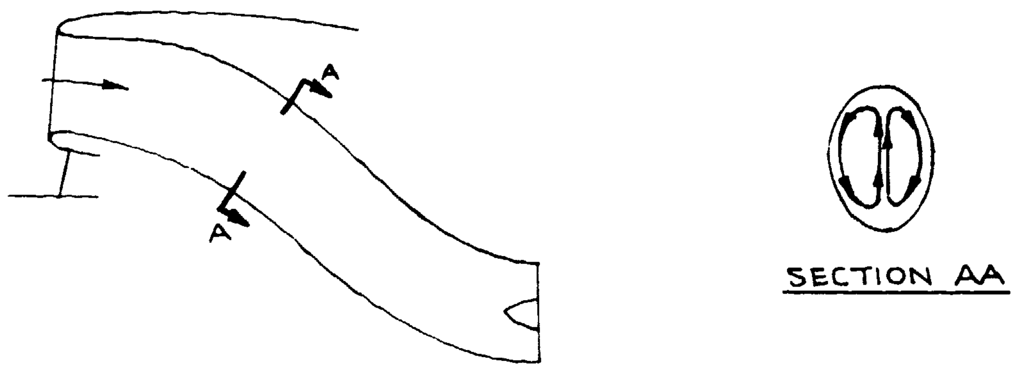

In order to have a better understanding of the development of the secondary flow, a traversing u-shaped rake with 5 total pressure probes was employed to measure the total pressure at lower wall body stations 1160.4, 1209.1 and 1277.4. The traversing rake is capable of moving four inches from the lower wall into the stream. To insure an undisturbed flow upstream of each traversing station, the measurements were taken in three separate runs, one for each traversing station. Figure 12 shows the pressure recovery at the stations. The pressure profile at lower wall body station 1160.4 is abnormal (not symmetrical to lower wall vertical plane) and is probably chargeable to design tolerance and flexibility of the rake installation. The effect of secondary flow on boundary layer growth is not very severe up to the mid-point of the first bend (station 1209.1). The accumulation of low energy flow is evident at station 1277.4.

Steady-state radial and circumferential distortions for the bare duct at the 160 knot, takeoff airflow condition are shown in Figures 13, 14 and 15.

The distortion limits as defined by the engine manufacturer, P&WA, are for the instantaneous total pressure (steady-state plus dynamic). The limits are also plotted in the same figures. It is seen that the 60-degree distortion limit was exceeded by the steady-state levels alone. In order to meet the distortion requirement imposed by the engine manufacturer, it was concluded that flow control devices would be required.

The following flow control devices were tested in the wind tunnel to evaluate their performance:

1) Vortex generators
2) Boundary layer fences
3) Turning vanes

4.4.2.1 Vortex Generators

- <u>Mechanism of Vortex Generators</u>

  The principle of boundary layer control by vortex generators relies on the increased mixing between the external streams and the boundary layer. This mixing is promoted by vortices trailing longitudinally over the surface, adjacent to the edge of the boundary layer. Fluid particles with high momentum in the stream direction are swept along helical paths toward the surface to mix with and to some extent replace the retarded air at the surface. This is a continuous process and so provides a continuous source of re-energization to counter the natural boundary-layer retardation and growth caused by surface friction and adverse pressure gradients. Large adverse pressure gradients can thus be imposed without causing separation.

The principle of reducing pressure distortion at the compressor face which is caused by the accumulation of low-energy flow due to secondary flow relies on increased momentum for fluid particles in the boundary layer and induced cross flows which counteract the secondary flow. By increasing the velocity in the boundary layer, the flow particles near the wall have a higher momentum, thus reducing the amount of secondary flow.

o Description of the Vortex Generators

The vortex generators tested were the vane-type generators which were used in the production 727 airplanes and the Phase I model "S" duct. They consist of a row of airfoils or small plates that project normal from the surface and are set at an angle of incidence to the local flow to produce single trailing vortices. The vanes can all be set at the same angle to produce a set of co-rotating vortices, or they can be set alternately at positive and negative angles to produce counter-rotating pairs of vortices.

The performance of vane-type vortex generators was evaluated by Taylor (Reference 4) of United Aircraft Corporation for diffusers and airfoils at low speeds, and by several NACA experiments (References 5 and 6) for airfoils and aircraft wings at high speeds. This work provides trends in effectiveness for certain vortex generator design variables, such as their angle of attack, height, distance ahead of separation, etc. Attention was, however, focused on the detailed changes that were produced in the boundary layer profile upstream of the imposed pressure gradient. Pearcy and Stuart (Reference 7) extended the study of the effects of various design parameters and concluded that the strength and disposition of the individual vortices was more important than the details of the boundary layer profile just upstream of the imposed gradient.

Counter-rotating, equal-strength vortex generators were used on both the lower and upper walls of the production 727 airplanes and the Phase I model "S" duct. This type of vortex generator is very effective in reducing flow separation if the vortex generator is placed slightly ahead of the point of separation. The disadvantages, compared to co-rotating vortex generators, are: (1) the induced vortices tend to lift off the surface as they proceed downstream; consequently, their effectiveness in reducing separation diminishes very rapidly downstream; (2) higher loss in inlet pressure; and (3) higher pressure distortion in the compressor face core region when used on the lower wall of the "S" duct.

Co-rotating vortex generators, as indicated by Pearcy and Stuart, are very competitive in reducing flow separation if the vortex generators are properly selected and located. The main advantage of co-rotating type vortex generators are their downstream effectiveness resulting in more efficient usage of the vortex energy within the affected boundary layer. This type of vortex generator has a few special advantages when applied on the lower wall of the "S" duct: (1) the induced vortices will remain close to the wall; consequently, a cleaner core (primary) region will be obtained; (2) the induced cross flows at the walls tend to counteract the tendency of the secondary flow to deposit and accumulate low energy air at the 6 o'clock position.

During this Phase II test only the co-rotating type of vortex generator was evaluated in the first bend on the lower surface of the "S" duct since this type demonstrated a superior capability to the counter-rotating type tested in the Phase I model test.

4.4.2.2 Boundary Layer Fences and Turning Vanes

The low pressure region symmetrical about a vertical plane at the lower wall is attributed to the migration of boundary layer due to the bends of the "S" duct. Installation of boundary layer fences was considered as one way of reducing pressure distortion. Turning vanes, based on the work done in Reference 8 were also evaluated. The idea of turning vanes was to turn the airflow in the opposite direction of the secondary flow to obtain an even pressure at the compressor face.

4.4.2.3 Results and Selection of Flow Control Devices

The criteria used in the selection of the flow control configuration for further testing were based on parameters defined by P&WA. Steady-state radial and circumferential distortions at the 160-knot takeoff airflow condition for the better performing configurations are shown in Figures 16, 17 and 18 for comparison. Steady-state compressor face pressure maps for the same conditions are shown in Figures 19, 20 and 21. These contour maps were generated as part of the final data reduction program and were not available during the test.

Vortex generator configurations 7, 10 and 12 have comparable steady-state pressure distortions. Intensified pressure distortions (Section 4.6.3.1), i.e., steady state plus 1-RMS intensification, were calculated for configurations 10 and 12 and are shown in Figures 22 and 23 for radial distortion and in Figures 24 through 27 for 60 and 180-degree circumferential distortions. These two configurations are very competitive when judged by pressure distortion criteria. Vortex generator configuration 12, which has similar generator geometry in the second-bend upper surface to that of the production 727, was selected for use in subsequent testing of inflow angle variations and crosswind conditions. However, it is recommended that configurations 7, 10 and 12 should be further evaluated for engine/inlet compatibility by full-scale ground testing.

The compressor face pressure recovery map for the boundary layer fences (configuration 14) is shown in Figure 28. Pressure distortion at the lower wall is very similar to that of the bare duct as can be seen by comparing Figures 11 and 28. It is felt, however, that extending the boundary layer fences further downstream and/or incorporating more fences may help to improve the lower wall pressure distortion.

The compressor face pressure recovery map for the turning vanes (configuration 16) is shown in Figure 29. It is seen that pressure distortion is worse than that of the bare duct. Pressure recovery was considerably lower than the vortex generator configurations as shown in Figure 30.

4.4.3 Inlet Lip Configuration

4.4.3.1 Inlet Lip Crosswind Consideration

In the JT8D Refan Program considerable emphasis has been placed on the airplane's ability to perform satisfactorily in crosswind. As a result of this thinking, the "S" duct was tested statically in 90-degree crosswinds up to a wind velocity of 35 knots. This testing covered a range of engine airflows from a low level representative of rolling takeoff demands up to full takeoff airflow. In addition to the static condition, a 29-knot crosswind was simulated at 67-knot forward speed in the 9' x 9' LSWT at takeoff airflow. Three inlet lip variations were tested. Table III shows the characteristics of these lips. The lip contours are shown in Figure 1.

TABLE III

LIP CONFIG. NUMBER	CONTRACTION RATIO A_{HI}/A_{TH}	LIP CONTOUR	ELLIPSE AXIS RATIO a/b
1	1.30 (30% LIP)	"SUPER-ELLIPSE"	2.5
2	1.34 (34% LIP)	"SUPER-ELLIPSE"	2.5
3	1.30 (30% LIP)	"SUPER-ELLIPSE"	2.0

4.4.3.2 Results and Selection of Inlet Lip Configuration

Figure 31 shows the static crosswind pressure recovery performance of the three configurations tested. It would seem that the lip performance is satisfactory up to and including 10-knot crosswind for the full range of airflows tested. When increasing crosswind to 25 knots, the pressure recovery decreased for all three lip configurations. Configuration 1 crosswind performance is shown with both total airflow and primary only pressure recovery, Figure 32. Beyond 10-knot crosswind, the primary core flow recovery which usually approaches unity is indistinguishable from the total flow.

Steady-state radial and circumferential pressure distortions are shown for configurations 1 and 2 at takeoff airflow on Figures 33, 34, and 35. No discernible advantage is evident for either lip at the 10-knot crosswind condition with both possibly meeting

P&WA limits. At the 25-knot condition neither configuration will meet P&WA radial distortion criteria, both lips showing comparable performance. Configuration 3 showed no special merit and was eliminated from further discussion.

With rolling takeoff procedures both lip configurations demonstrate similar steady-state pressure distortion characteristics at initiation of takeoff roll with low airflow, Figures 36, 37 and 38. Upon attaining the not-to-exceed airplane roll speed for final setting of takeoff thrust the crosswind distortion effect is minimal; the resulting steady-state pressure distortions under this condition for configuration 1 only are shown on Figures 39, 40 and 41.

Because the alternate lips demonstrated insufficient crosswind performance improvement and can have adverse effect on external lines and/or additional cost of tailoring internal lip contours, configuration 1 lip was selected for Phase II ground rig testing. This inlet lip selection will also provide maximum correlation with the existing model-scale data bank.

4.4.4 Engine Nose Dome

The engine nose dome contour for this test was of an elliptical shape described by a 2.0 to 1.0 ellipse (ellipse major/minor axis). In addition, the inlet was selectively tested with a long nose dome (3.15 to 1.0 ellipse) at 160 knots and takeoff airflow to evaluate length sensitivity. Pressure recovery versus corrected airflow is shown in Figure 42 for both nose domes. Radial, 180-degree and 60-degree circumferential pressure distortions are shown in Figures 43, 44 and 45, respectively, for both nose domes. No discernible difference in either pressure recovery or distortion was observed. Therefore, for reasons of interchangeability with the side inlet and a requirement to provide additional acoustic treatment area, the long elliptical nose dome is recommended.

4.5 TOTAL PRESSURE RECOVERY

4.5.1 Total Pressure Recovery Without Vortex Generators

Tests were conducted for the duct without vortex generators at zero degree inflow angle for the forward speed conditions only because of excessive pressure distortion at upper wall and accumulation of low energy air at the lower wall. Total pressure recovery versus compressor face corrected airflow is shown in Figure 46 for 25-knot and 160-knot speed conditions.

4.5.2 Total Pressure Recovery with Vortex Generators

Vortex generators were introduced because of high pressure distortion. Vortex generator configuration 12 was found most effective in reducing pressure distortion and was used in subsequent testing at inflow angle variation and crosswind conditions.

Pressure recovery versus airflow is shown in Figure 47 for zero-degree inflow angle and in Figure 48 for inlet inflow angle variations. It is seen that inlet inflow angle variations within the 727 airplane normal operating regime (-5 to 5 degrees) have no effect on pressure recovery. The penalty in pressure recovery due to vortex generators at takeoff airflow with forward speed is 0.10 percent, Figures 46 and 47. Phase I testing demonstrated that inlet performance was insensitive to inflow angle variation up to 15-degree downflow; therefore, this corner condition was not repeated in this Phase II program.

Crosswind pressure recovery versus airflow is shown in Figure 32. Pressure recovery at a 25-knot crosswind and takeoff airflow is 96 percent for Phase II "S" duct as compared to 93.5 percent for the 727-100 "S" duct (1/9 model scale, unpublished data). At 10-knot crosswind condition the Phase II "S" duct performance is comparable to that of the 727-200 "S" duct.

Total pressure recovery of the Phase II duct has improved 0.1 percent over the Phase I duct at the 160-knot, takeoff airflow condition (see Figure 49). Pressure recovery of the bare ducts is identical between Phase I and Phase II ducts; therefore, the improvement is attributed to the better vortex generator configuration used on the Phase II duct. The improvement in pressure recovery is most pronounced at 6 o'clock position as can be seen in Figure 50.

4.6 TOTAL PRESSURE DISTORTION

4.6.1 Steady-State Compressor Face Pressure Recovery Maps

Steady-state compressor face pressure recovery maps for the bare duct (without flow control devices) at takeoff airflow conditions are shown in Figures 51 and 52 for 25 and 160 knots, respectively. Compressor face maps are identical for both the 25 and 160-knot conditions.

Steady-state compressor face pressure recovery maps for the duct with vortex generator configuration 12 installed are shown at takeoff airflow for the following conditions:

Figure 53	25-knot forward speed, inflow angle = 0 degrees
Figure 54	160-knot forward speed, inflow angle = 0 degrees
Figure 55	160-knot forward speed, inflow angle = 5 degrees
Figure 56	160-knot forward speed, inflow angle = -5 degrees
Figure 57	0-knot, 90-degree crosswind condition
Figure 58	10-knot, 90-degree crosswind condition
Figure 59	25-knot, 90-degree crosswind condition
Figure 60	35-knot, 90-degree crosswind condition
Figure 61	73-knot, 23-degree yaw condition (simulates 29-knot crosswind at 67-knot forward speed condition).

It is seen from Figures 54, 55 and 56 that the inlet inflow angle variation within the 727 airplane normal operating regime (-5 to 5 degrees) has no effect on total pressure distortion. Total pressure distortion is more pronounced at high crosswind conditions. Rolling takeoff, which is a common airline operational procedure, sets takeoff power at about 67 knots. To simulate 67-knot forward speed and 29-knot crosswind conditions, the "S" duct was set at a 23-degree yaw and tested at a 73-knot forward speed condition. Pressure distortion at this condition is identical to that of the 160-knot forward speed condition as shown by comparing Figures 55 and 61; therefore, it is probable that the "S" duct can be operated successfully at 29-knot crosswinds by using a rolling takeoff procedure.

4.6.2 Compressor Face Dynamic Pressure (RMS) Maps

The $RMS/P_{T\infty}$ compressor face map at 160 knots and takeoff airflow is shown in Figure 62. A steady-state compressor face pressure recovery map for the same condition is shown in Figure 21. Some correlation between steady-state pressure recovery and $RMS/P_{T\infty}$ compressor face maps can be noted: (1) in the core region, pressure recovery is 100 percent (no steady-state pressure gradient) while $RMS/P_{T\infty}$ is zero. (2) At the 6 o'clock position both the steady-state data and the $RMS/P_{T\infty}$ data show better performance (high recovery and low RMS) outside the core region than at other circumferential locations. (3) At the upper wall, the large steady-state pressure gradients exist between each pair of vortex generators and are well reflected in the $RMS/P_{T\infty}$ map.

4.6.3 Distortion Criteria

4.6.3.1 Pratt & Whitney Criteria

Radial and circumferential pressure distortions are used by P&WA, Reference 9, to define the limits. All limits, radial and circumferential, are based on instantaneous pressure measurements. As prescribed by P&WA, the distortions were first calculated for steady-state alone and then intensified with 1 RMS.

The distortion parameters are defined as follows:

- Radial distortion $= \dfrac{P_{T\ MAX\ RING} - P_{T\ LOCAL\ RING}}{P_{T\ MAX\ RING}}$

  where $P_{T\ LOCAL\ Ring}$ is averaged over 360 degrees for a given radius and $P_{T\ MAX\ RING}$ is the maximum $P_{T\ LOCAL\ RING}$

- Circumferential distortion $= \dfrac{P_{T\ RING\ AVG} - P_{T\ MIN\ SECTOR\ AVG}}{P_{T\ RING\ AVG}}$

  Where $P_{T\ MIN\ SECTOR\ AVG}$ is the lowest average total pressure in any 180-degree or 60-degree arc at a given radius having an average pressure of $P_{T\ RING\ AVG}$.

The intensification techniques employed by P&WA to get from steady-state to estimated instantaneous distortion parameters are illustrated in Figure 63. For the radial pressure distortion, one RMS value was added to the maximum ring readings and subtracted from all the other probe readings, and the radial parameter calculated. For the circumferential factors, one RMS value was subtracted from the probes in the minimum sectors and added to all other probes. From these new values, circumferential parameters were recalculated. Radial and 60-degree circumferential pressure distortions are shown in Figures 64, 65, 23 and 25 for takeoff airflow at the static and the 160-knot conditions. It is seen that the "S" duct pressure distortions are within P&WA distortion limits. The 180-degree circumferential distortions are not critical with respect to the limits (see Figure 27).

4.6.3.2 Boeing Criteria

The criterion used by Boeing in assessing the "S" duct is: the steady-state pressure distortions for the Phase II "S" duct will be no more than that of the 727-200 "S" duct. A typical compressor face pressure recovery map for the 727-200 "S" duct is shown in Figure 66. It is seen that pressure measurements were taken at 45-degree intervals. For the Phase II "S"-duct model test, pressure measurements were taken at 10-degree intervals. In order to make a fair comparison, the model test data was reconstructed to show the pressure recovery at 45-degree intervals, similar to that of 727-200. The pressure recoveries at the 0-, 90-, 180- and 270-degree locations were taken directly from the model test data. At the 45-, 135-, 225- and 325-degree locations, the pressure recoveries were obtained by averaging the two neighboring pressure probes; for example, the pressure recoveries at the 45-degree location were the average of the 40- and 50-degree locations.

Pressure distortion $(P_{TAVG} - P_{TMIN})/P_{T\ AVG}$ vs. corrected airflow is shown in Figure 67 for both Phase II and 727-200 "S" ducts. It is seen that in the range of takeoff and cruise corrected airflows, the two ducts have comparable distortion.

Steady-state radial and circumferential pressure distortions, using P&WA parameters are shown in Figures 68 and 69 for both the Phase II and 727-200 ducts. Figure 68 shows that the Phase II duct has lower radial distortion in the critical core region (lower engine limits) than the 727-200 Production duct. Outside the core region, where the engine limits are higher, the Phase II duct has higher radial distortion than the current Production duct. Except for an isolated point outside the core region, the Phase II duct has lower circumferential distortion everywhere as shown in Figure 69.

Pressure distortion in the core region is very critical from the standpoint of engine/inlet compatibility. It is very important that pressure distortion in the core region be kept to a minimum because the engine is less tolerant of distortion in this region (i.e., the limits are low). Since the Phase II duct has lower pressure distortion in the core region, and P&WA claims the JT8D-100 engine and the current JT8D engines have comparable tolerance to distortion, it is concluded that the Phase II duct should provide improved engine/inlet compatibility compared to the 727-200 duct.

4.7 MAXIMUM AIRFLOW CAPABILITY

Maximum airflow obtained with installation of a 19-percent screen is approximately 500 lb/sec. To investigate "S" duct performance at higher airflow conditions, tests were conducted at a 160-knot forward speed with the screen removed. Maximum corrected airflow tested was 585 lb/sec, pressure recovery is 95.9 percent. Pressure recovery versus corrected airflow is shown in Figure 49.

RMS pressure data was taken at corrected airflow of 527.6 lb/sec (V_T = 160 knot). Radial and circumferential pressure distortion calculated based on P&WA criteria are shown in Figures 70 and 71. It is seen that pressure distortions are within the limits set by P&WA. Maximum test airflow at the static condition was 467 lb/sec. It is believed that higher airflow can be achieved statically with modification of lip geometry to stay within the P&WA distortion limits.

4.8 DATA REPEATABILITY

Pressure recovery and distortion at inlet inflow angles of 5, 0 and -5 degrees are expected to be the same, consequently, measured data at these angles can be compared as a check of data repeatability. Figures 72, 73 and 74 are compressor face pressure recovery maps at 100 knot and takeoff airflow condition for inlet airflow angles of 5, 0 and -5 degrees respectively. It is seen that both pressure recovery and distortion are consistent from run to run.

5.0 CONCLUSIONS

- The required airflow was achieved with acceptable pressure recovery (comparable to the current 727-200 duct).

- Pressure recovery for the Phase II center duct inlet is 0.1 percent better than that of the Phase I duct at 160 knots, takeoff airflow conditions (with best vortex generators installed for both Phase I and Phase II ducts).

- Installation of co-rotating type vortex generators on the lower wall improved pressure distortion in the core region when compared to the 727-200 or Phase I ducts. Therefore, the Phase II center duct should provide improved engine/inlet compatibility.

- Pressure distortion at static and forward speed, takeoff airflow conditions is within P&WA limits for the Phase II duct when equipped with vortex generator configuration 12. (P&WA is independently assessing the results of the test program to determine if the model test results indicate that the engine and "S" duct are compatible. Findings have not yet been received).

- Static crosswind operation up to 10 knots appears feasible at full takeoff power. Somewhere between 10 knots and 25 knots, a thrust setting procedure involving rolling takeoff would be required. This rolling takeoff procedure is the prescribed method shown in the 727 Boeing Operations Manual for all takeoff conditions.

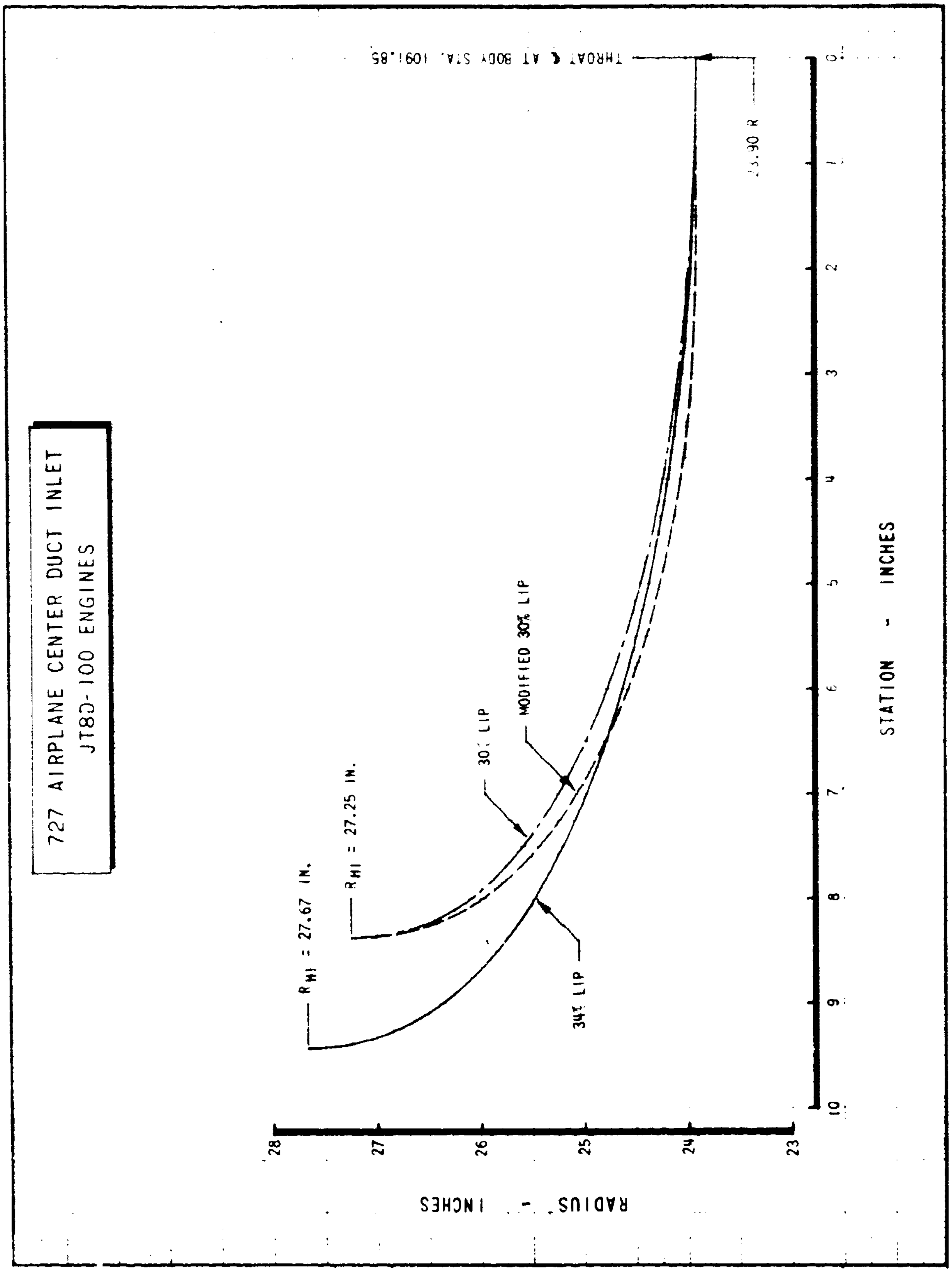

FIGURE 1. - INLET LIP CONTOURS

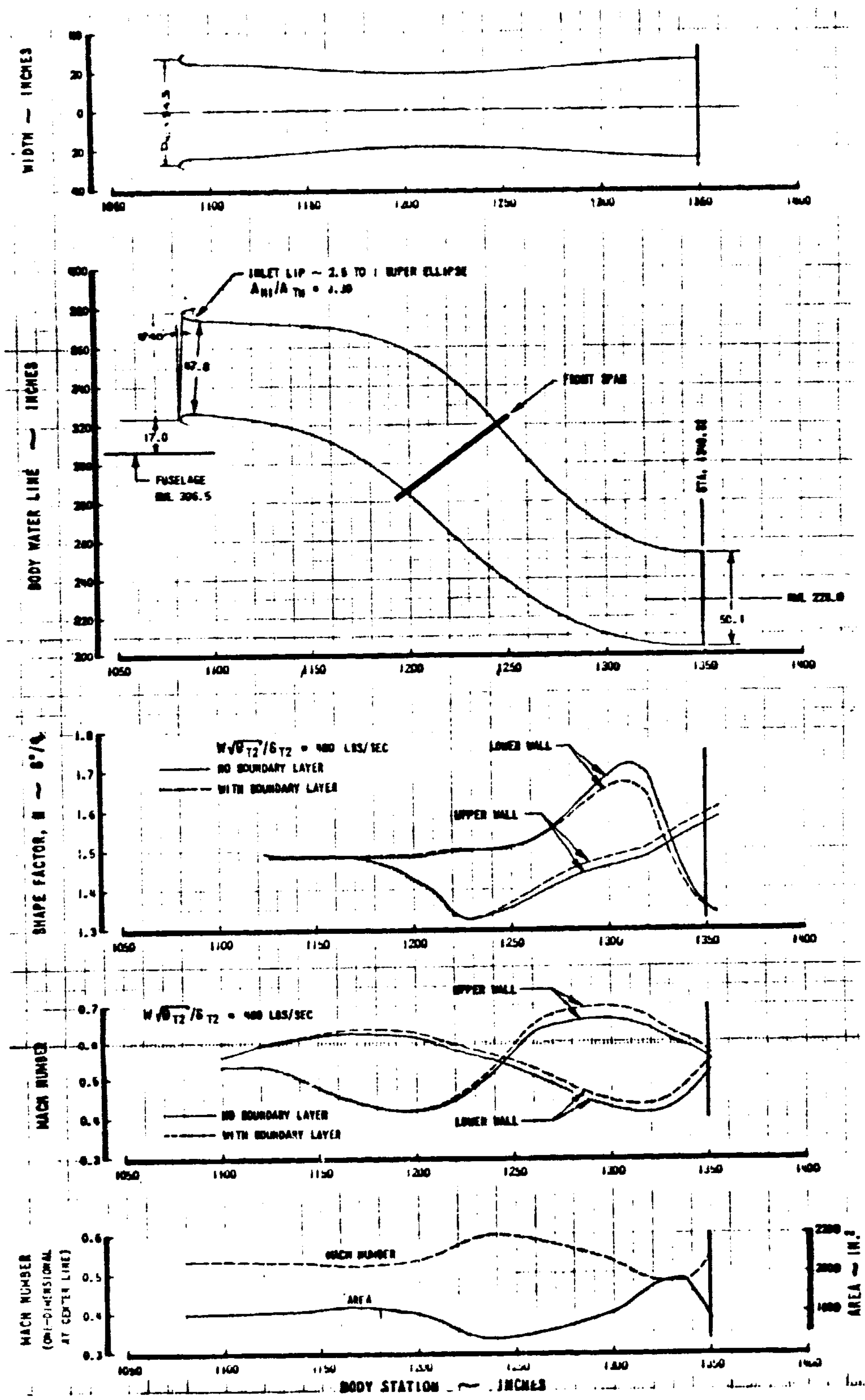

FIGURE 2. - DUCT CONTOUR, SURFACE MACH NUMBER AND SHAPE FACTOR DISTRIBUTIONS

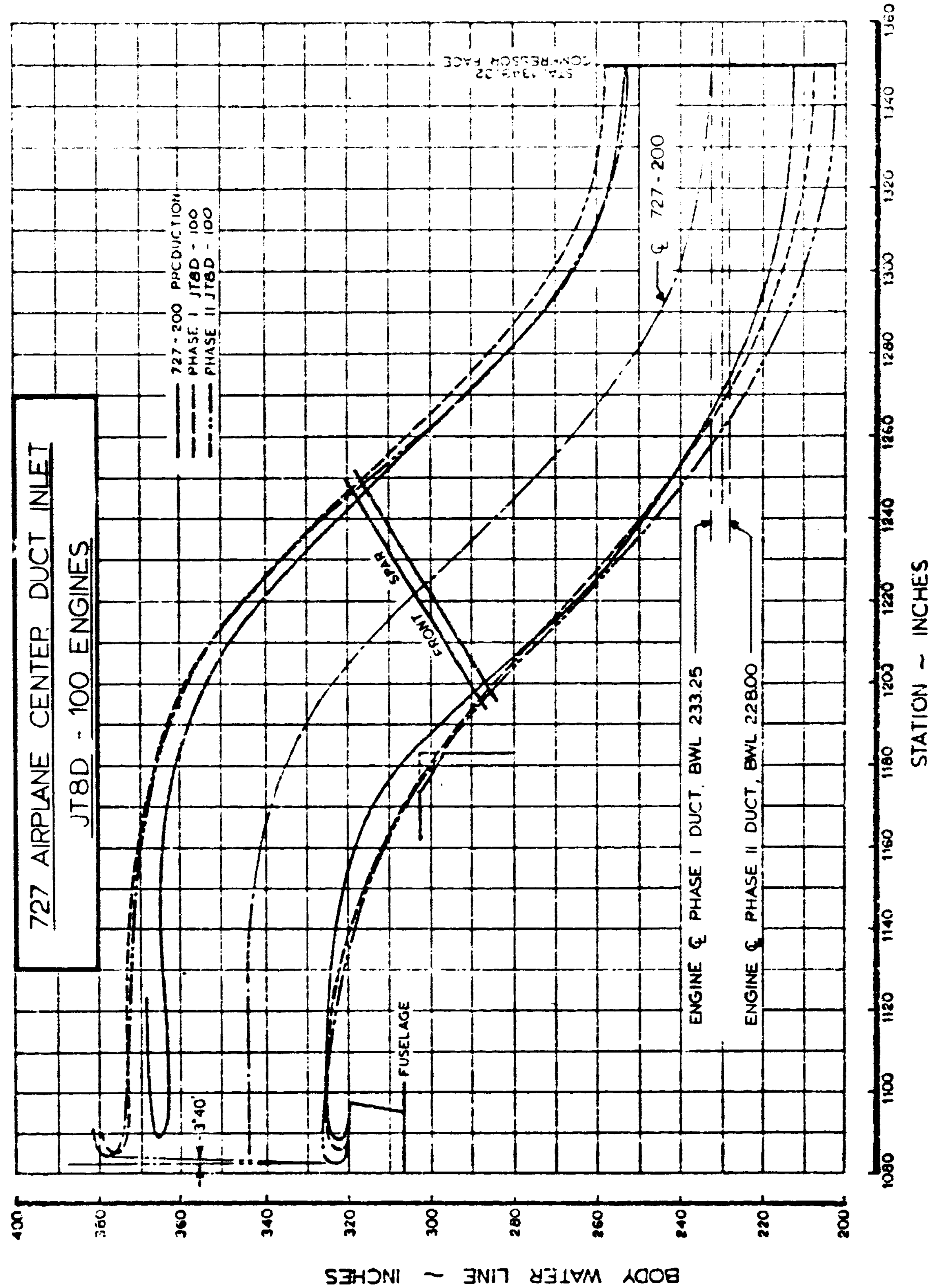

FIGURE 3. - CENTER DUCT INLET WALL CONTOURS

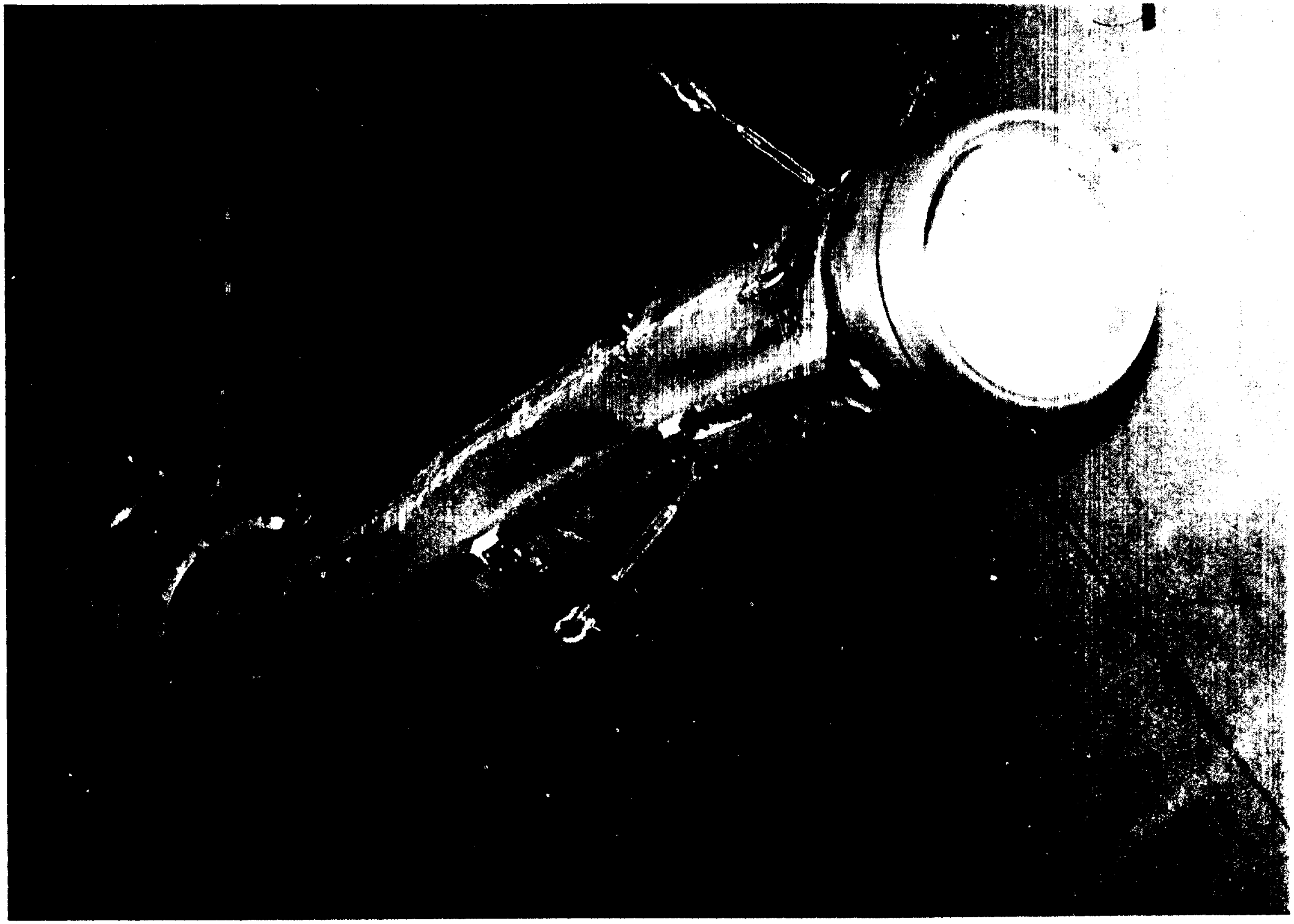

FIGURE 4.-DUCT MODEL W/O FUSELAGE SIMULATION FORWARD SPEED ORIENTATION

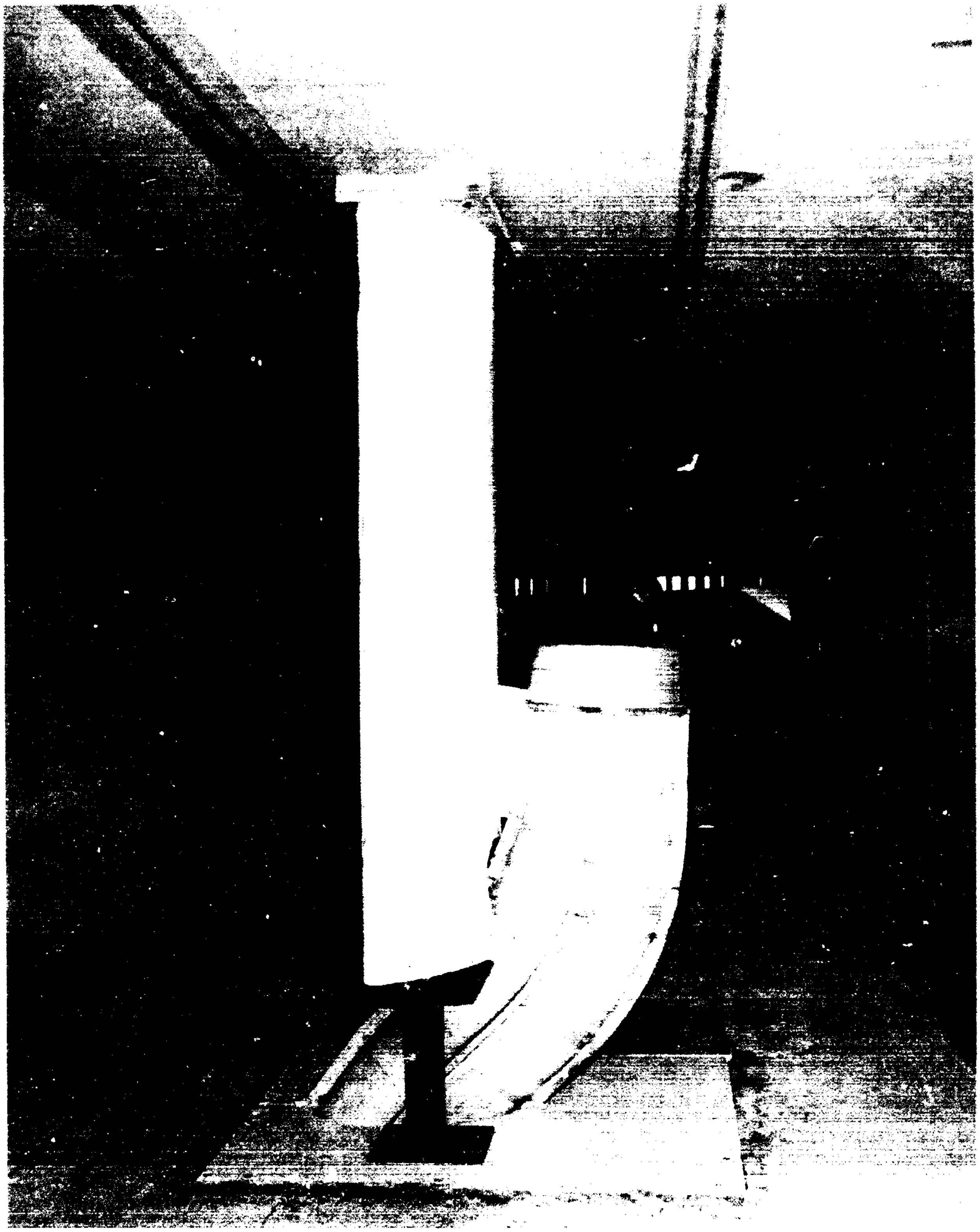

FIGURE 5.-DUCT MODEL WITH FUSELAGE SIMULATION CROSSWIND ORIENTATION

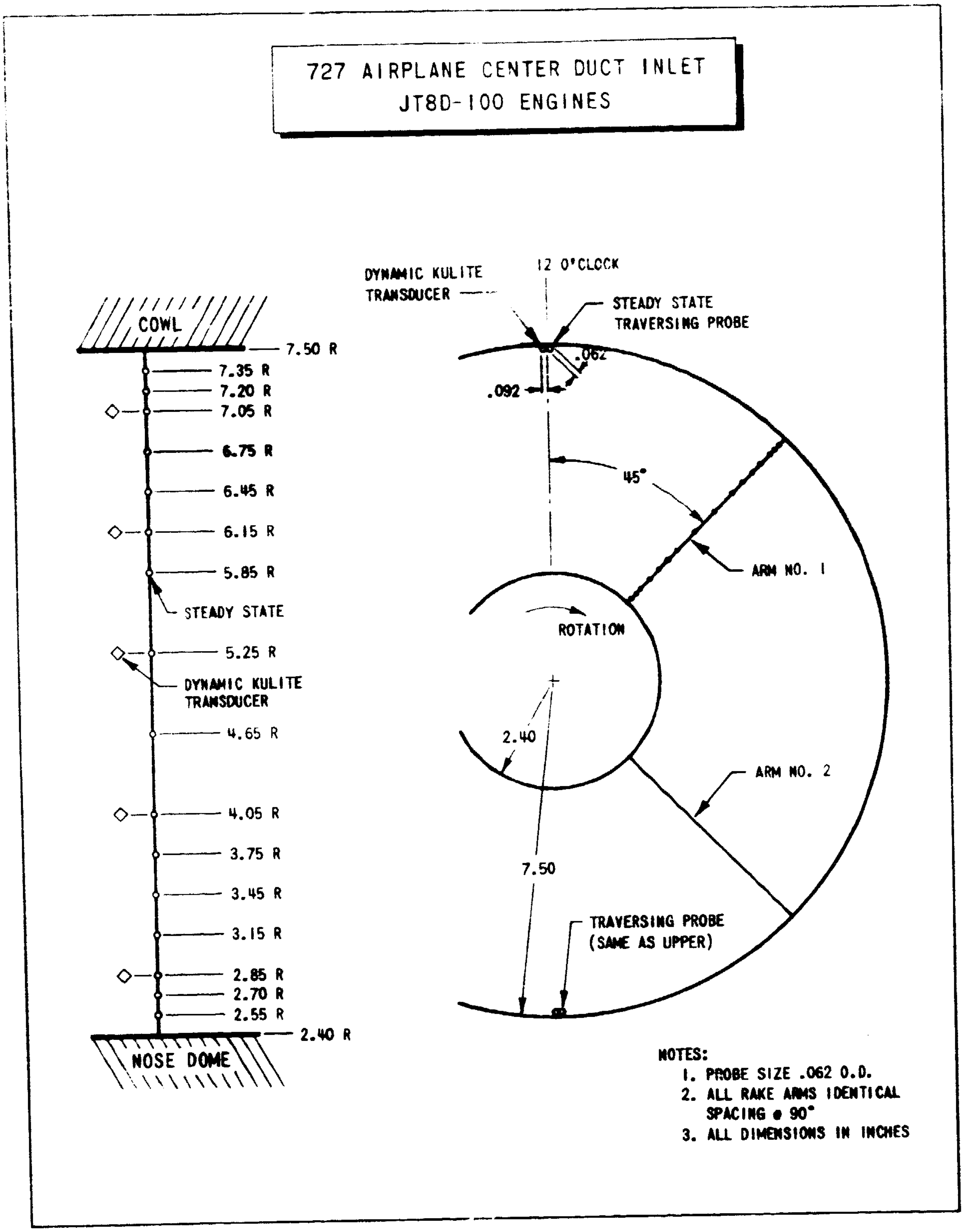

FIGURE 6. - ROTATING TOTAL PRESSURE RAKE (STEADY STATE AND DYNAMIC)

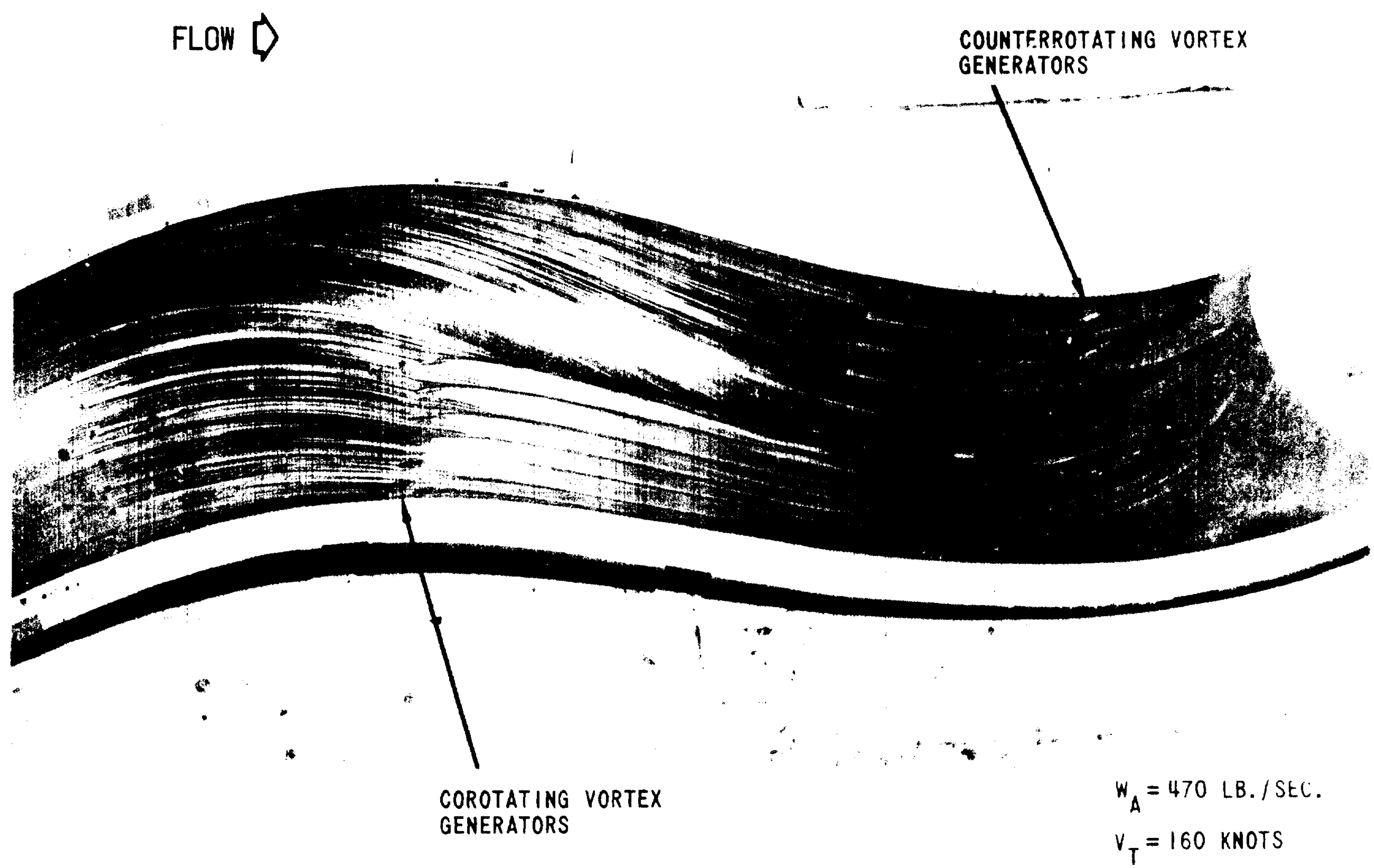

FIGURE 7.-OIL FLOW PATTERN WITH VORTEX GENERATORS
Vortex Generator Configuration 12

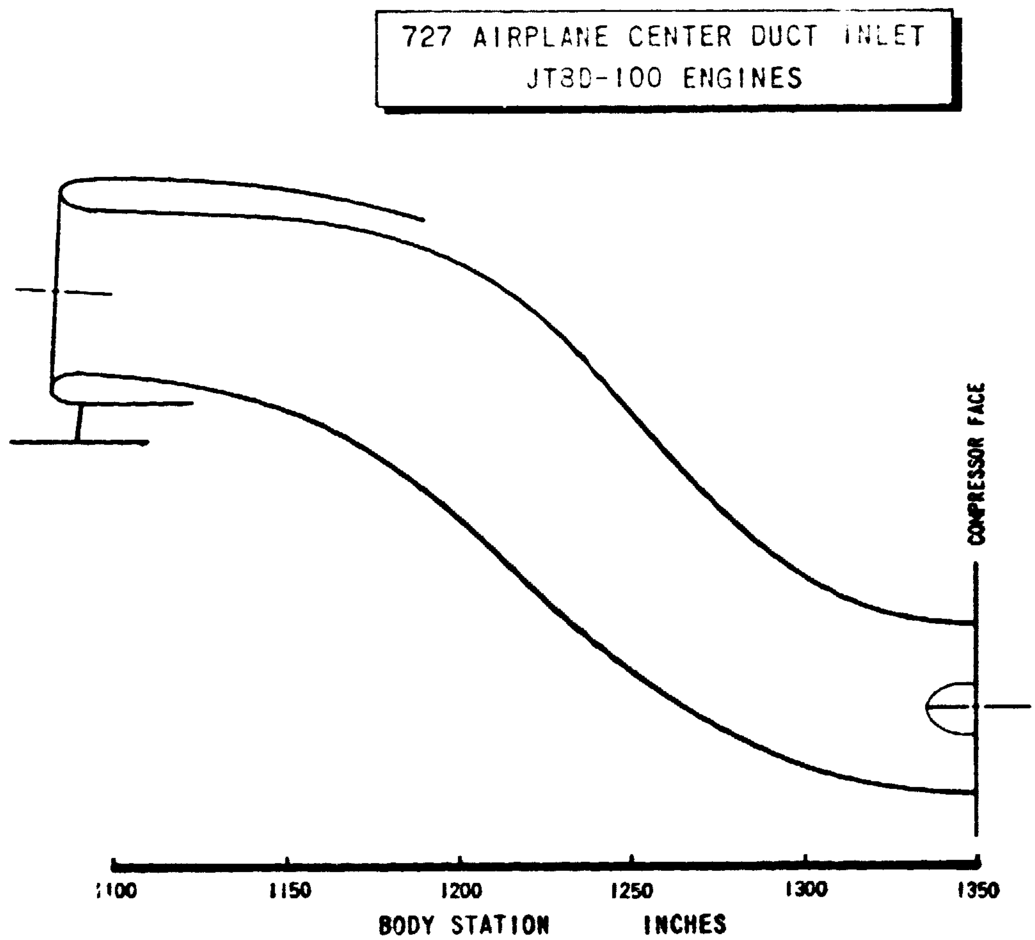

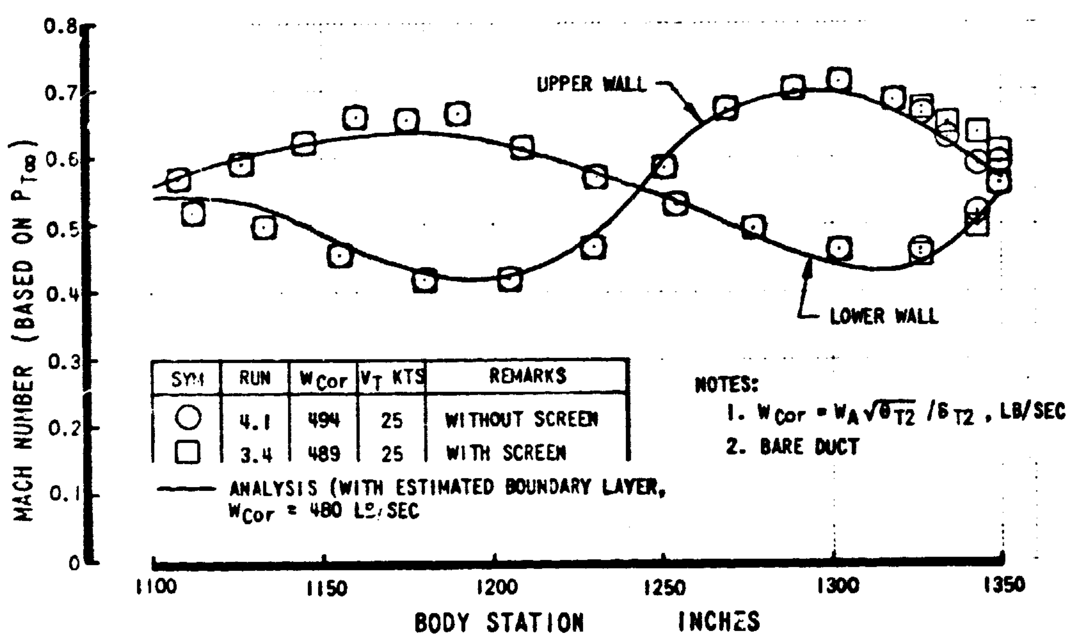

FIGURE 8. - DUCT WALL MACH NUMBER DISTRIBUTION,
EFFECT OF 19% BLOCKAGE SCREEN AT FAN STA.

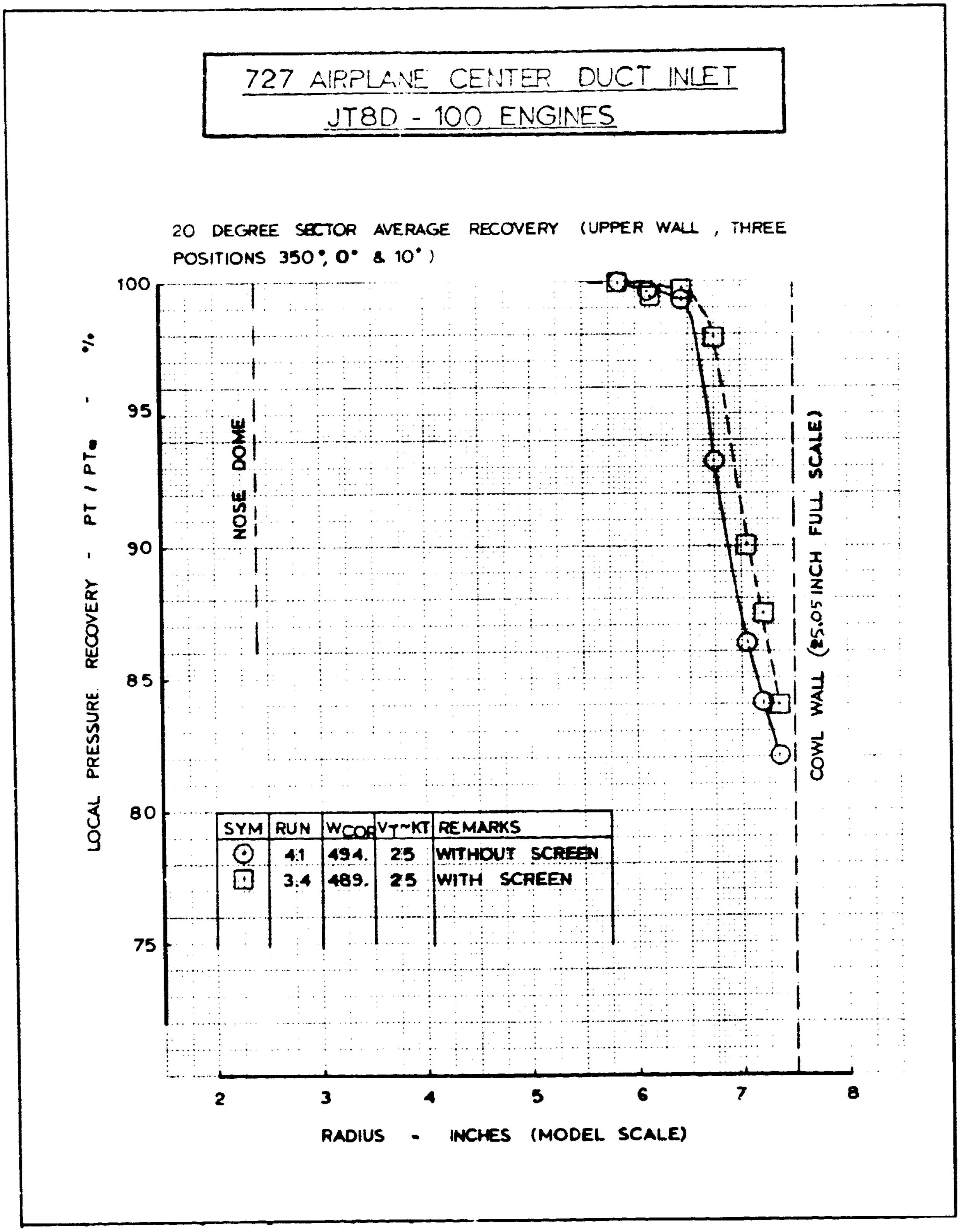

FIGURE 9. - LOCAL PRESSURE RECOVERY (20° SECTOR), EFFECT OF 19% BLOCKAGE SCREEN AT FAN STA.

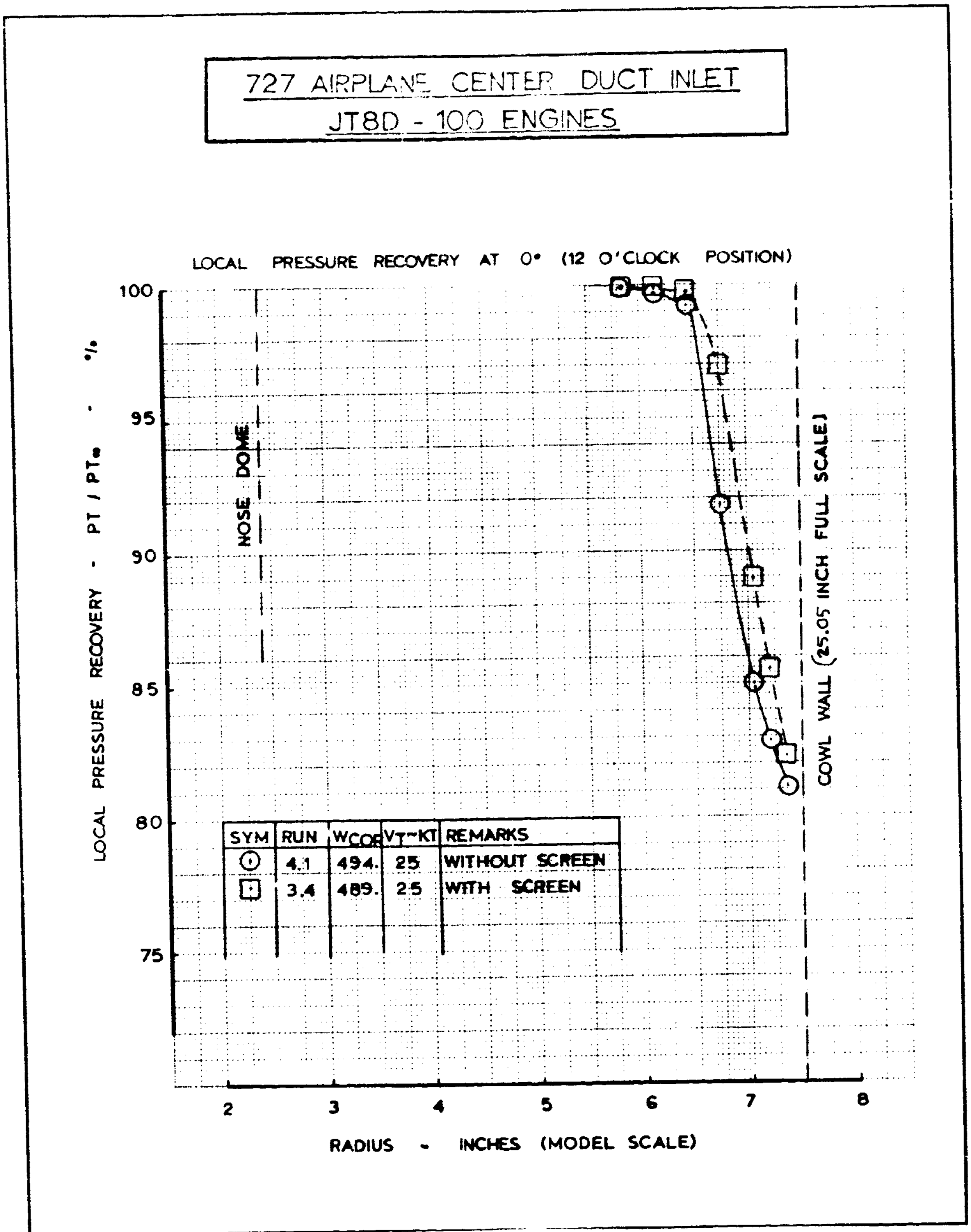

FIGURE 10. - LOCAL PRESSURE RECOVERY (12 O'CLOCK), EFFECT OF 19% BLOCKAGE SCREEN AT FAN STA.

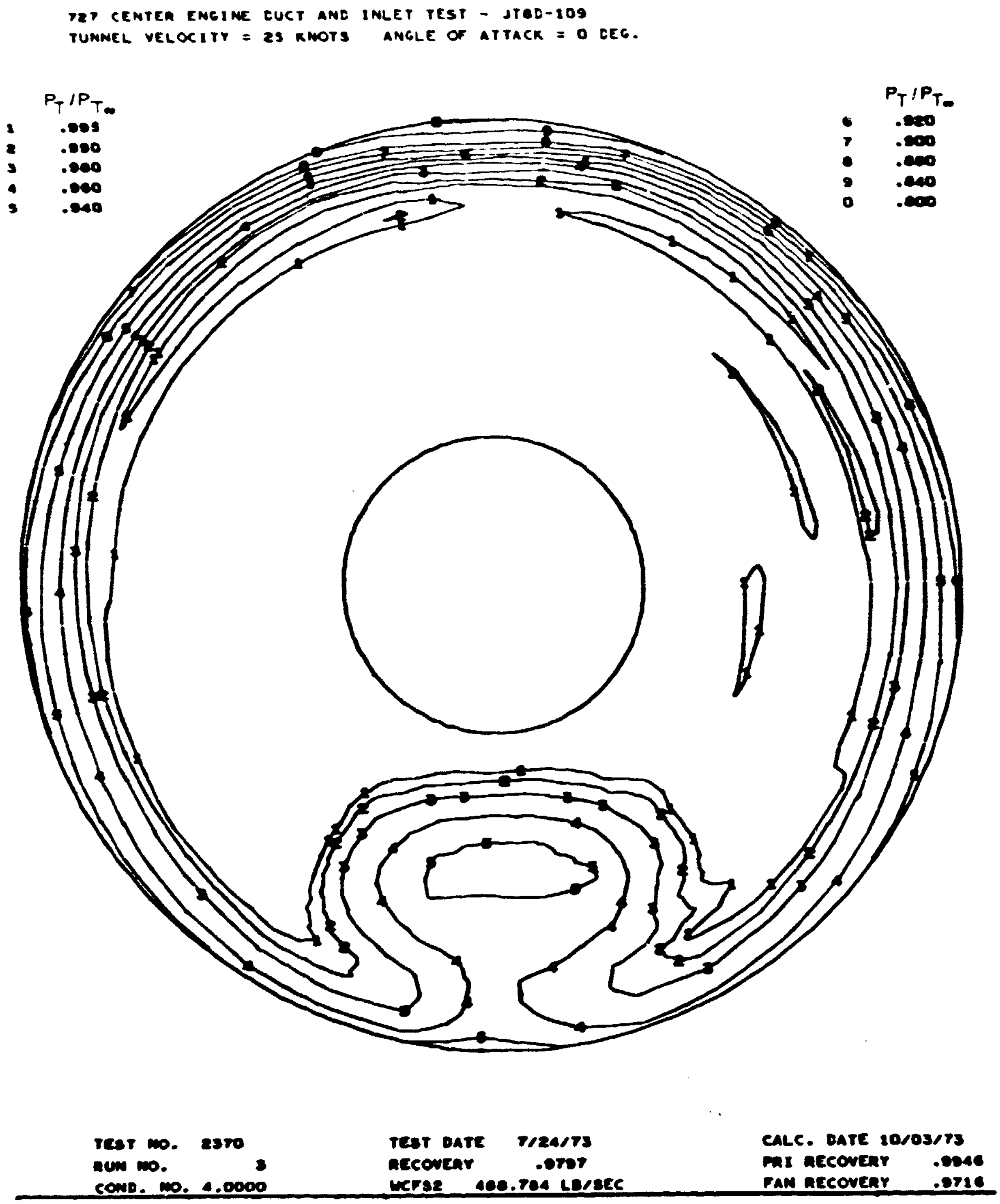

FIGURE 11. - 25-KNOT STEADY-STATE COMPRESSOR FACE PRESSURE PECOVERY
MAP WITHOUT FLOW CONTROL DEVICES

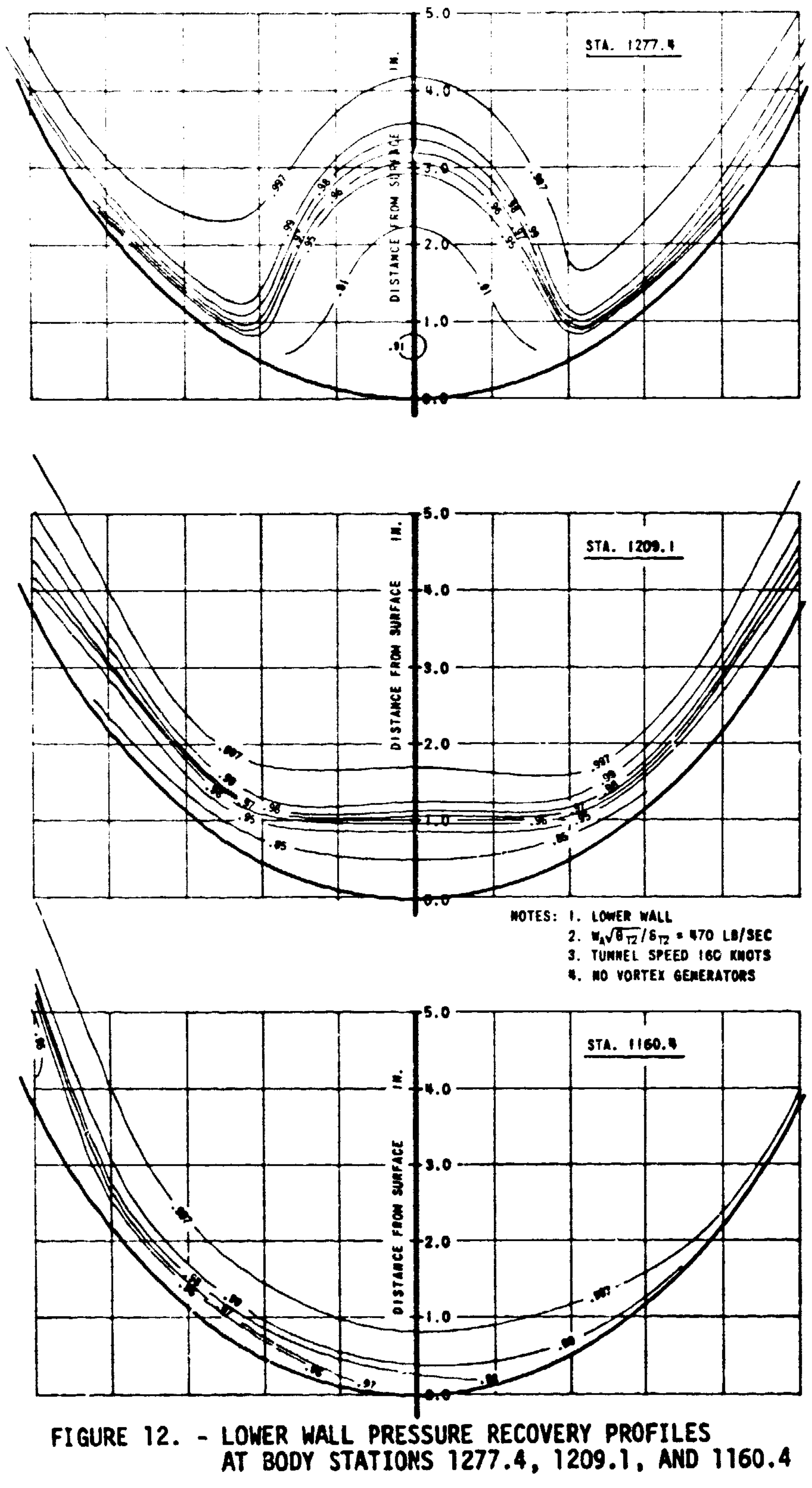

FIGURE 12. - LOWER WALL PRESSURE RECOVERY PROFILES AT BODY STATIONS 1277.4, 1209.1, AND 1160.4

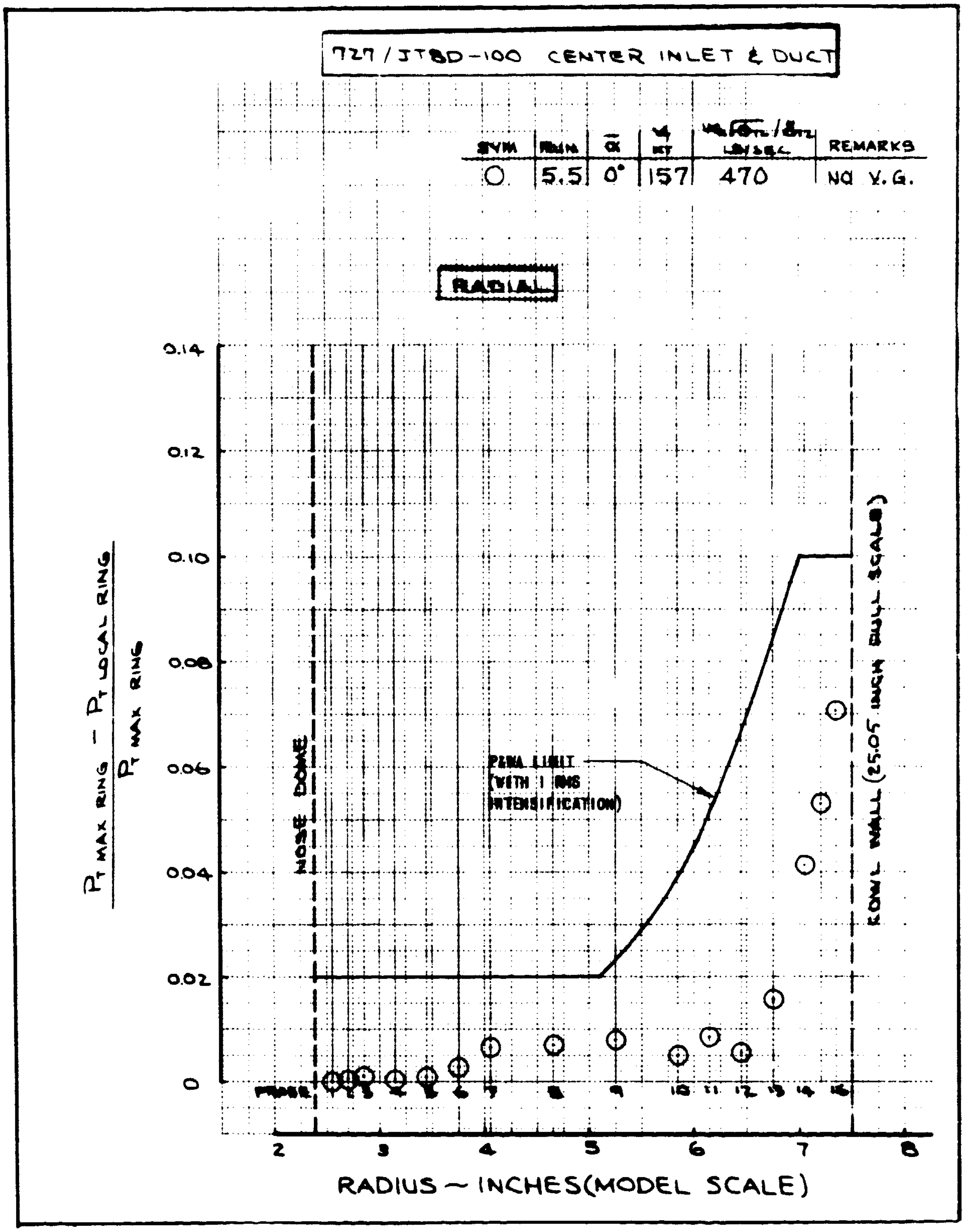

FIGURE 13. - 160-KNOT STEADY-STATE RADIAL PRESSURE DISTORTION
(WITHOUT FLOW CONTROL DEVICES)

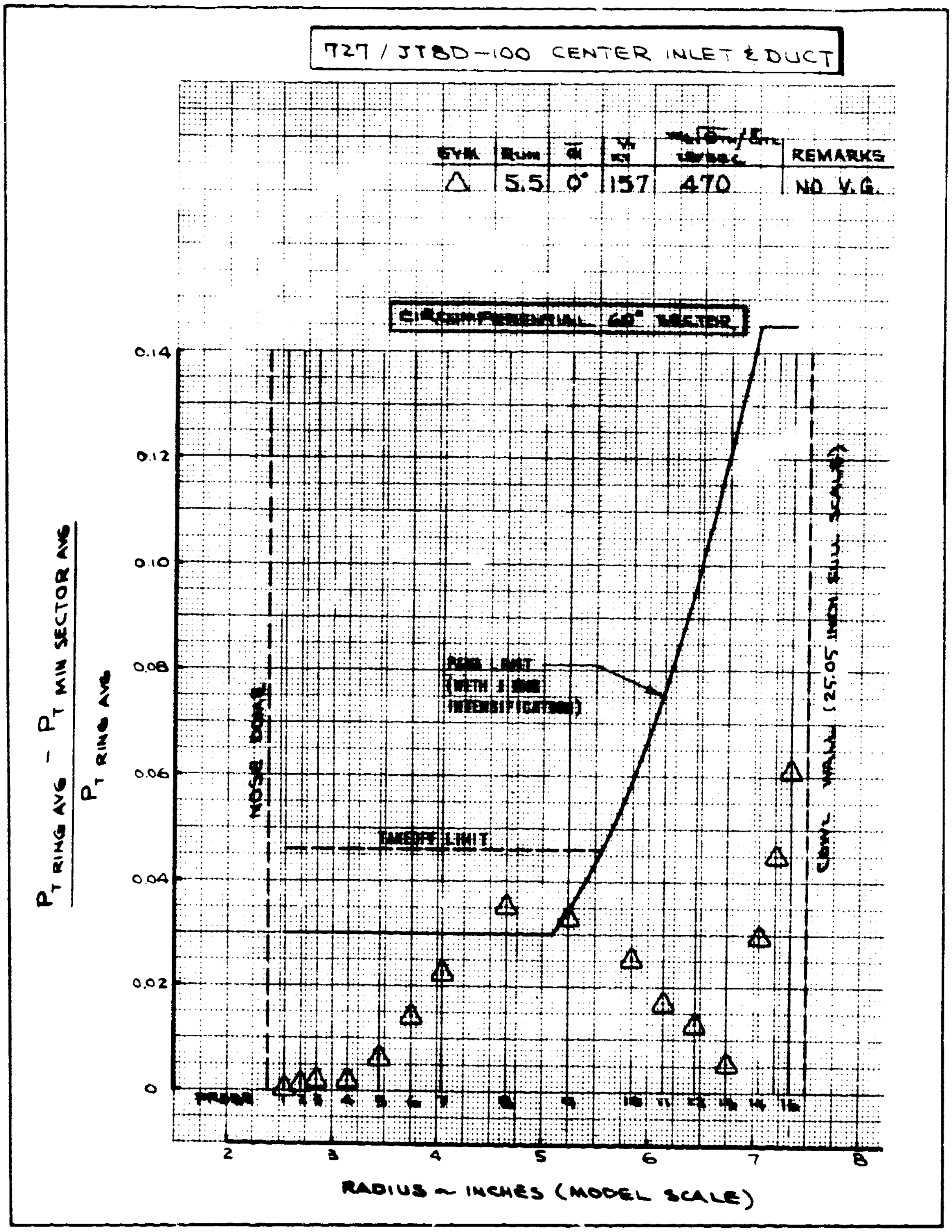

FIGURE 14. - 160-KNOT STEADY-STATE 60°-SECTOR CIRCUMFERENTIAL PRESSURE DISTORTION (WITHOUT FLOW CONTROL DEVICES)

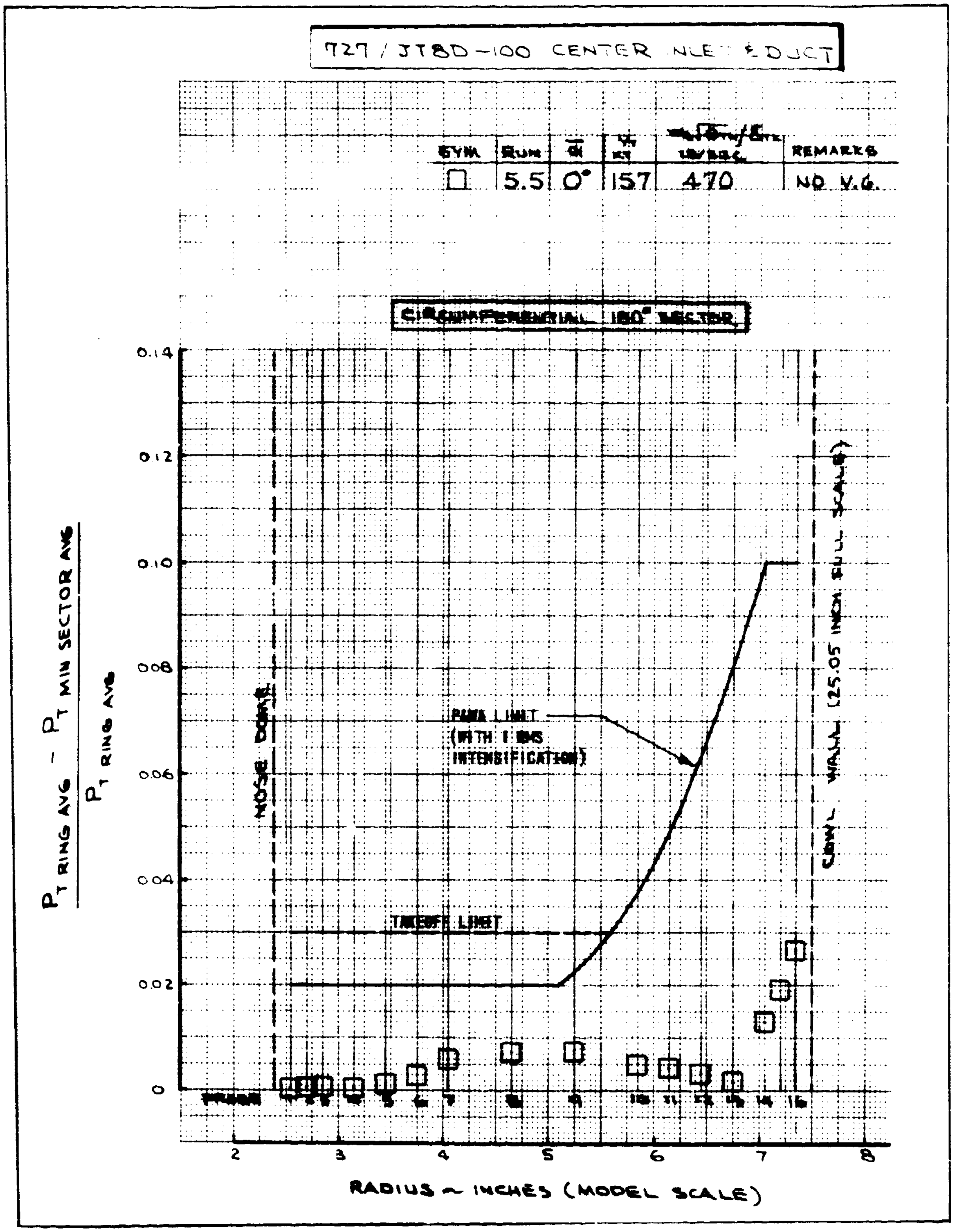

FIGURE 15. - 160-KNOT STEADY-STATE 180°-SECTOR CIRCUMFERENTIAL PRESSURE DISTORTION (WITHOUT FLOW CONTROL DEVICES)

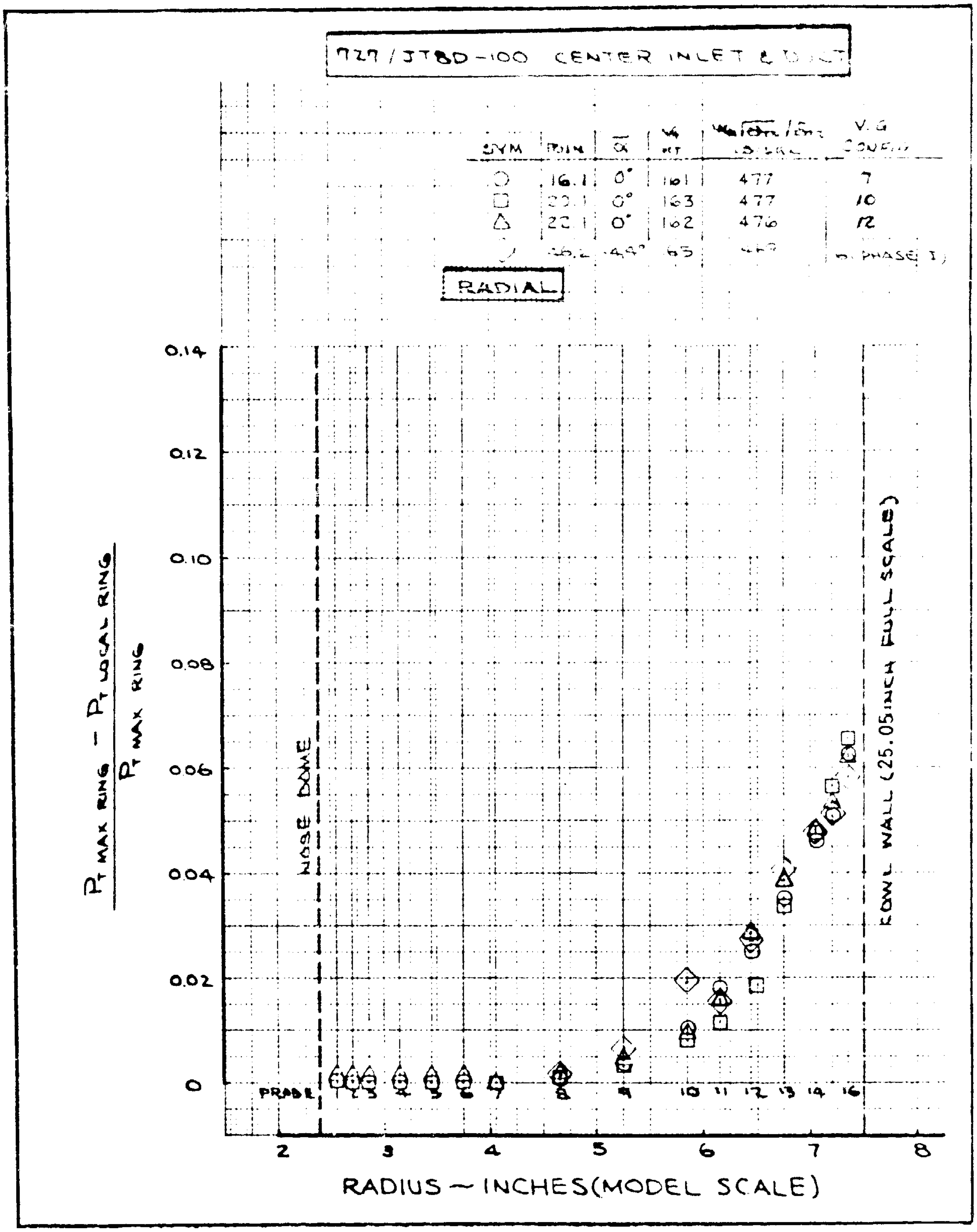

FIGURE 16. - 160-KNOT STEADY-STATE RADIAL PRESSURE DISTORTION, VORTEX GENERATOR CONFIG. 7, 10, and 12

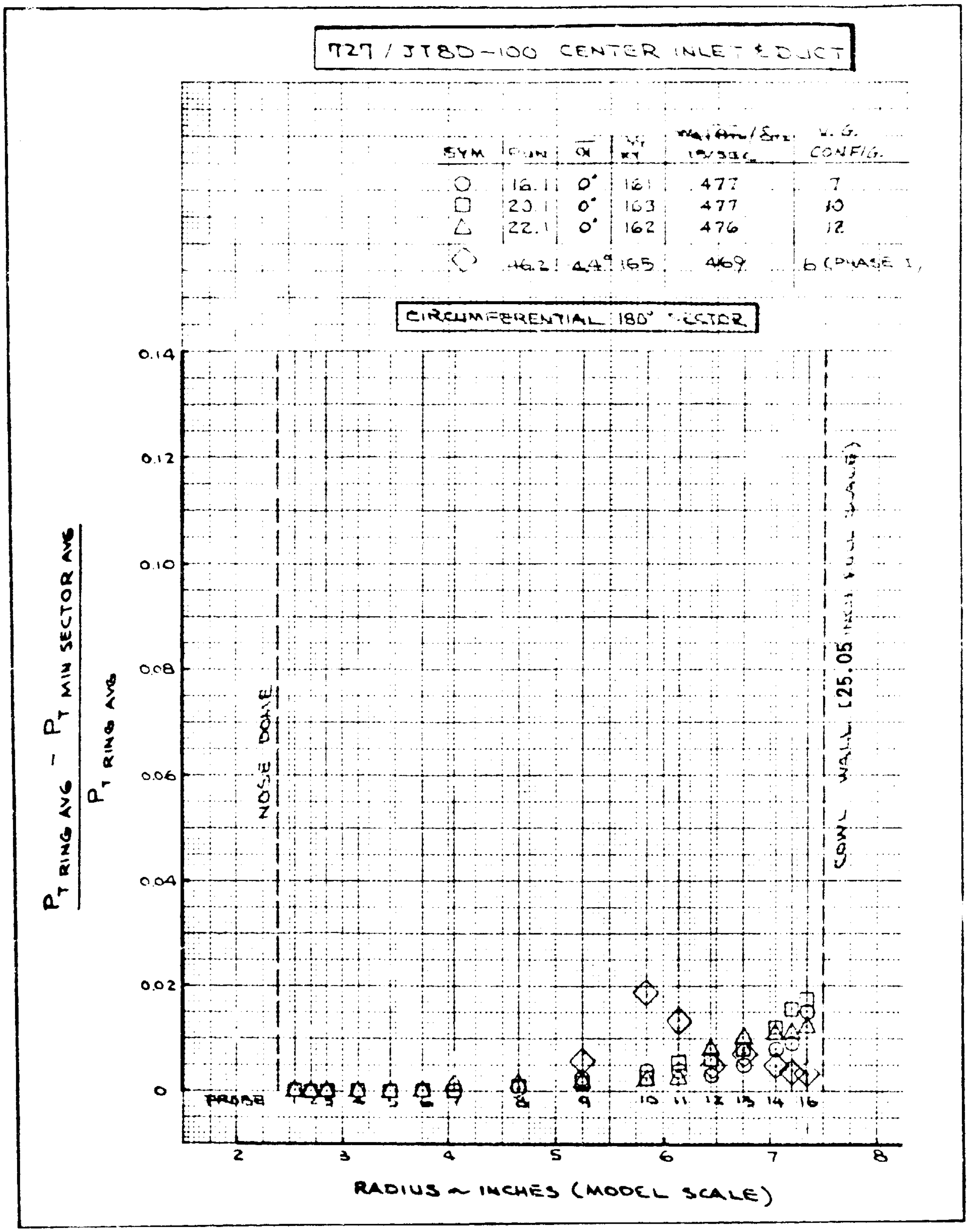

FIGURE 17. - 160-KNOT STEADY-STATE 180°-SECTOR CIRCUMFERENTIAL PRESSURE DISTORTION, VORTEX GENERATOR CONFIG. 7, 10 and 12

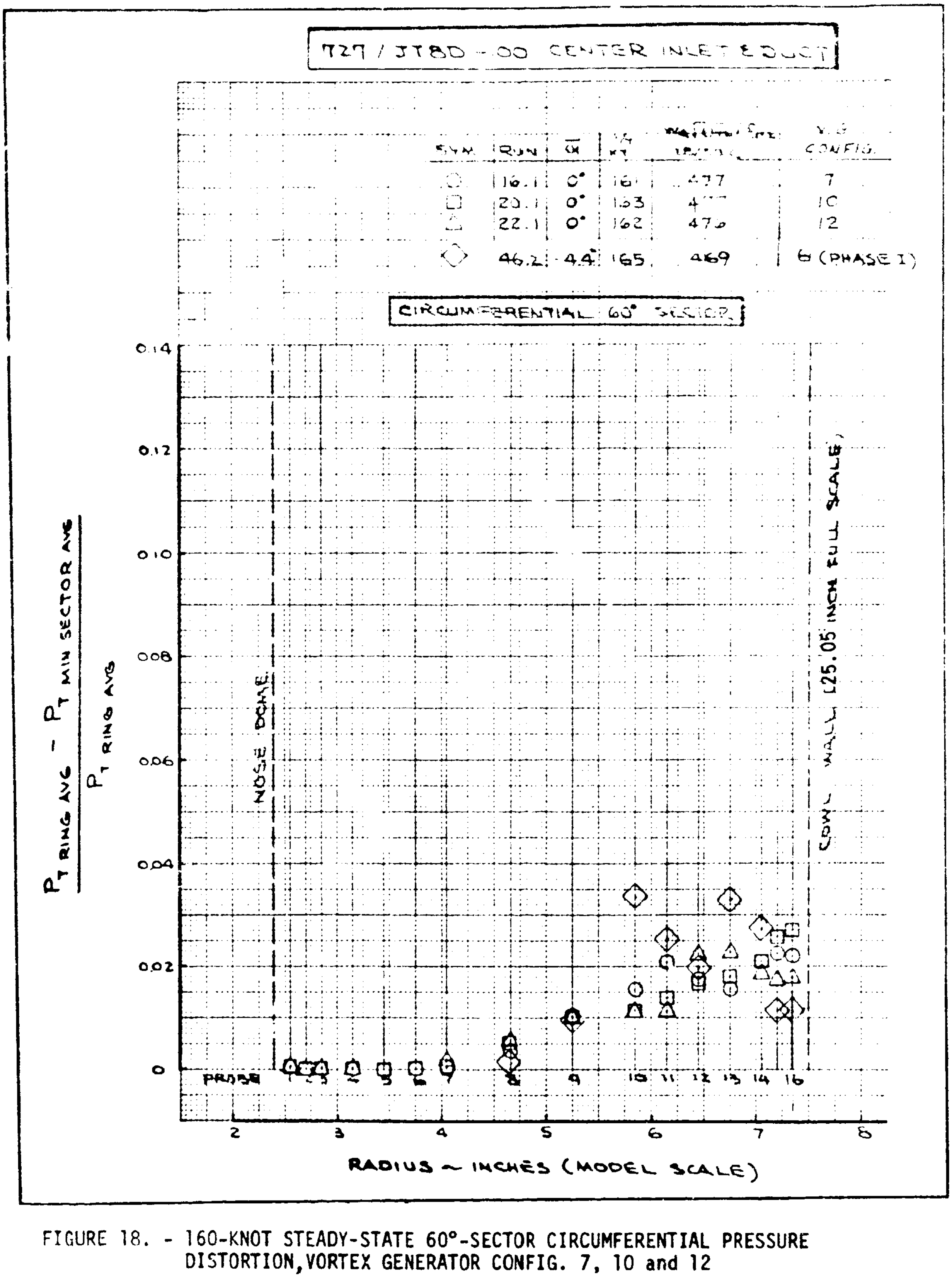

FIGURE 18. - 160-KNOT STEADY-STATE 60°-SECTOR CIRCUMFERENTIAL PRESSURE DISTORTION,VORTEX GENERATOR CONFIG. 7, 10 and 12

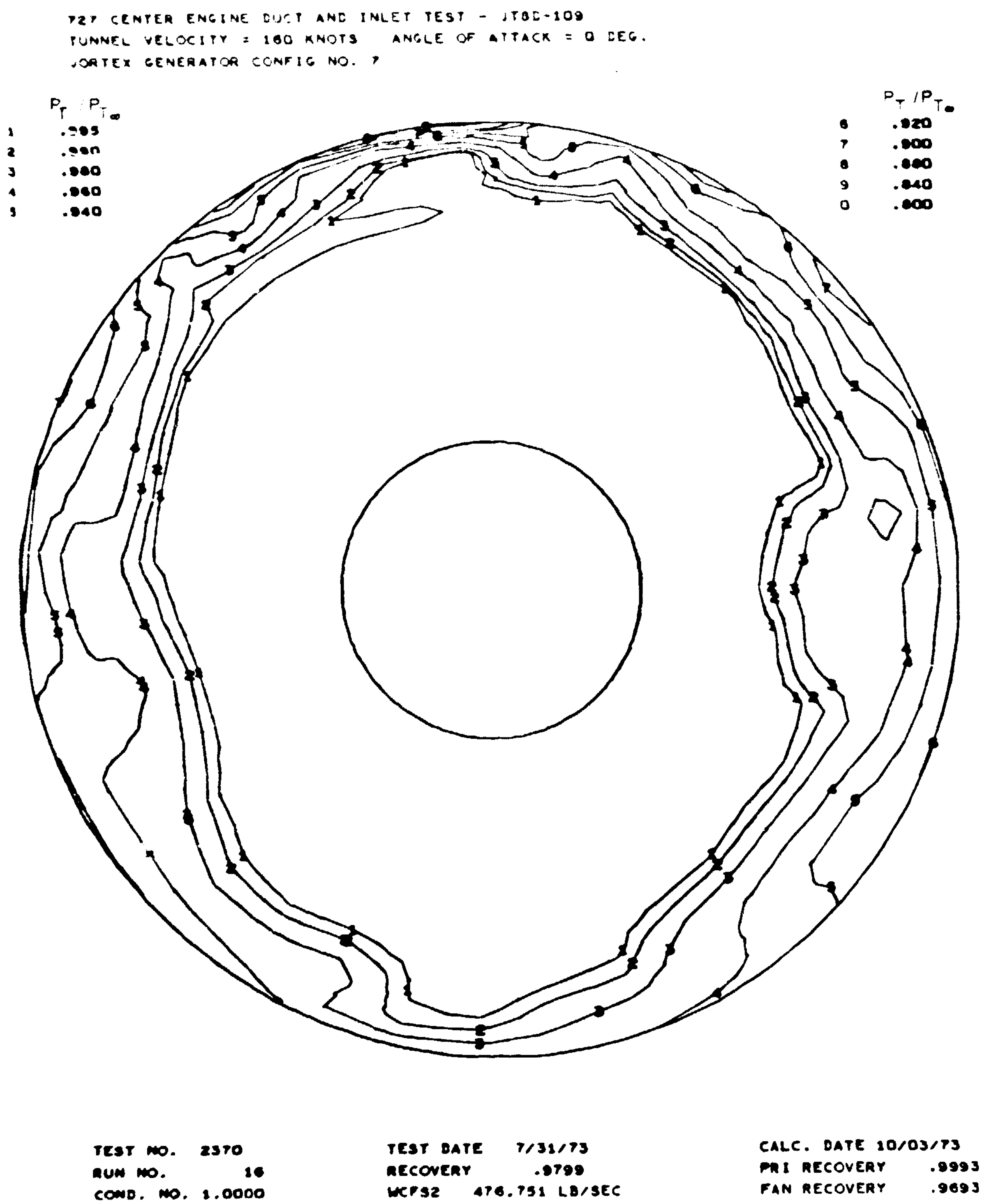

FIGURE 19. - 160-KNOT STEADY-STATE COMPRESSOR FACE PRESSURE RECOVERY MAP, WITH VORTEX GENERATOR CONFIG. 7

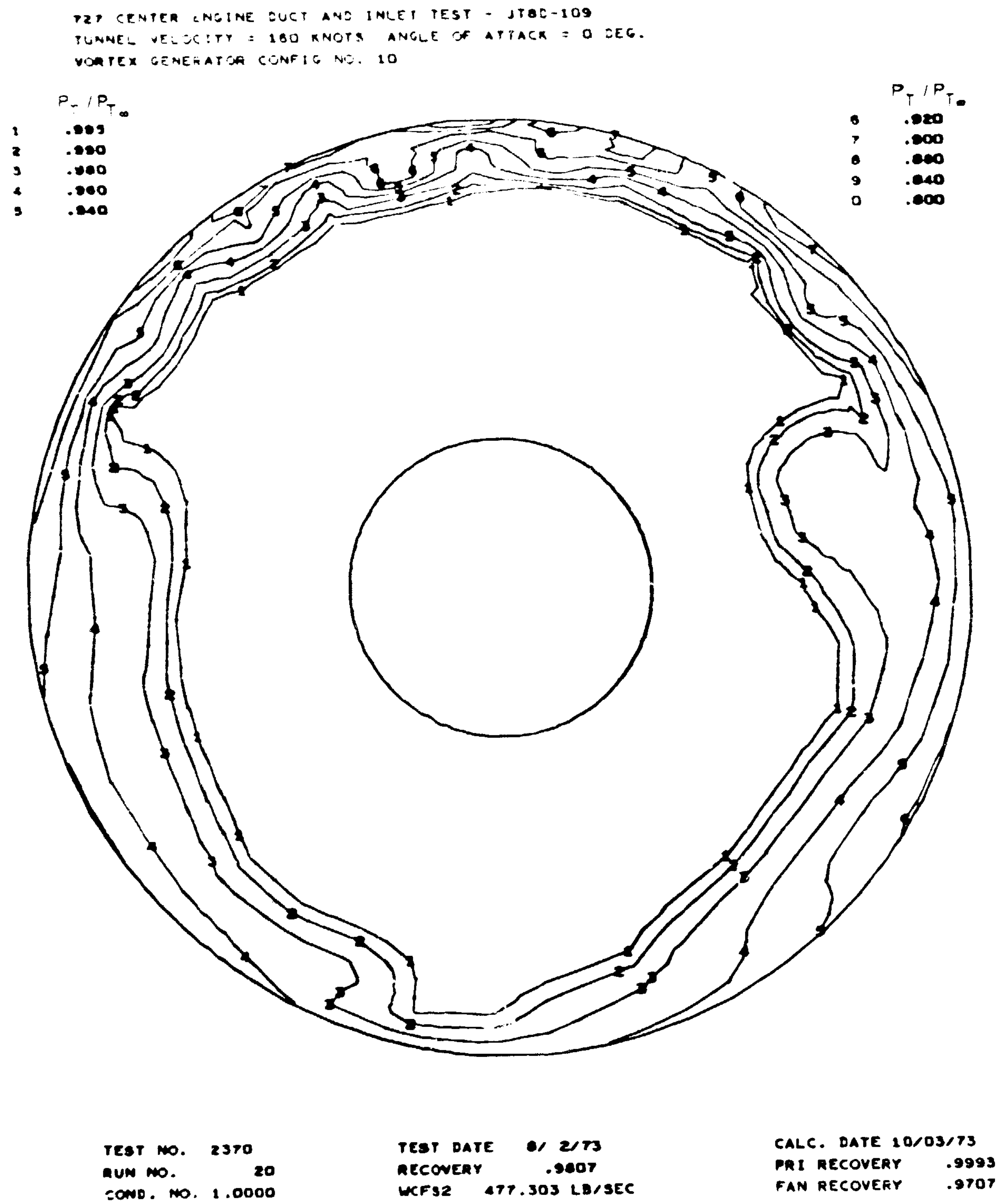

FIGURE 20. - 160-KNOT STEADY-STATE COMPRESSOR FACE PRESSURE RECOVERY MAP, WITH VORTEX GENERATOR CONFIG. 10

727 CENTER ENGINE DUCT AND INLET TEST - J780-103
TUNNEL VELOCITY = 160 KNOTS   ANGLE OF ATTACK = 0 DEG.
VORTEX GENERATOR CONFIG NO. 12

	$P_T/P_{T\infty}$		$P_T/P_{T\infty}$
1	.995	6	.920
2	.990	7	.900
3	.980	8	.880
4	.960	9	.840
5	.940	0	.800

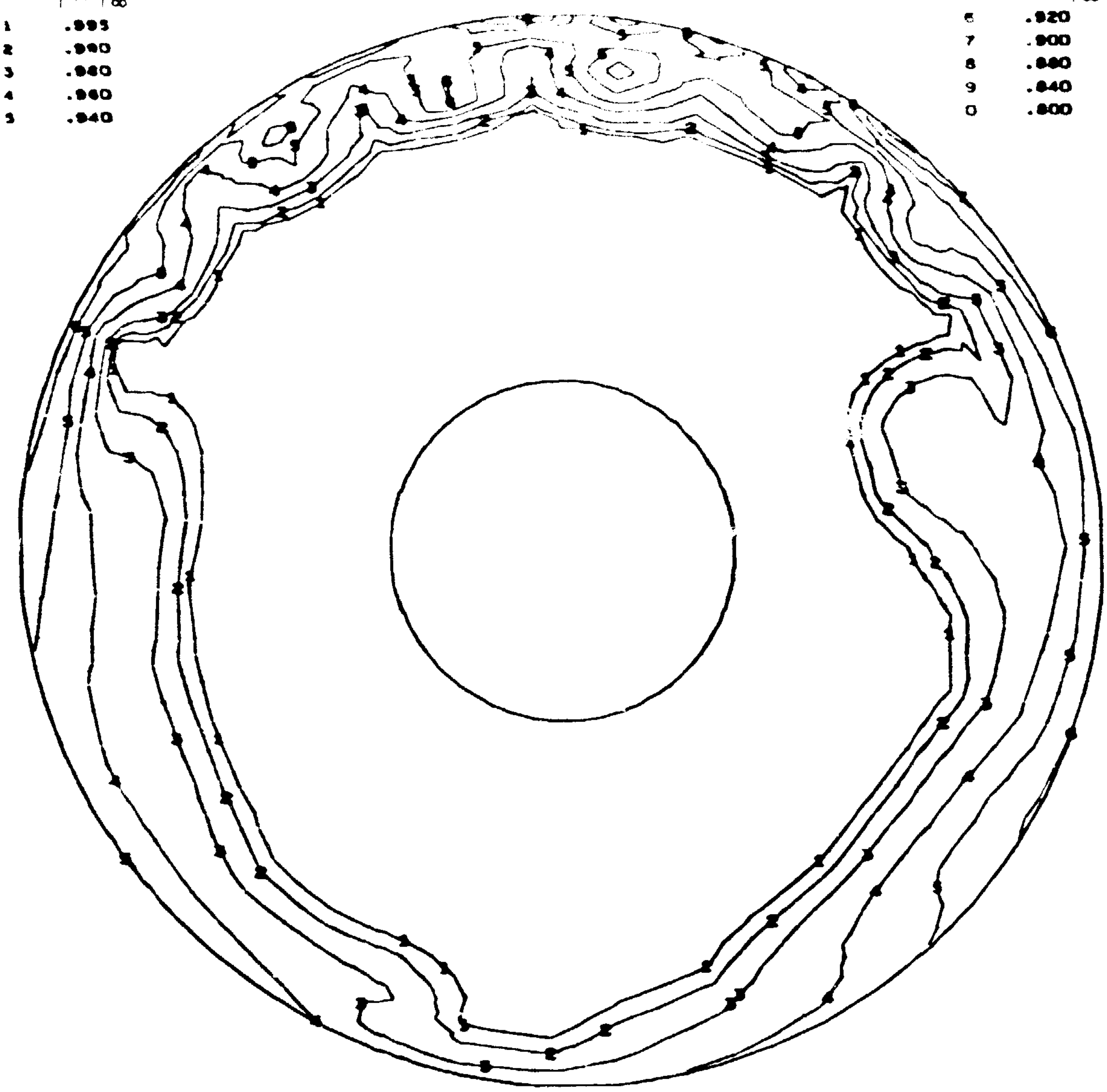

TEST NO.	2370	TEST DATE	8/ 3/73	CALC. DATE	10/03/73
RUN NO.	22	RECOVERY	.9805	PRI RECOVERY	1.0000
COND. NO.	1.0000	WCFS2	476.038 LB/SEC	FAN RECOVERY	.9699

FIGURE 21. - 160-KNOT STEADY-STATE COMPRESSOR FACE PRESSURE RECOVERY MAP, WITH VORTEX GENERATOR CONFIG. 12

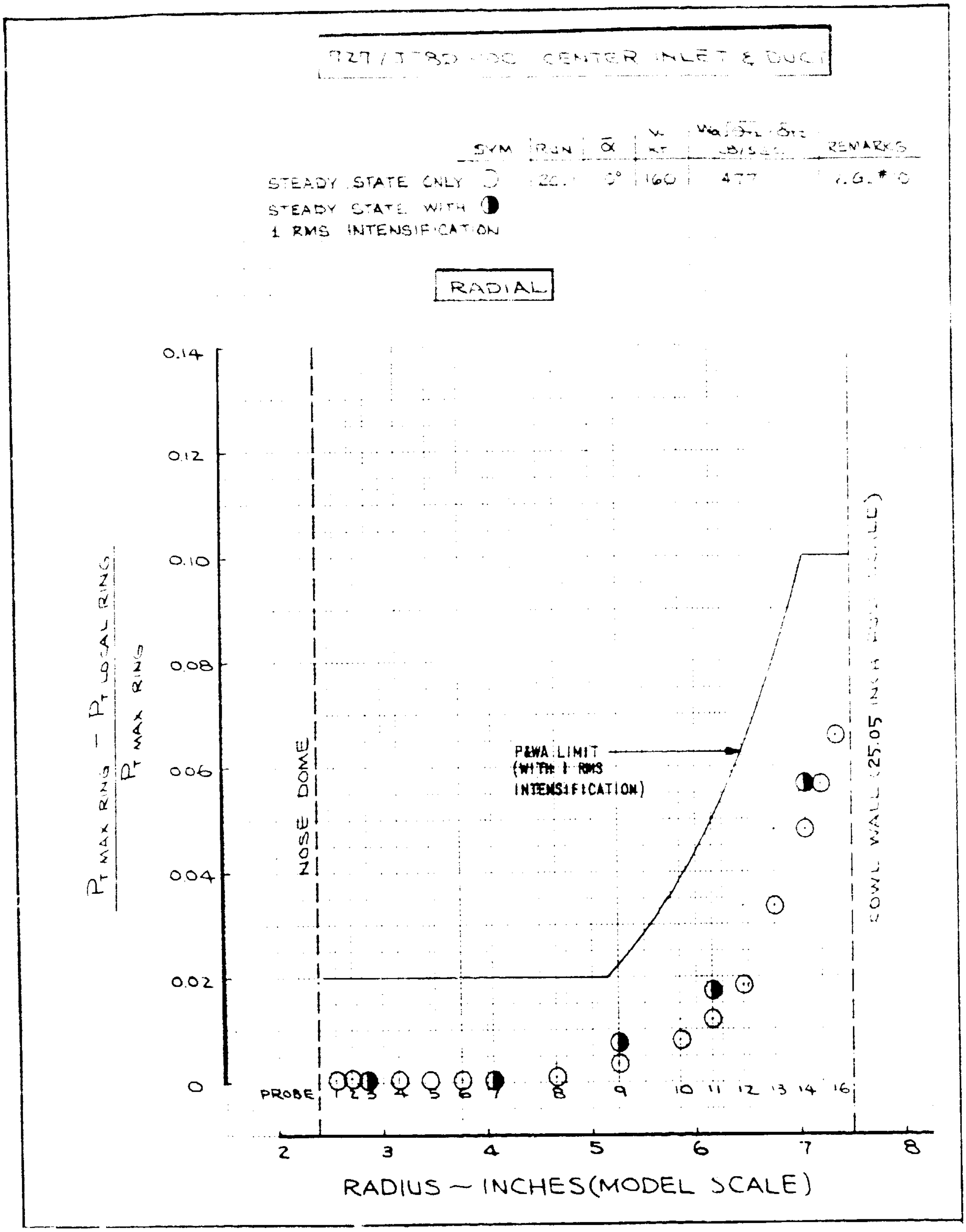

FIGURE 22. - 160-KNOT (P&WA METHOD) RADIAL PRESSURE DISTORTION, WITH VORTEX GENERATOR CONFIG. 10

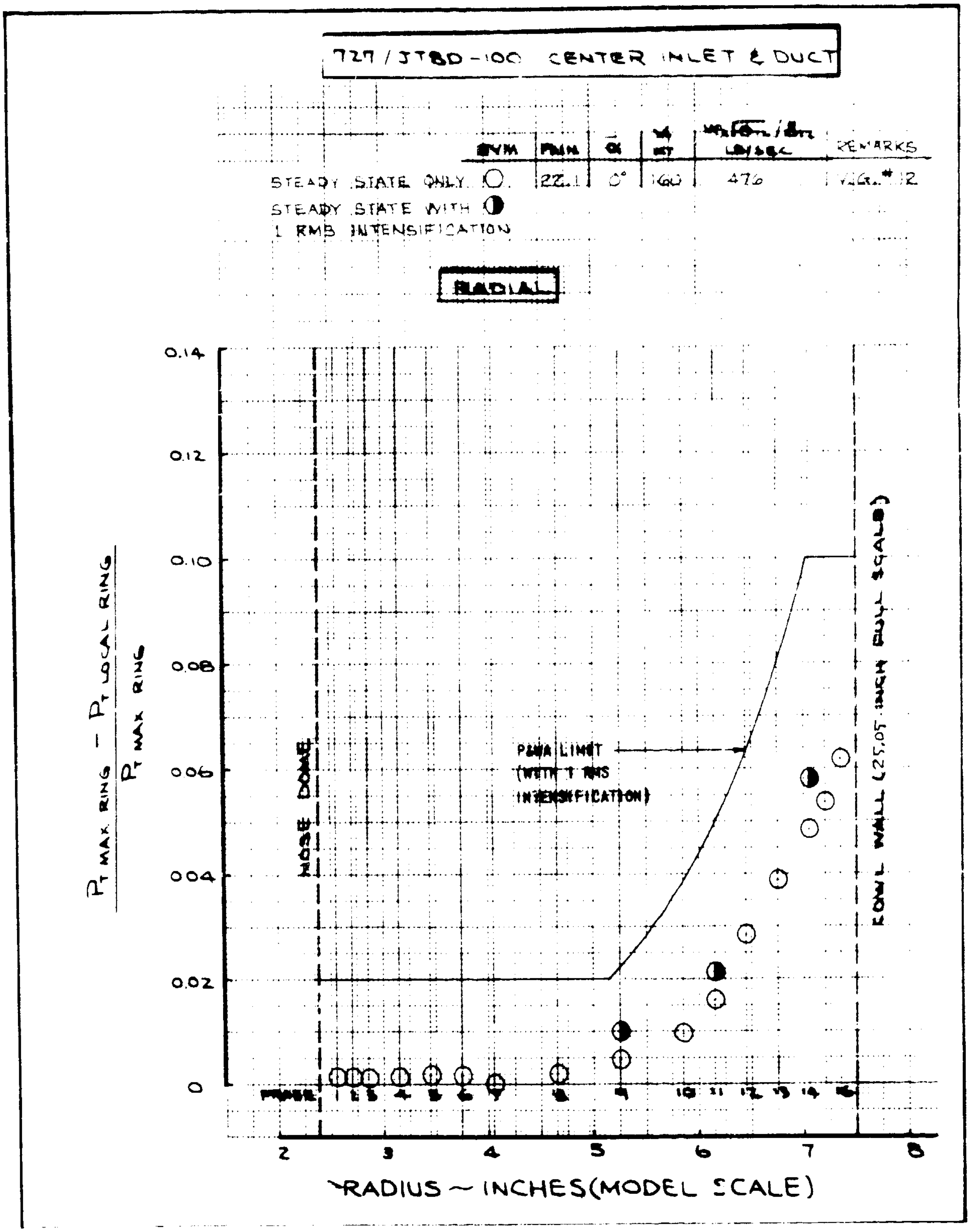

FIGURE 23. - 160 KNOT (P&WA METHOD) RADIAL PRESSURE DISTORTION, WITH VORTEX GENERATOR CONFIG. 12

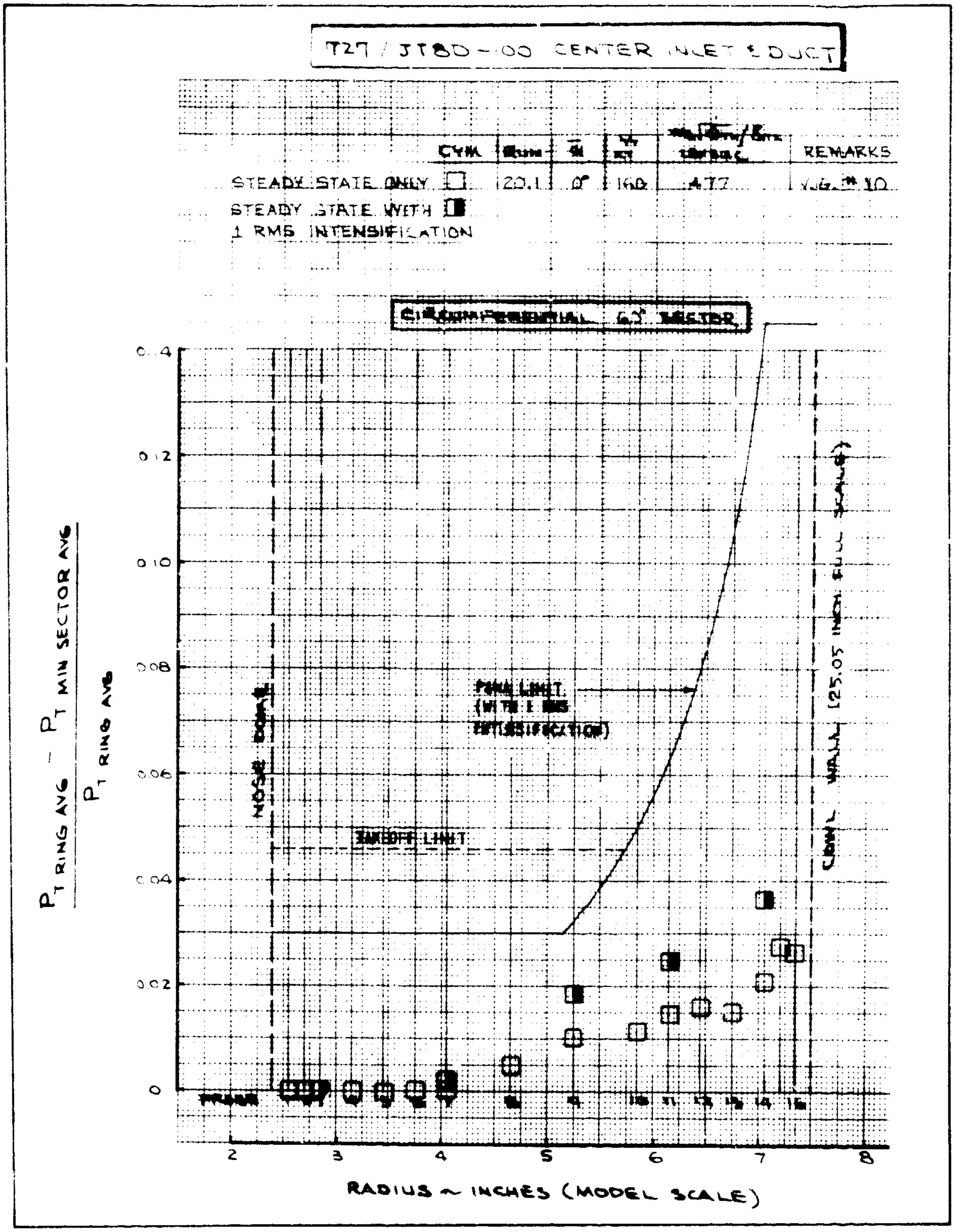

FIGURE 24. - 160-KNOT (P&WA METHOD) 60°-SECTOR CIRCUMFERENTIAL PRESSURE DISTORTION, WITH VORTEX GENERATOR CONFIG. 10

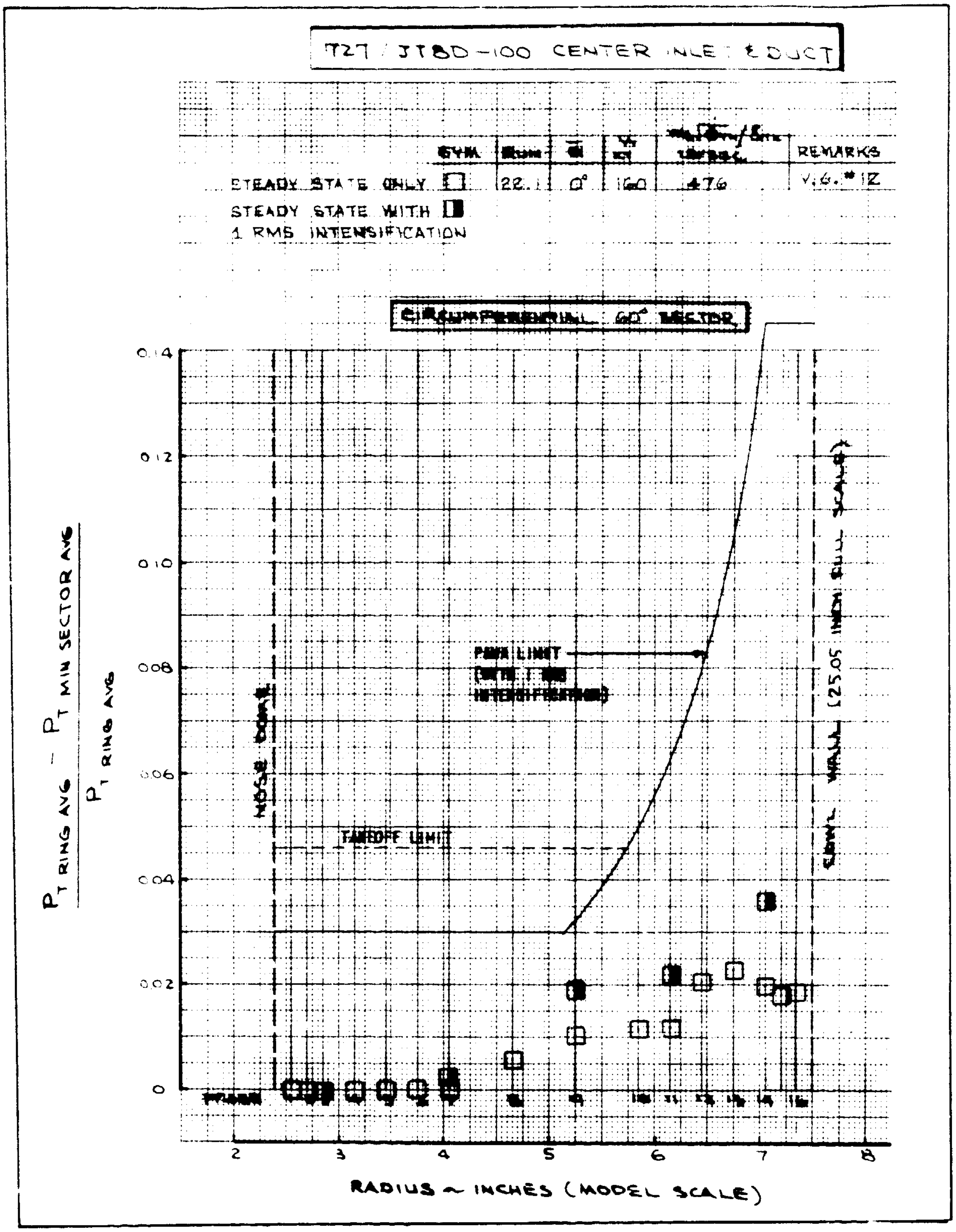

FIGURE 25. - 160-KNOT (P&WA METHOD) 60°-SECTOR CIRCUMFERENTIAL PRESSURE DISTORTION,WITH VORTEX GENERATOR CONFIG. 12

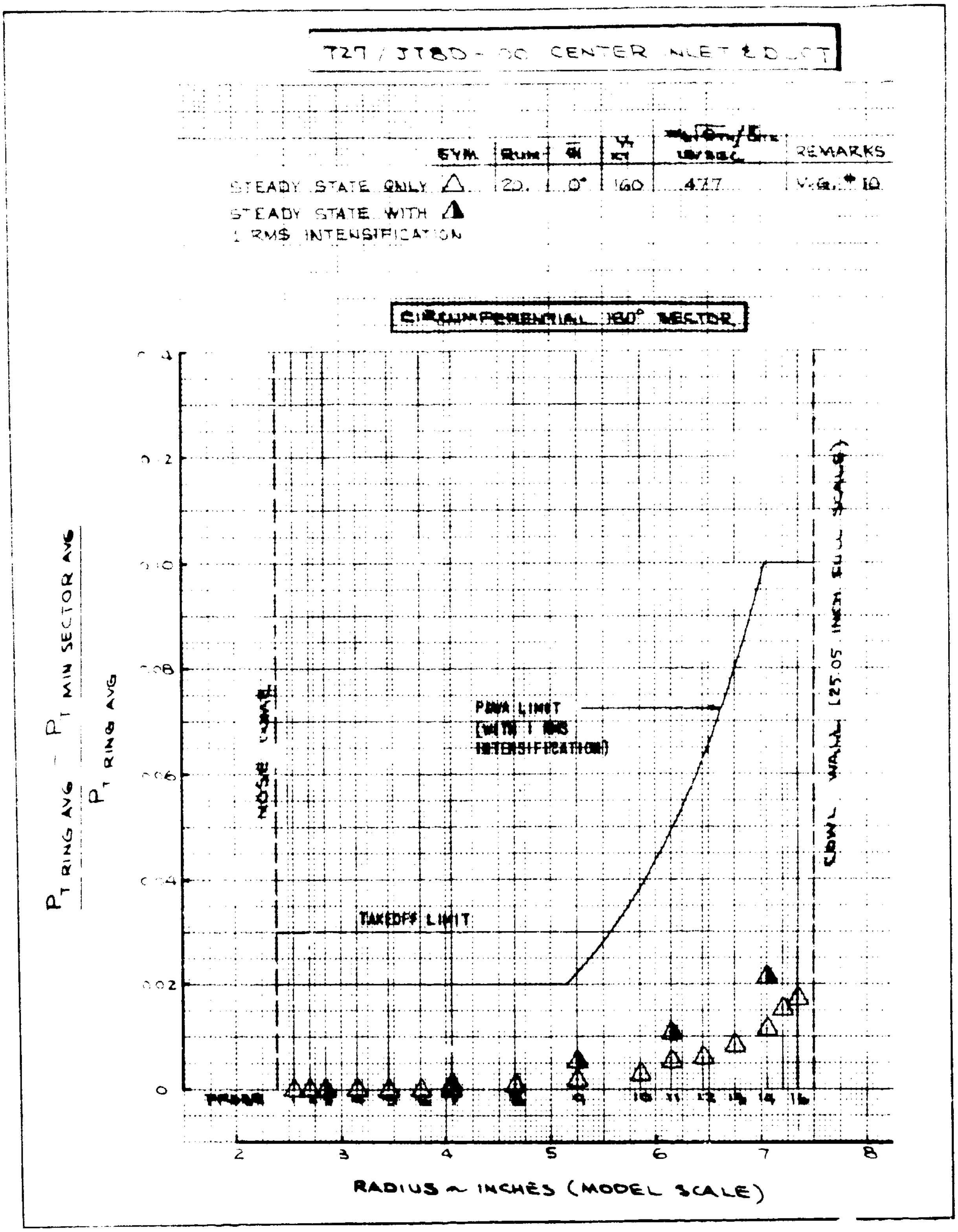

FIGURE 26. - 160-KNOT (P&WA METHOD) 180° SECTOR CIRCUMFERENTIAL PRESSURE DISTORTION, WITH VORTEX GENERATOR CONFIG. 10

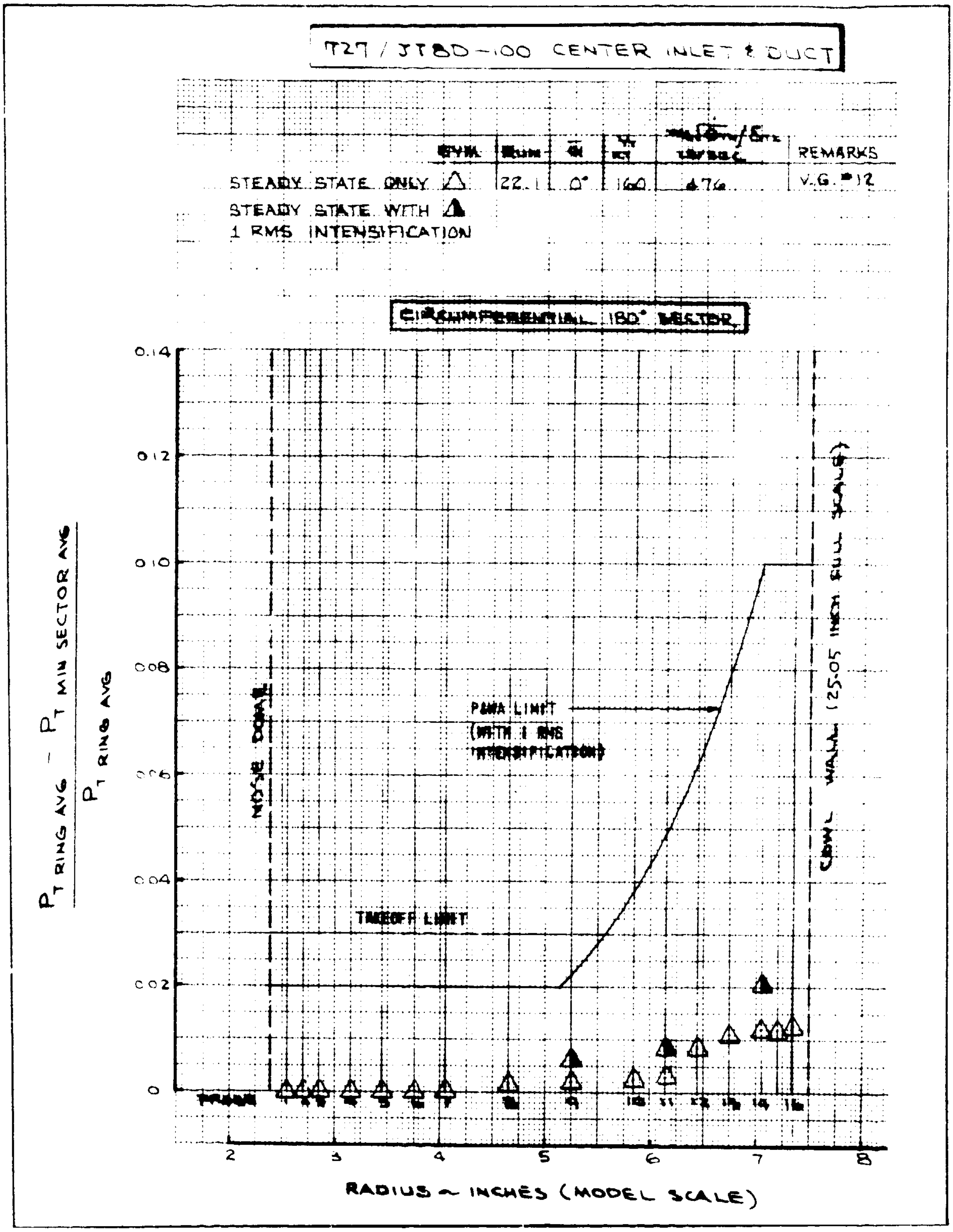

FIGURE 27. - 160-KNOT (P&WA METHOD) 180°-SECTOR CIRCUMFERENTIAL PRESSURE DISTORTION,WITH VORTEX GENERATOR CONFIG. 12

727 CENTER ENGINE DUCT AND INLET TEST - JT8D-109
TUNNEL VELOCITY = 160 KNOTS ANGLE OF ATTACK = 0 DEG.
VORTEX GENERATOR CONFIG NO. 14

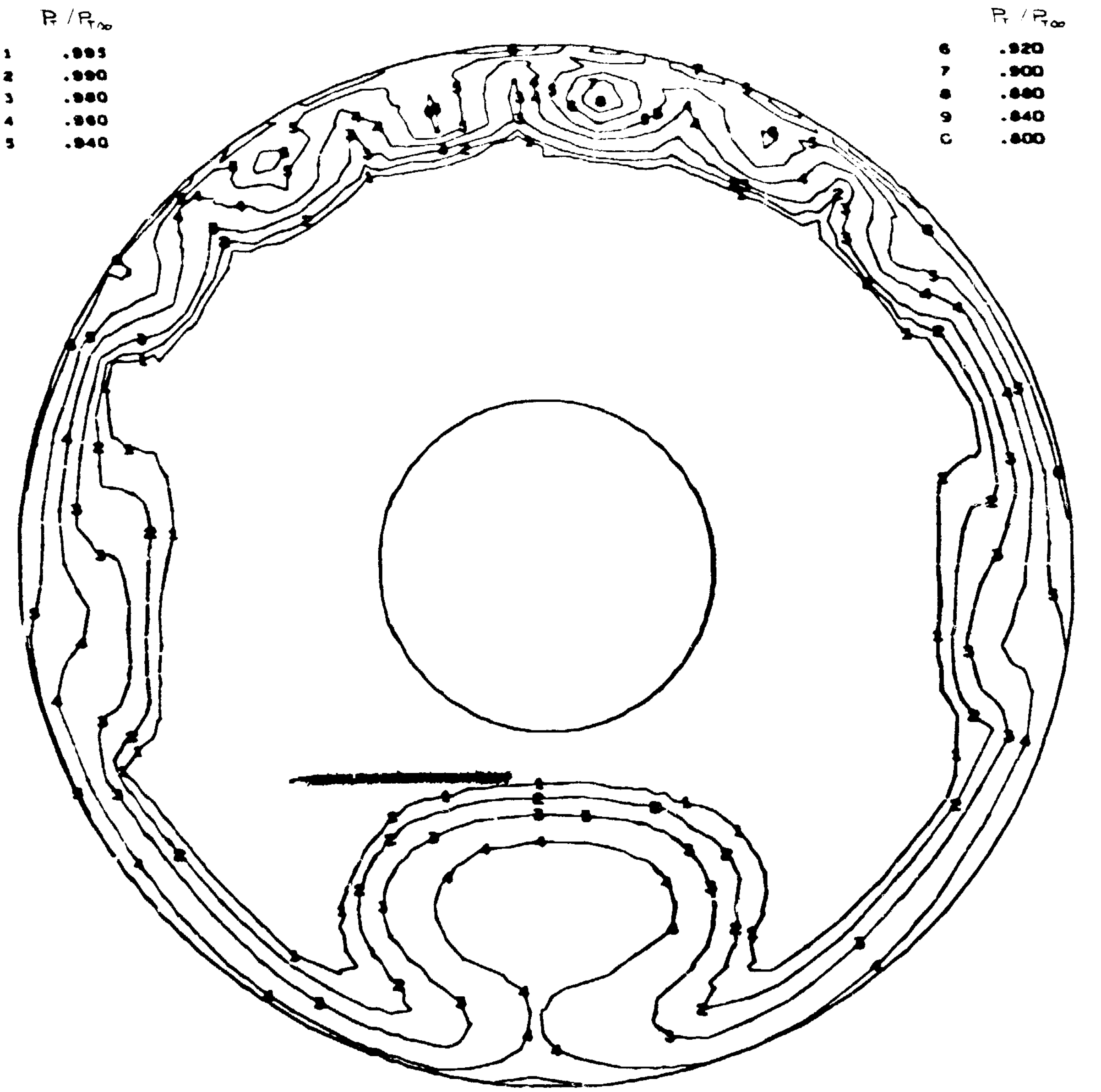

TEST NO. 2370	TEST DATE 8/ 6/73	CALC. DATE 10/03/73
RUN NO. 24	RECOVERY .9810	PRI RECOVERY .9963
COND. NO. 1.0000	WCFS2 476.697 LB/SEC	FAN RECOVERY .9727

FIGURE 28. - 160-KNOT STEADY-STATE COMPRESSOR FACE PRESSURE RECOVERY MAP, WITH BOUNDARY LAYER FENCES (CONFIG. 14)

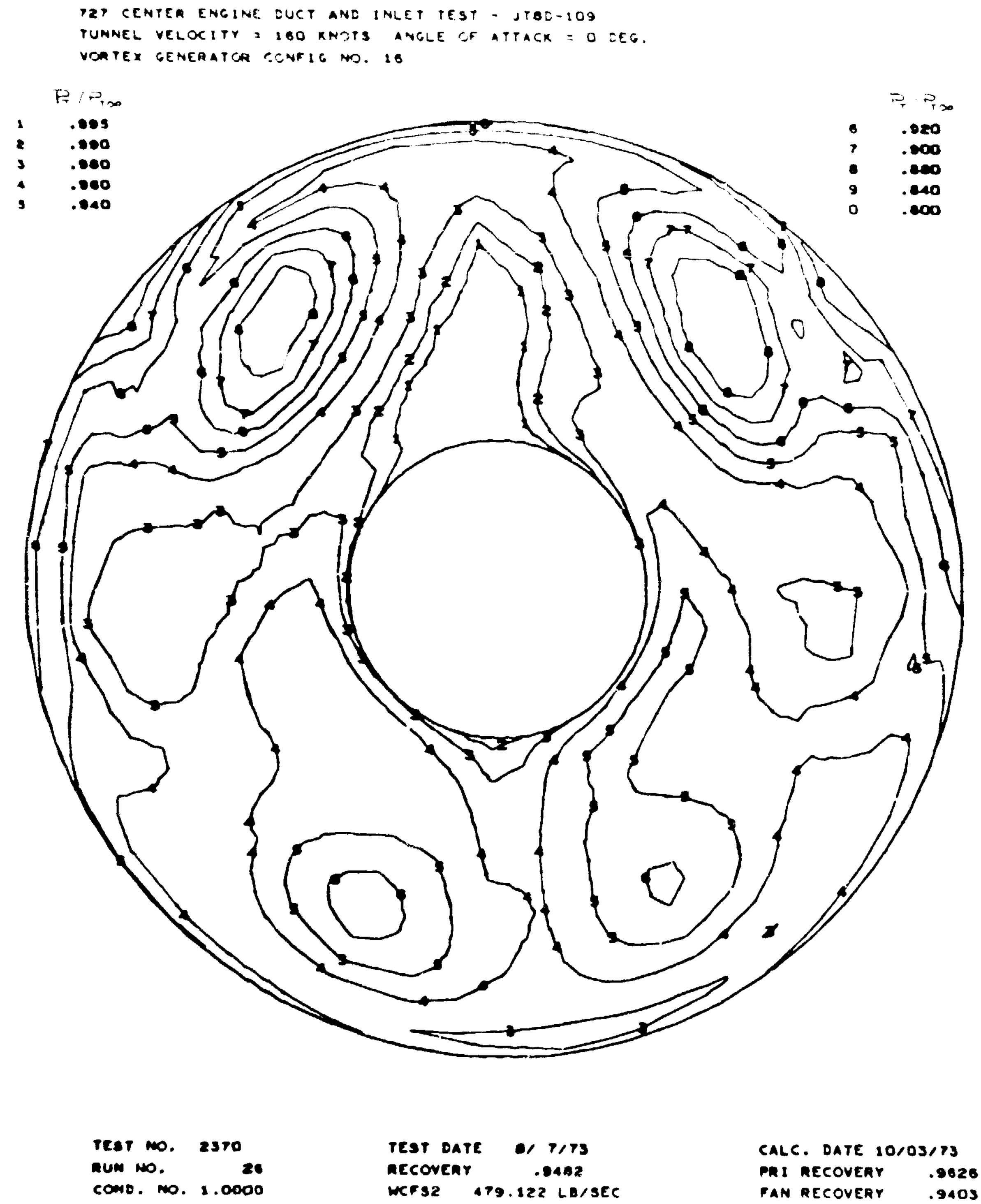

FIGURE 29. - 160-KNOT STEADY-STATE COMPRESSOR FACE PRESSURE RECOVERY MAP, WITH TURNING VANES (CONFIG. 16)

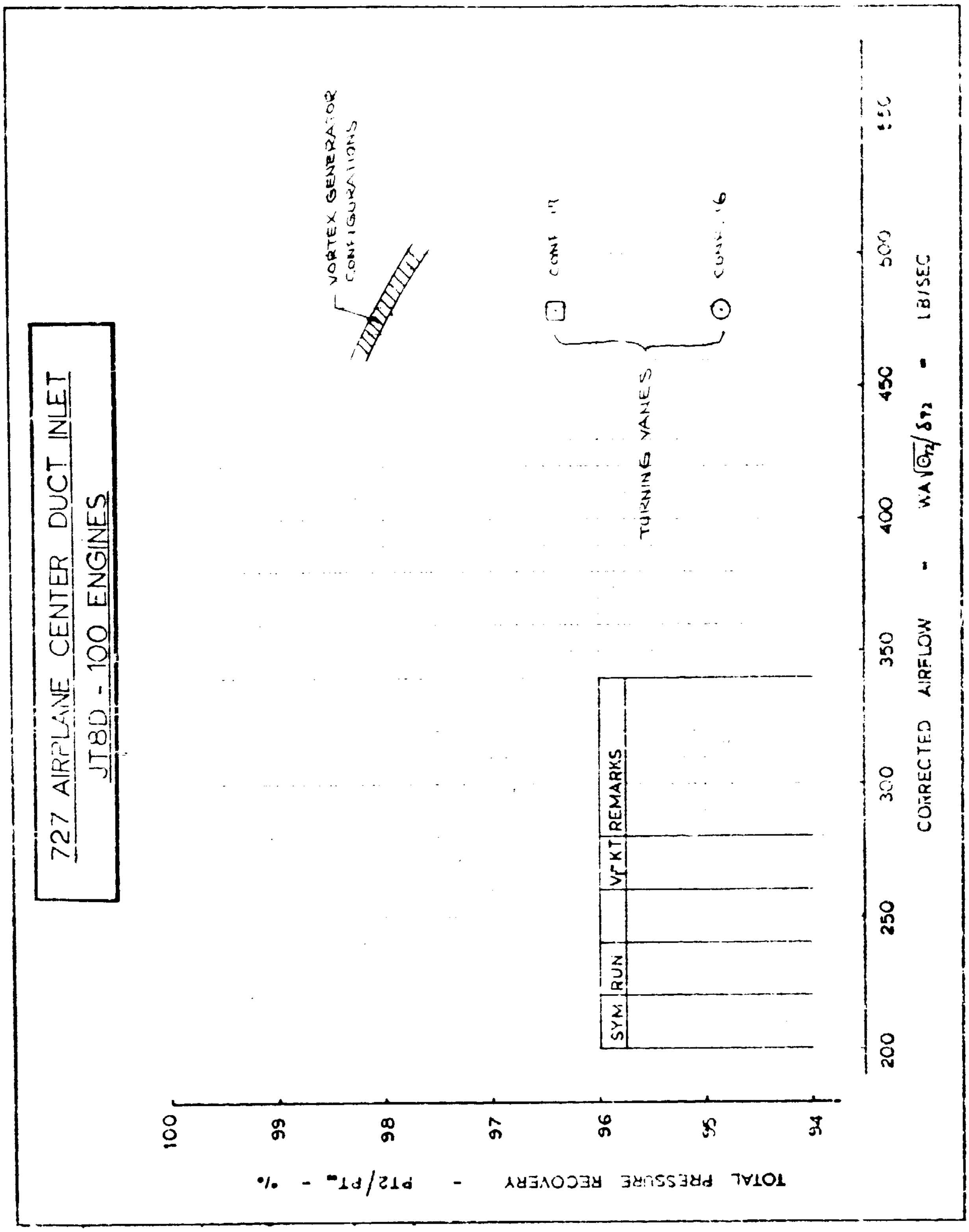

FIGURE 30. - TOTAL PRESSURE RECOVERY VS. AIRFLOW, TURNING VANES (CONFIGURATIONS 16 AND 17)

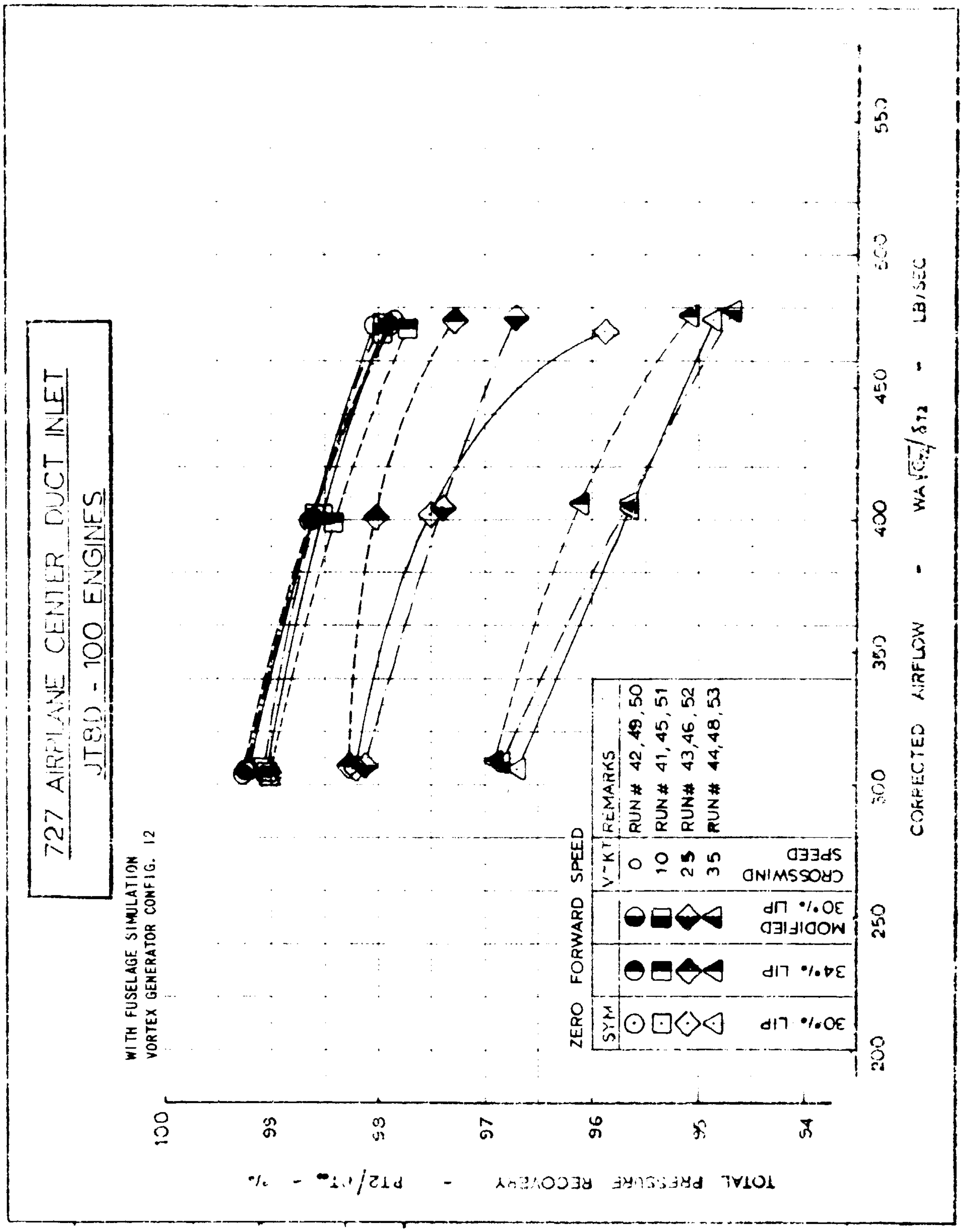

FIGURE 31. - CROSSWIND PRESSURE RECOVERY, WITH VORTEX GENERATOR CONFIG. 12 (LIP CONTOUR STUDY)

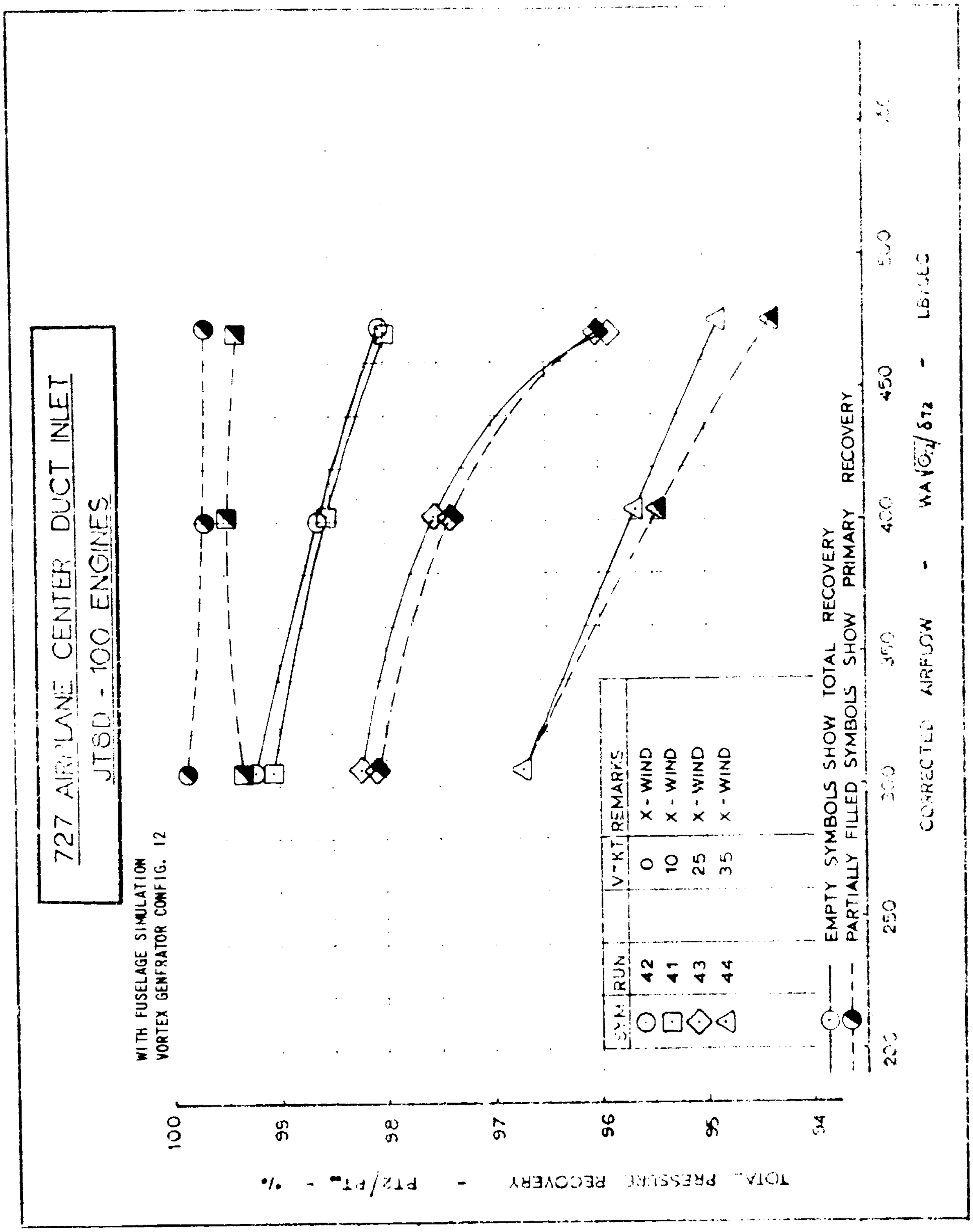

FIGURE 32. - CROSSWIND PRIMARY AND TOTAL PRESSURE RECOVERIES, WITH VORTEX GENERATOR CONFIG. 12 (30% LIP)

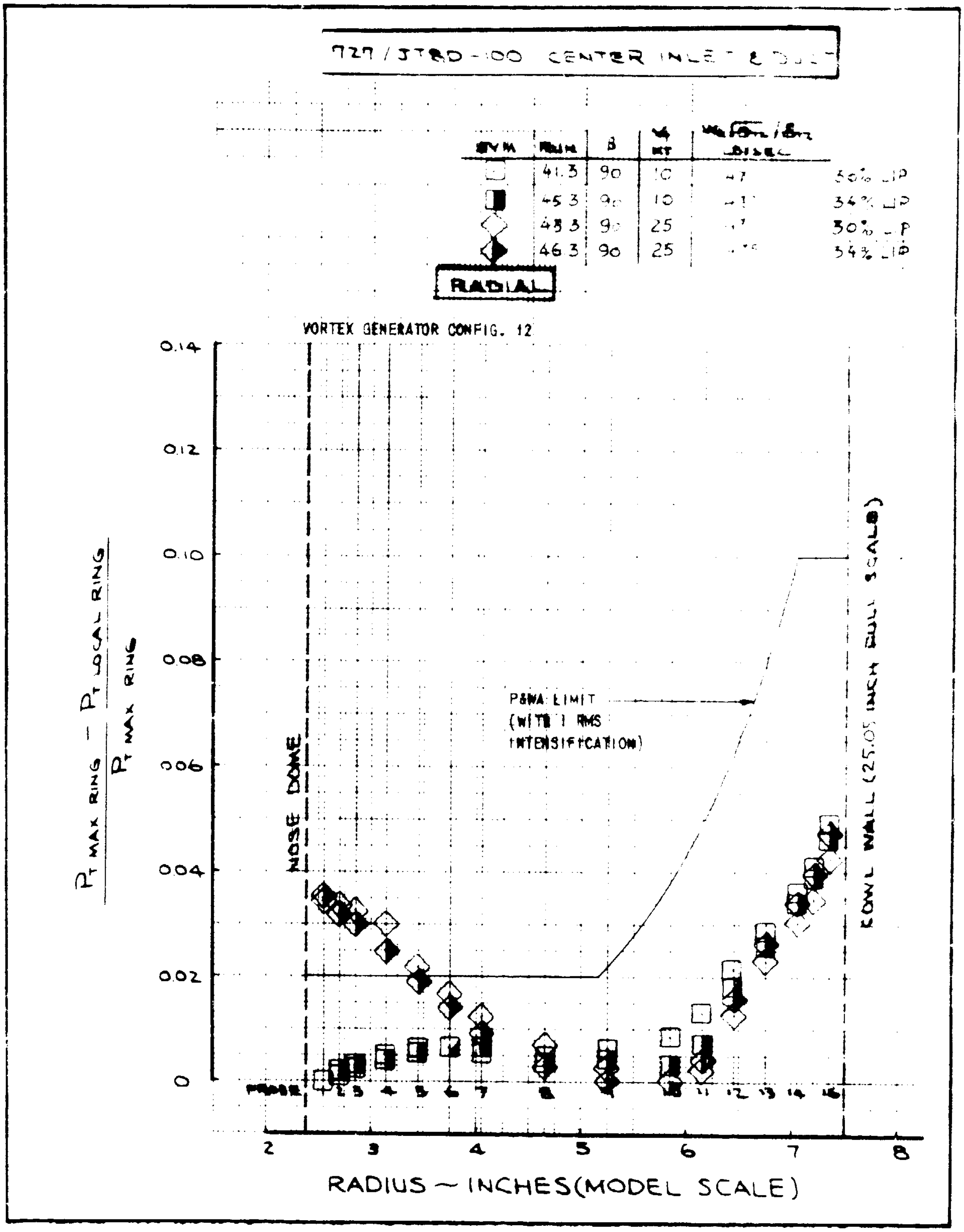

FIGURE 33. - CROSSWIND STEADY STATE RADIAL PRESSURE DISTORTION, WITH VORTEX GENERATOR CONFIG. 12 (30% vs. 34% LIP)

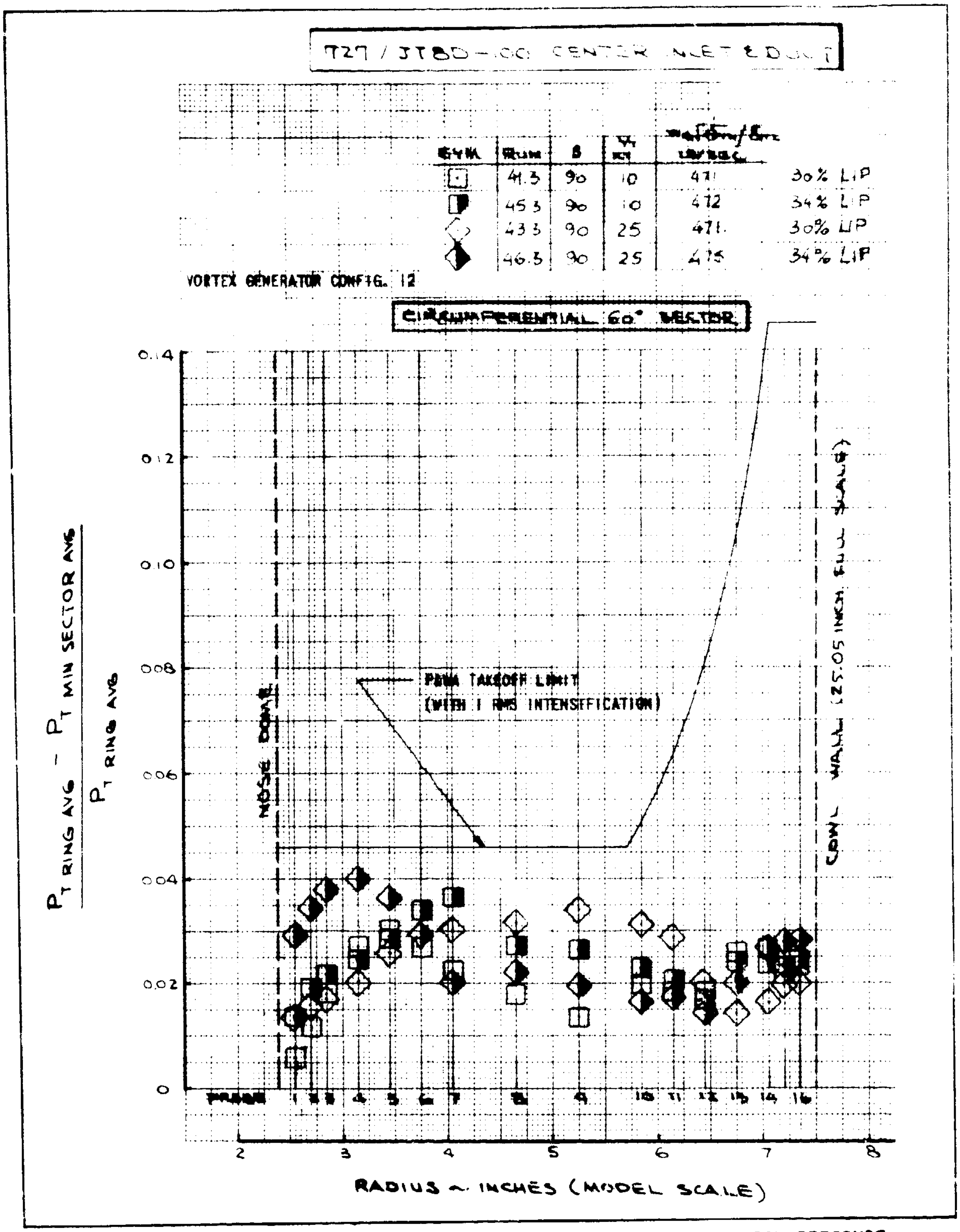

FIGURE 34. - CROSSWIND STEADY-STATE 60°-SECTOR CIRCUMFERENTIAL PRESSURE DISTORTION, WITH VORTEX GENERATOR CONFIG. 12 (30% vs. 34% LIP)

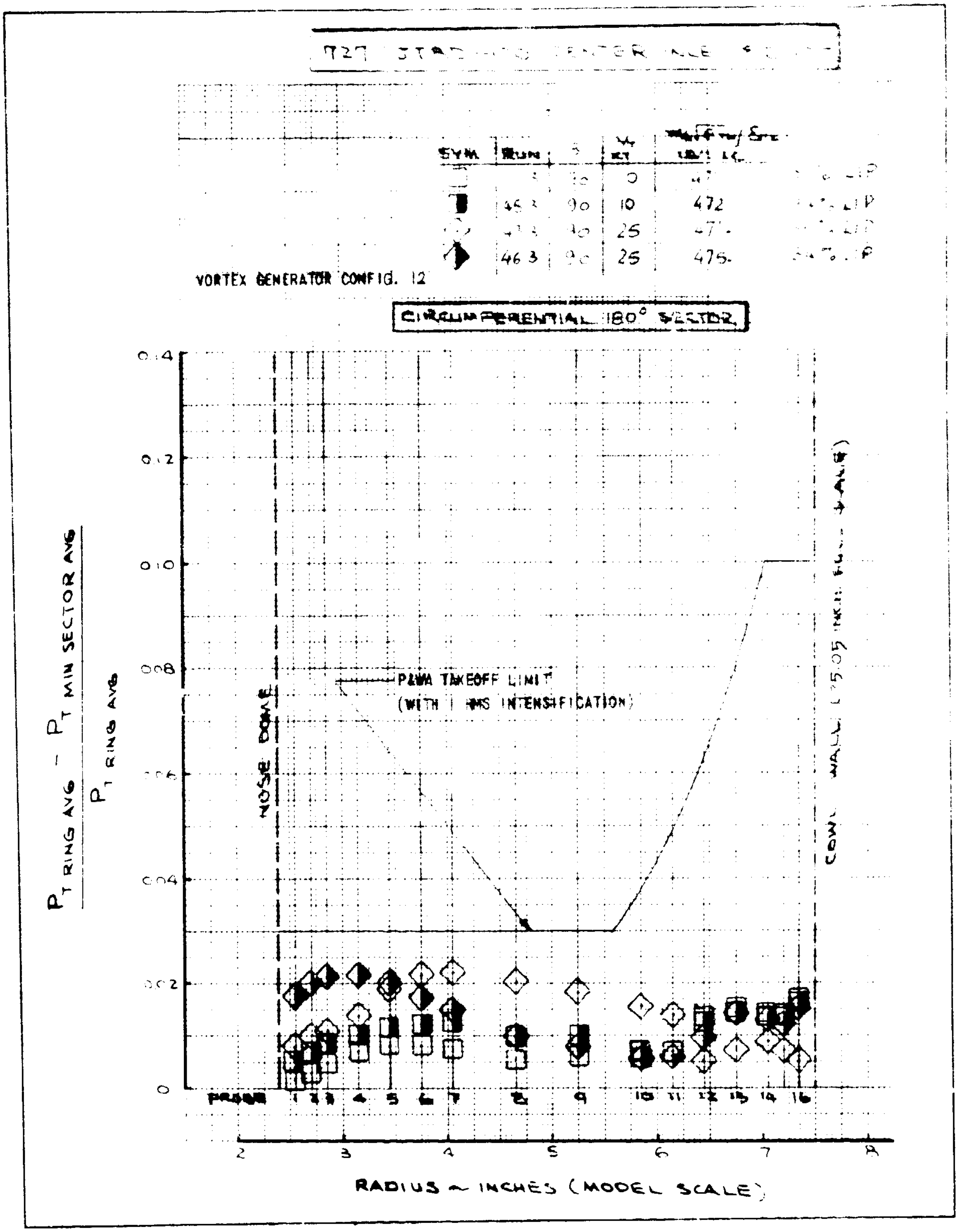

FIGURE 35. - CROSSWIND STEADY-STATE 180°-SECTOR CIRCUMFERENTIAL PRESSURE DISTORTION, WITH VORTEX GENERATOR CONFIG. 12 (30% vs. 34% LIP)

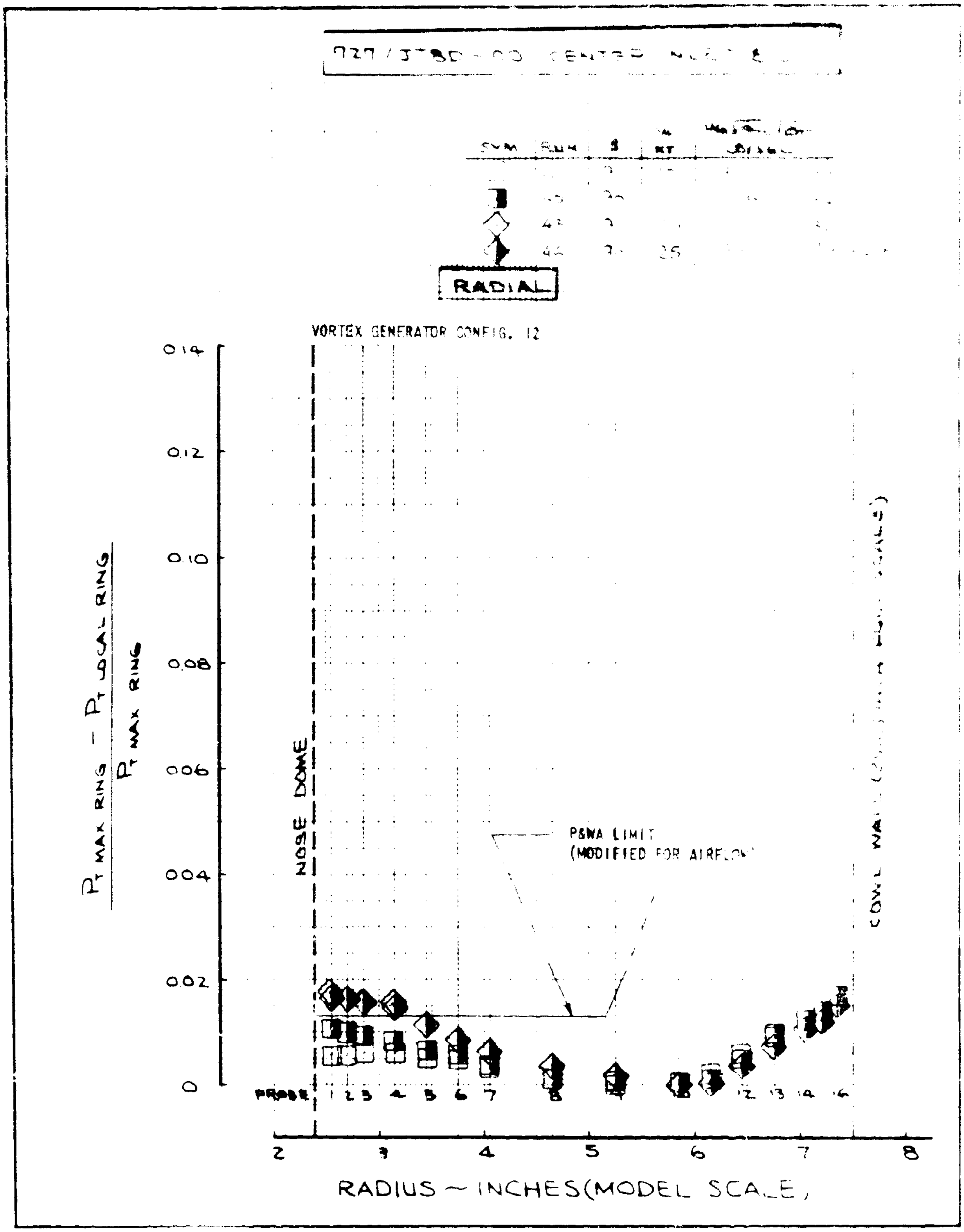

FIGURE 36. - CROSSWIND STEADY-STATE RADIAL PRESSURE DISTORTION, WITH VORTEX GENERATOR CONFIG. 12 AT REDUCED AIRFLOW (30% vs. 34% LIP)

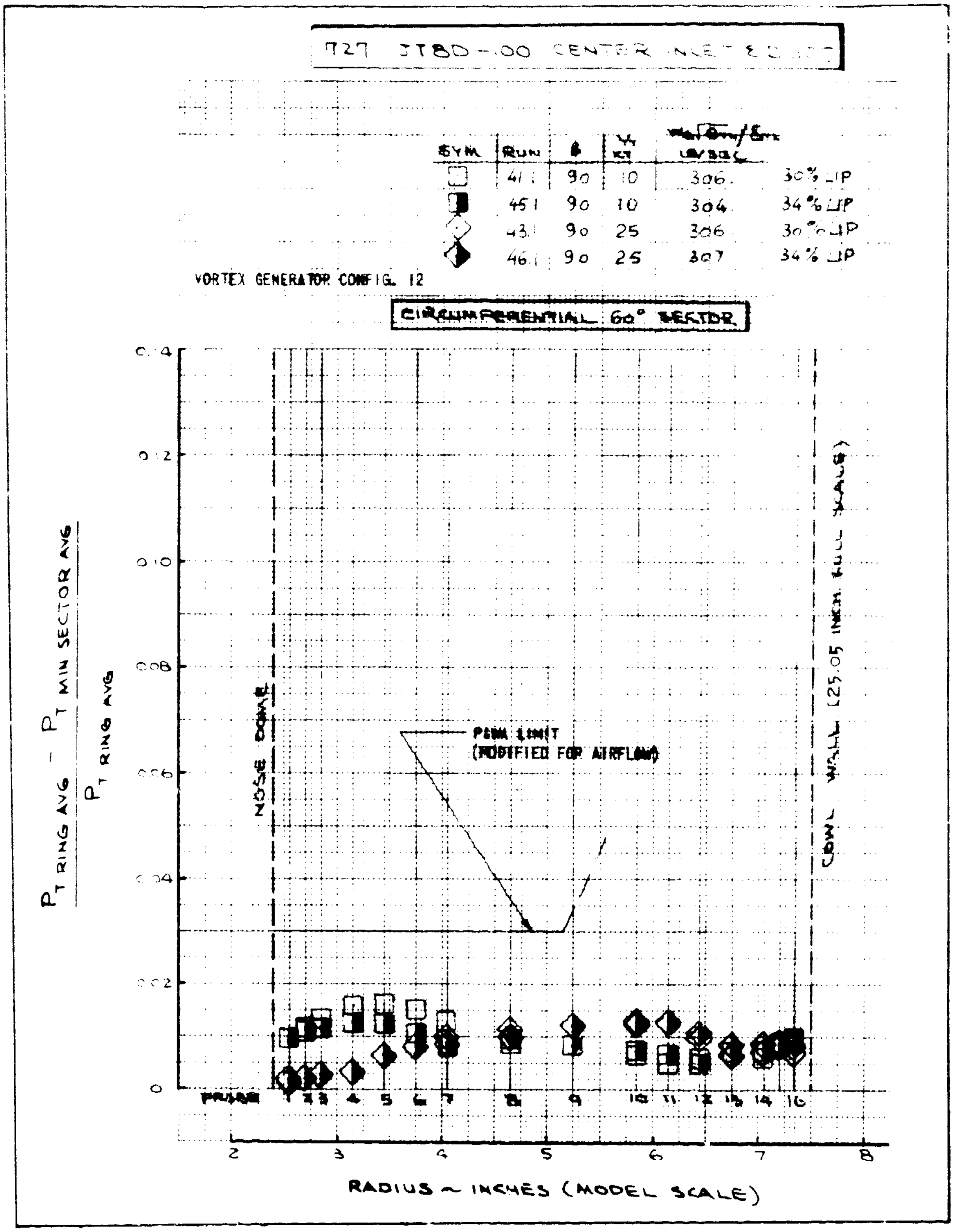

FIGURE 37. - CROSSWIND STEADY-STATE 60°-SECTOR CIRCUMFERENTIAL PRESSURE DISTORTION, WITH VORTEX GENERATOR CONFIG. 12 AT REDUCED AIRFLOW (30% vs. 34% LIP)

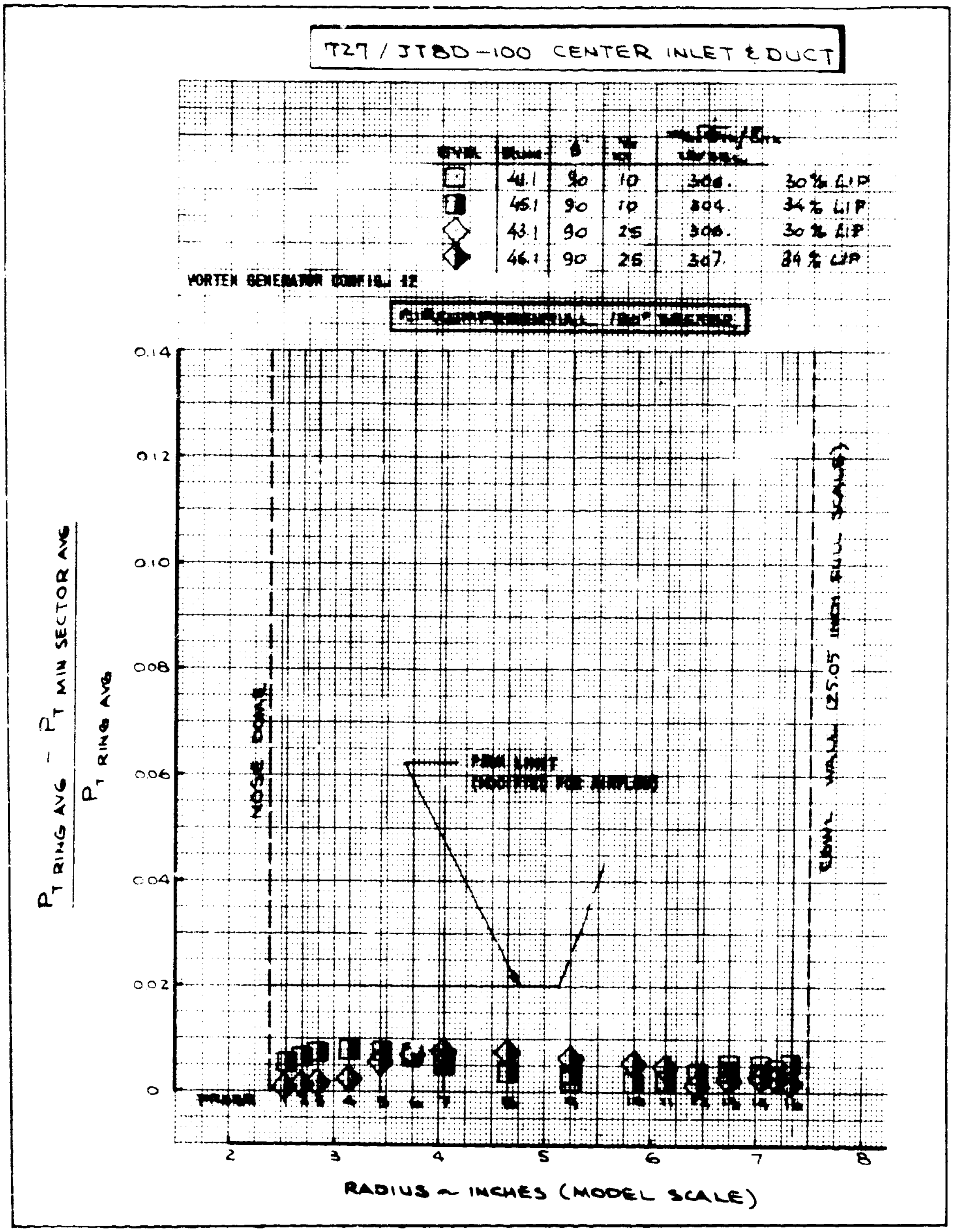

FIGURE 38. - CROSSWIND STEADY-STATE 180°-SECTOR CIRCUMFERENTIAL PRESSURE DISTORTION, WITH VORTEX GENERATOR CONFIG. 12 AT REDUCED AIRFLOW (30% vs. 34% LIP)

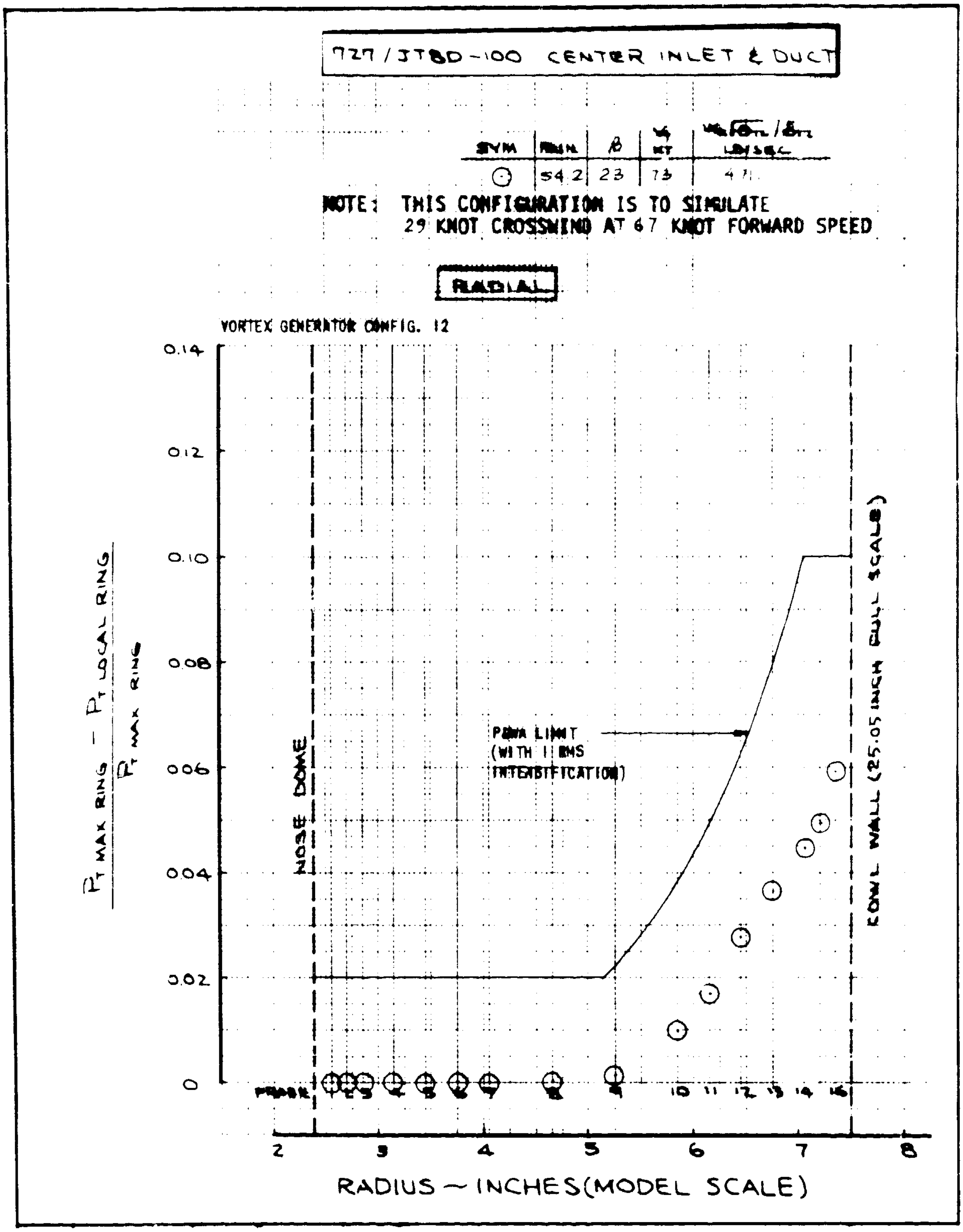

FIGURE 39. - 67-KNOT STEADY-STATE RADIAL PRESSURE DISTORTION, WITH VORTEX GENERATOR CONFIG. 12 AT 23 DEGREE YAW

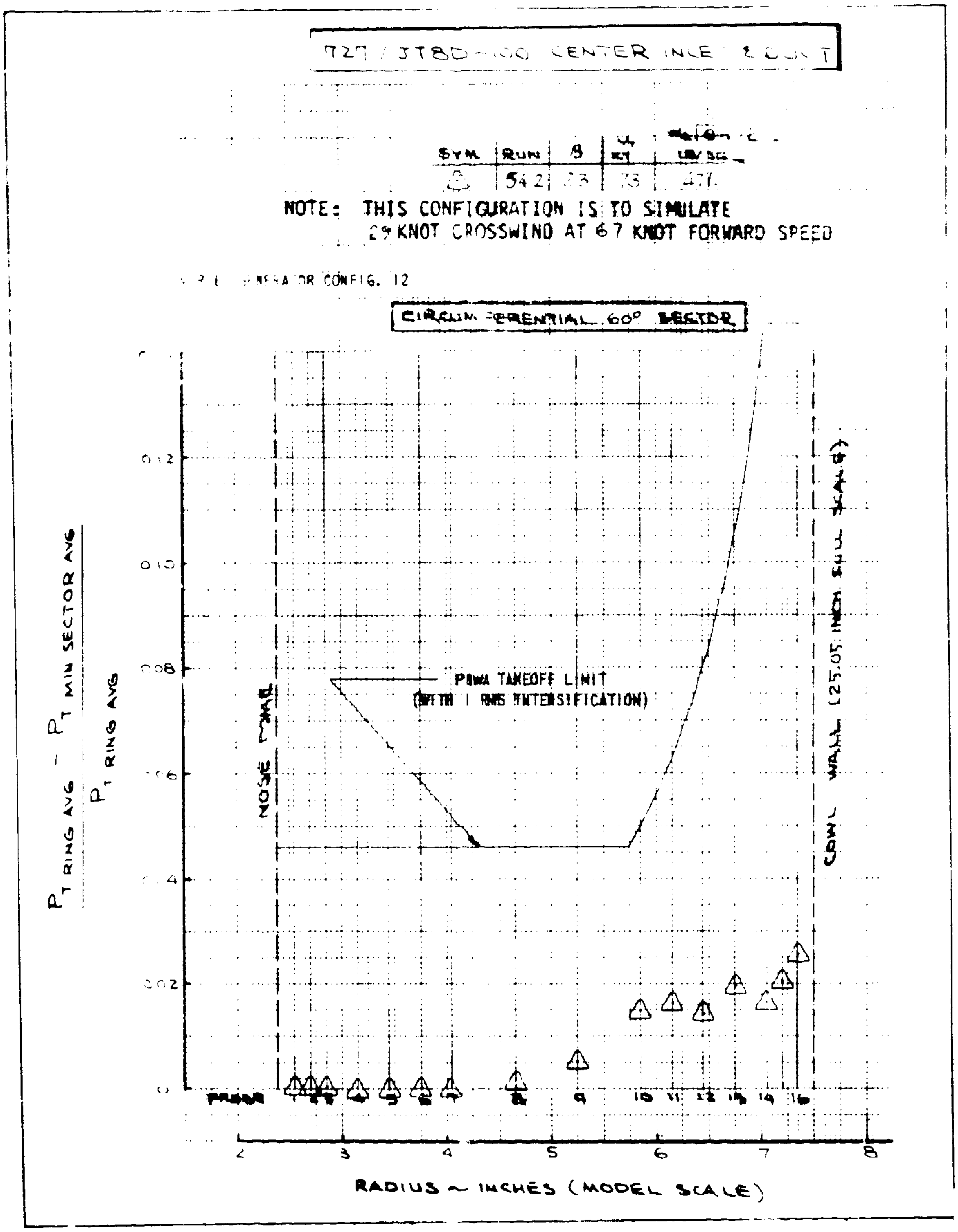

FIGURE 40. - 67-KNOT STEADY-STATE 60°-SECTOR CIRCUMFERENTIAL PRESSURE DISTORTION, WITH VORTEX GENERATOR CONFIG. 12 AT 23 DEGREE YAW

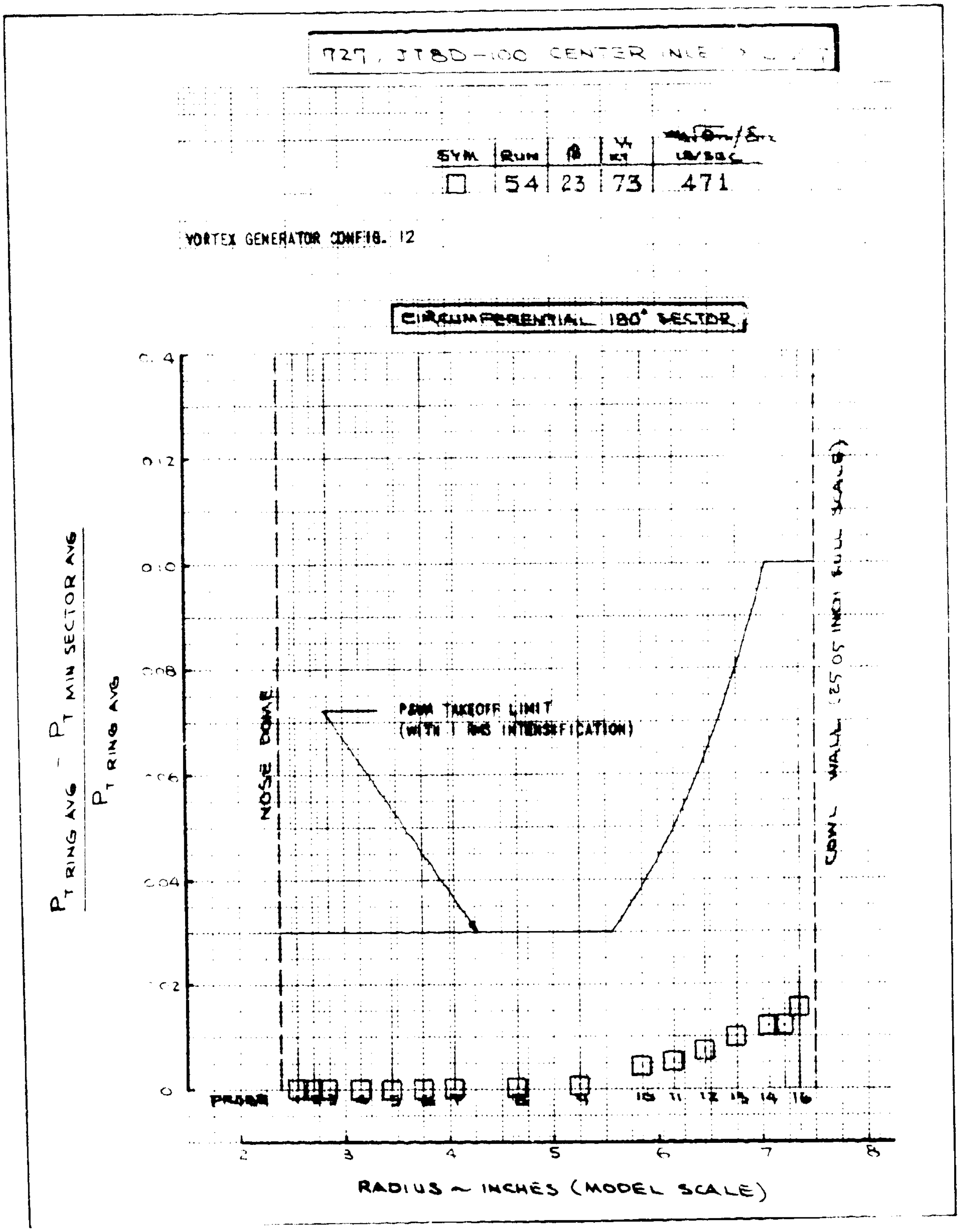

FIGURE 41. - 67-KNOT STEADY-STATE 180°-SECTOR CIRCUMFERENTIAL PRESSURE DISTORTION, WITH VORTEX GENERATOR CONFIG. 12 AT 23 DEGREE YAW

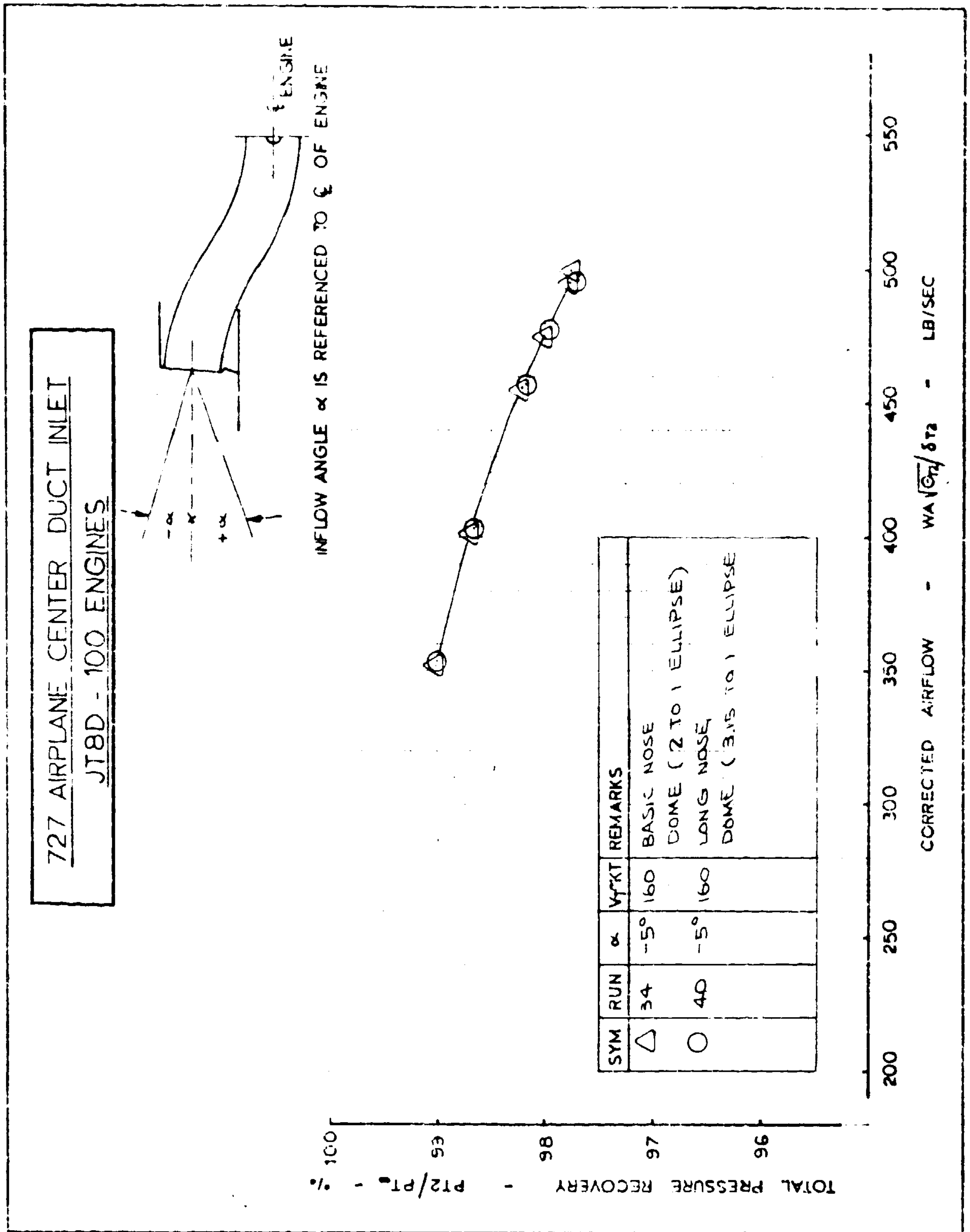

FIGURE 42. - TOTAL PRESSURE RECOVERY VS. AIRFLOW, EFFECT OF LENGTH OF NOSE DOME

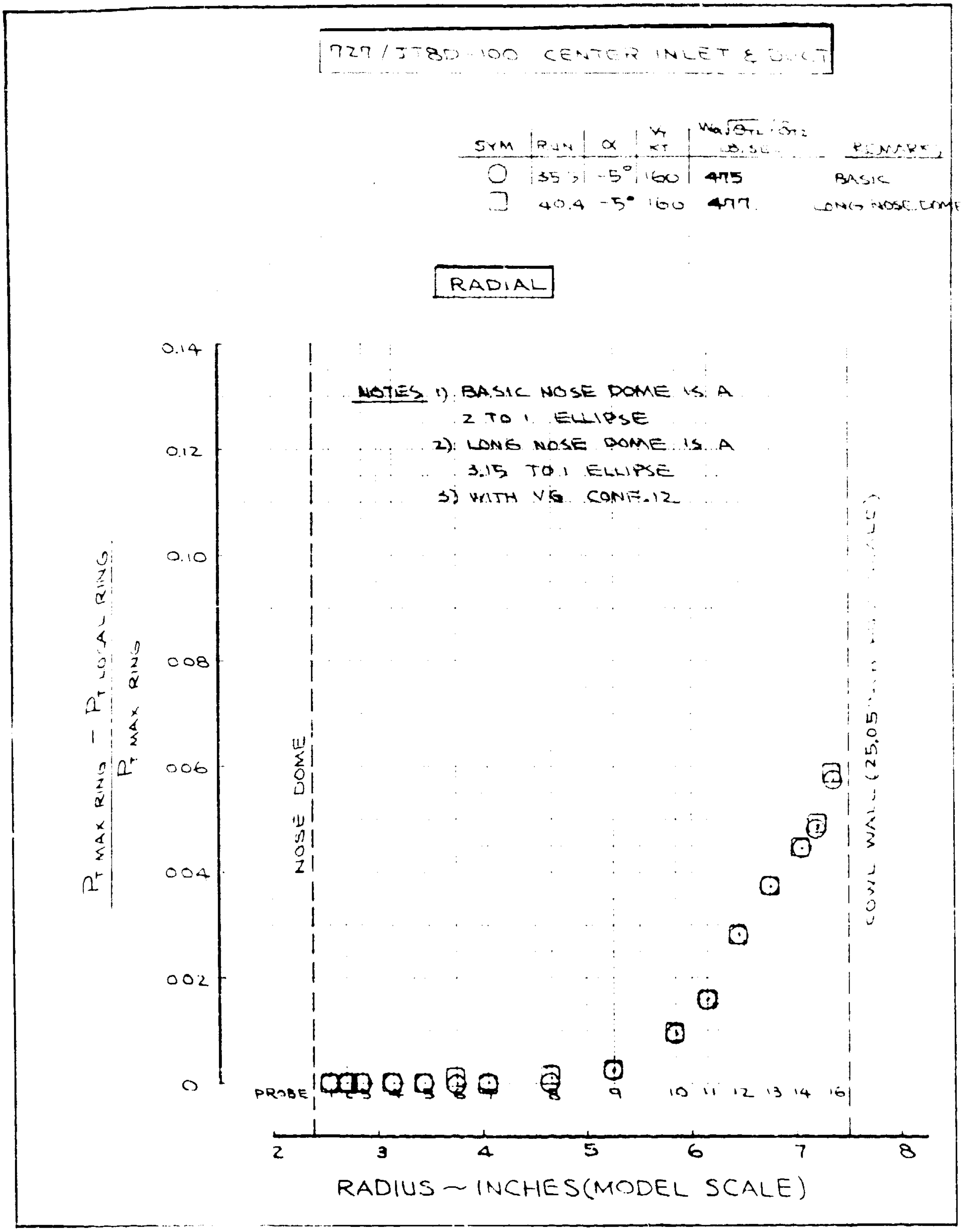

FIGURE 43. - 160-KNOT STEADY-STATE RADIAL PRESSURE DISTORTION, EFFECT OF LENGTH OF NOSE DOME

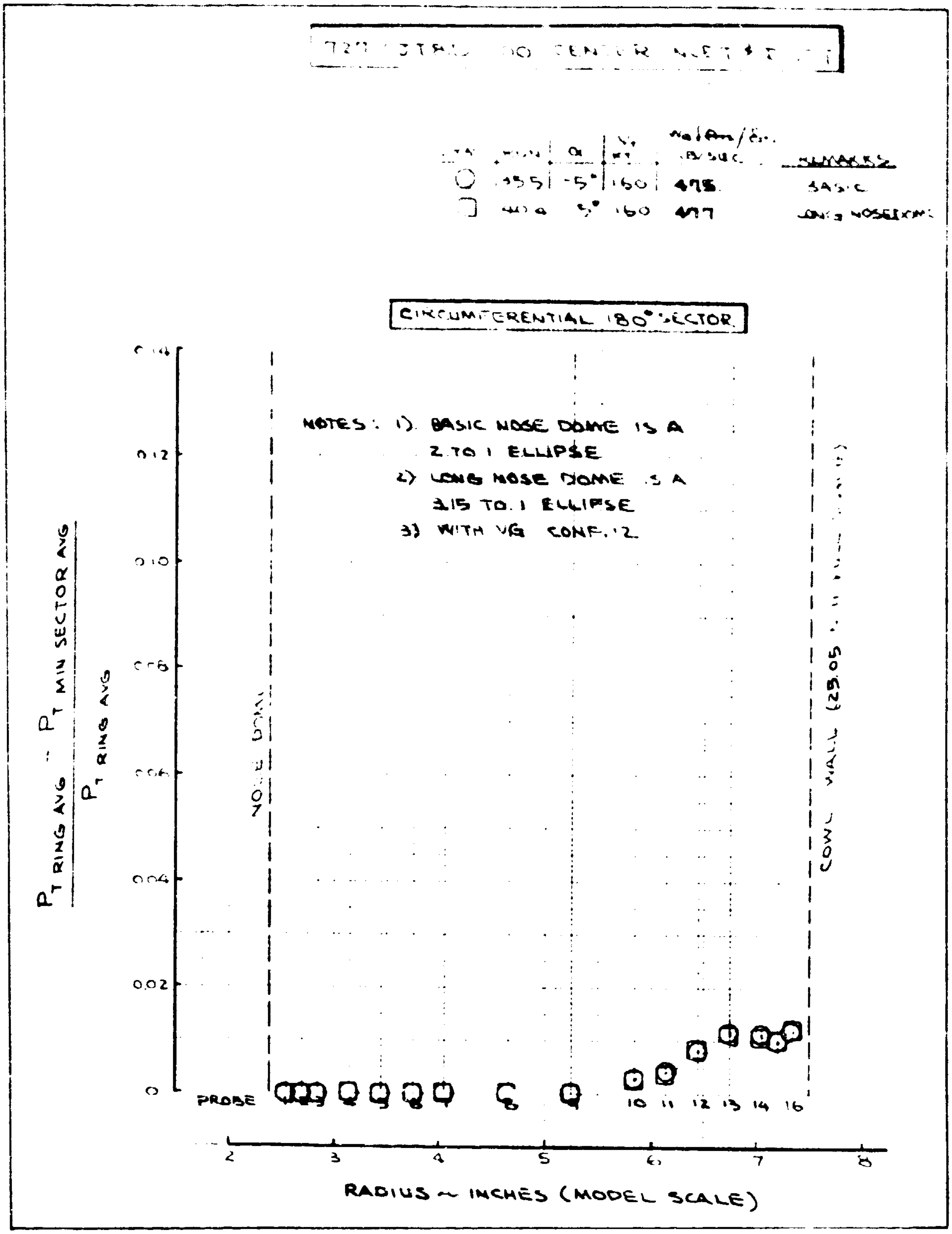

FIGURE 44. - 160-KNOT STEADY-STATE 180°-SECTOR CIRCUMFERENTIAL PRESSURE DISTORTION, EFFECT OF LENGTH OF NOSE DOME

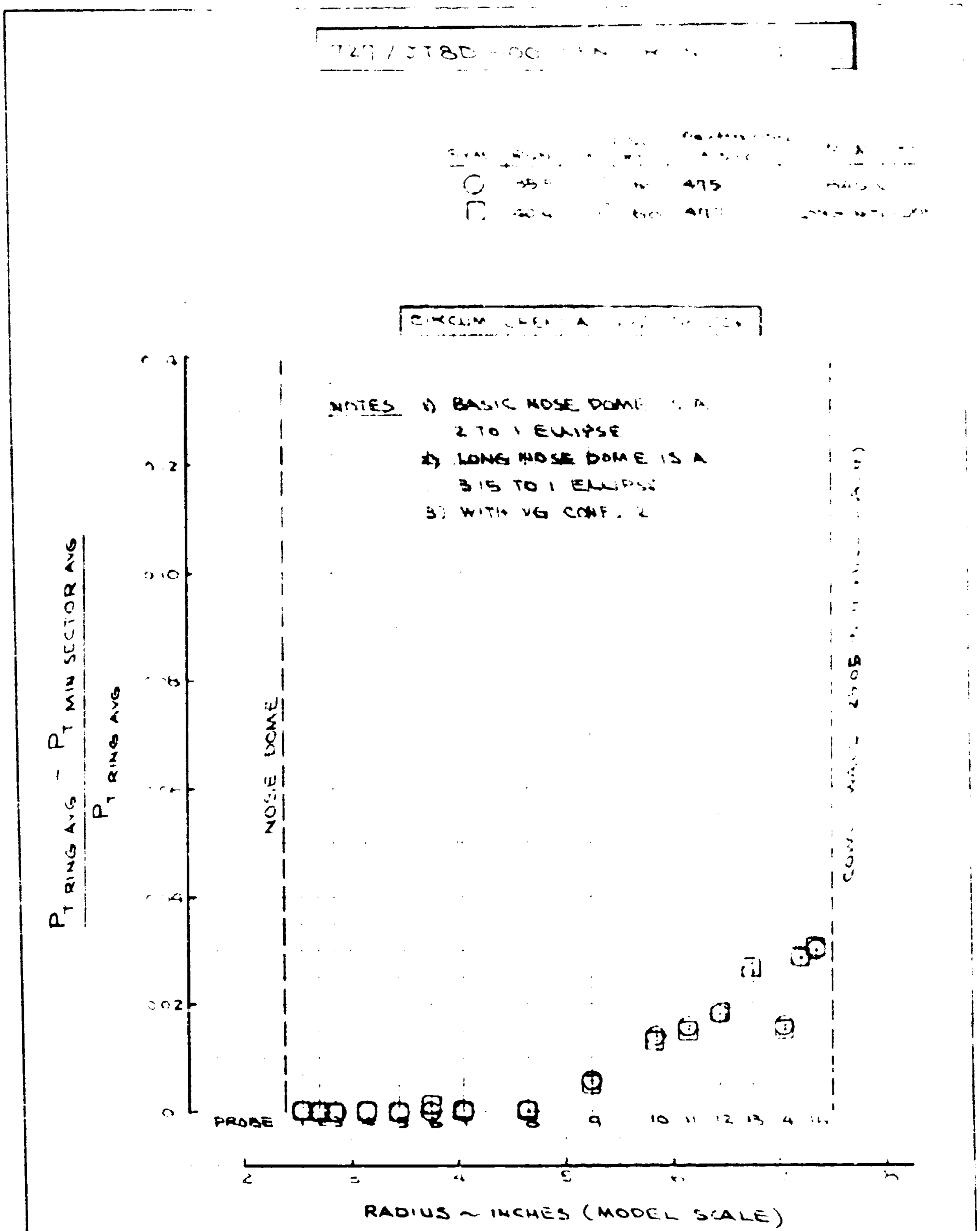

FIGURE 45. - 160-KNOT STEADY-STATE 60°-SECTOR CIRCUMFERENTIAL PRESSURE DISTORTION, EFFECT OF LENGTH OF NOSE DOME

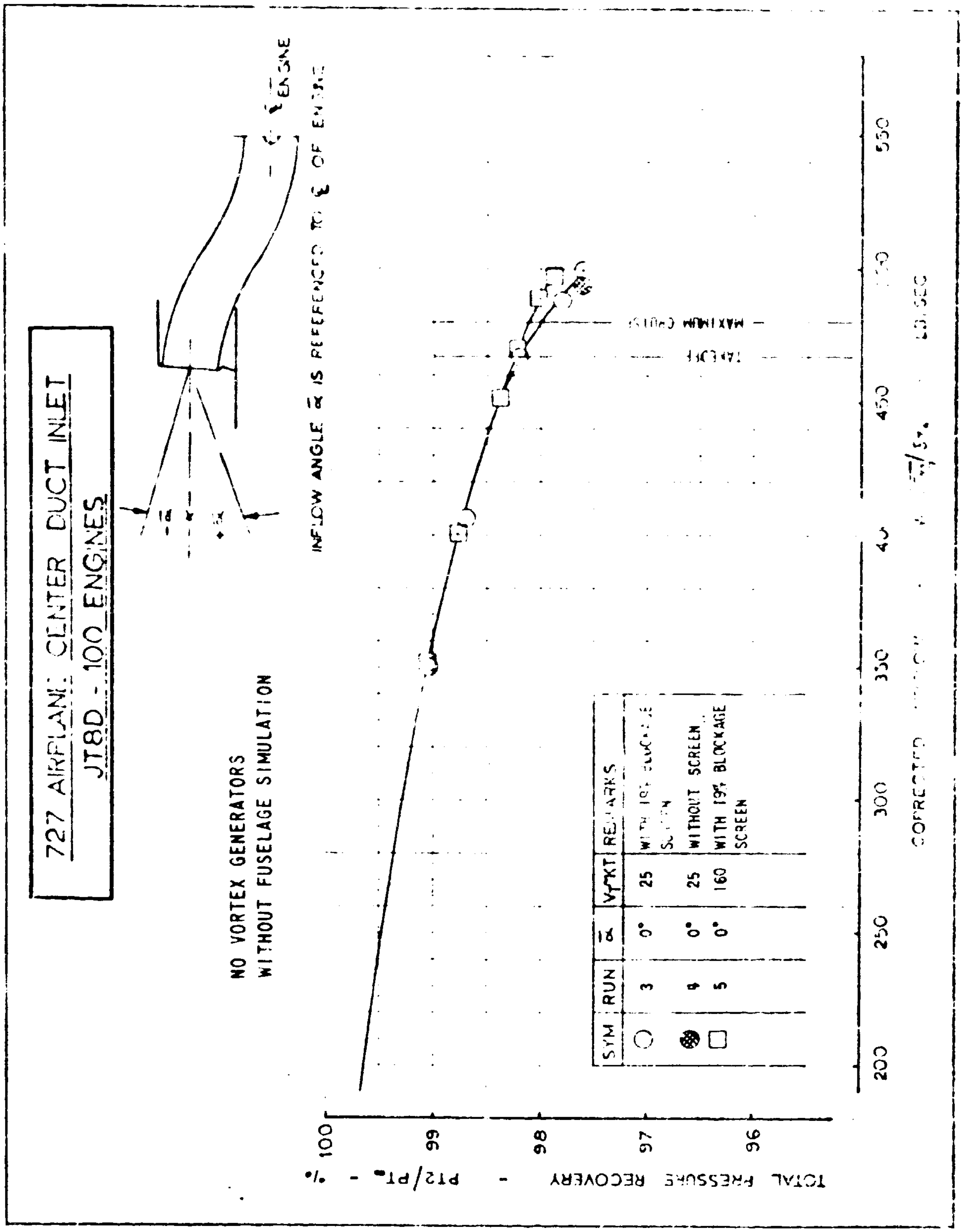

FIGURE 46. - PRESSURE RECOVERY vs. AIRFLOW, AT ᾱ = 0° WITH FORWARD SPEED (WITHOUT FLOW CONTROL DEVICES)

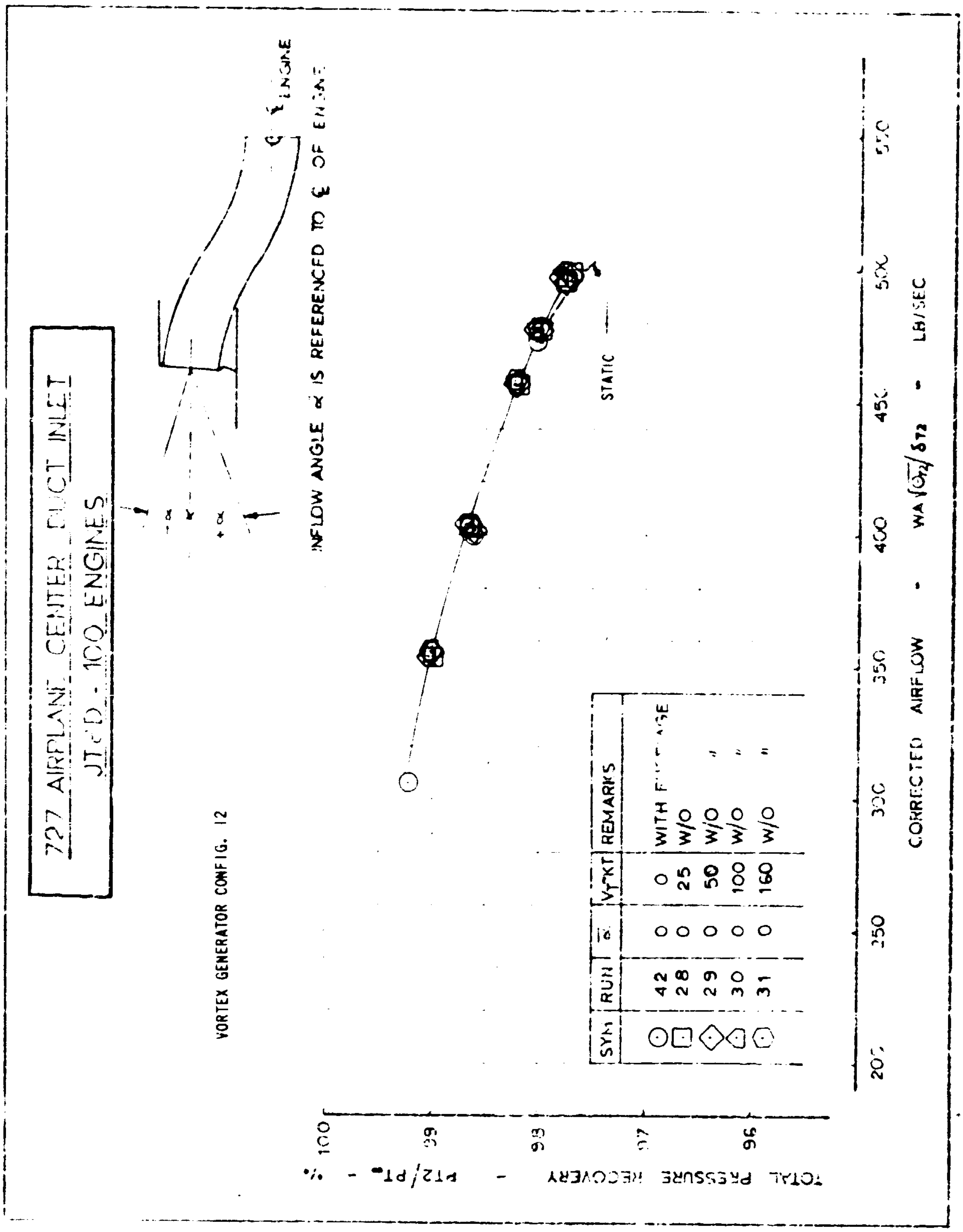

FIGURE 47. - PRESSURE RECOVERY VS. AIRFLOW,WITH VORTEX GENERATOR CONFIG. 12 ($\bar{\alpha}$ = 0°) EFFECT OF FORWARD SPEED

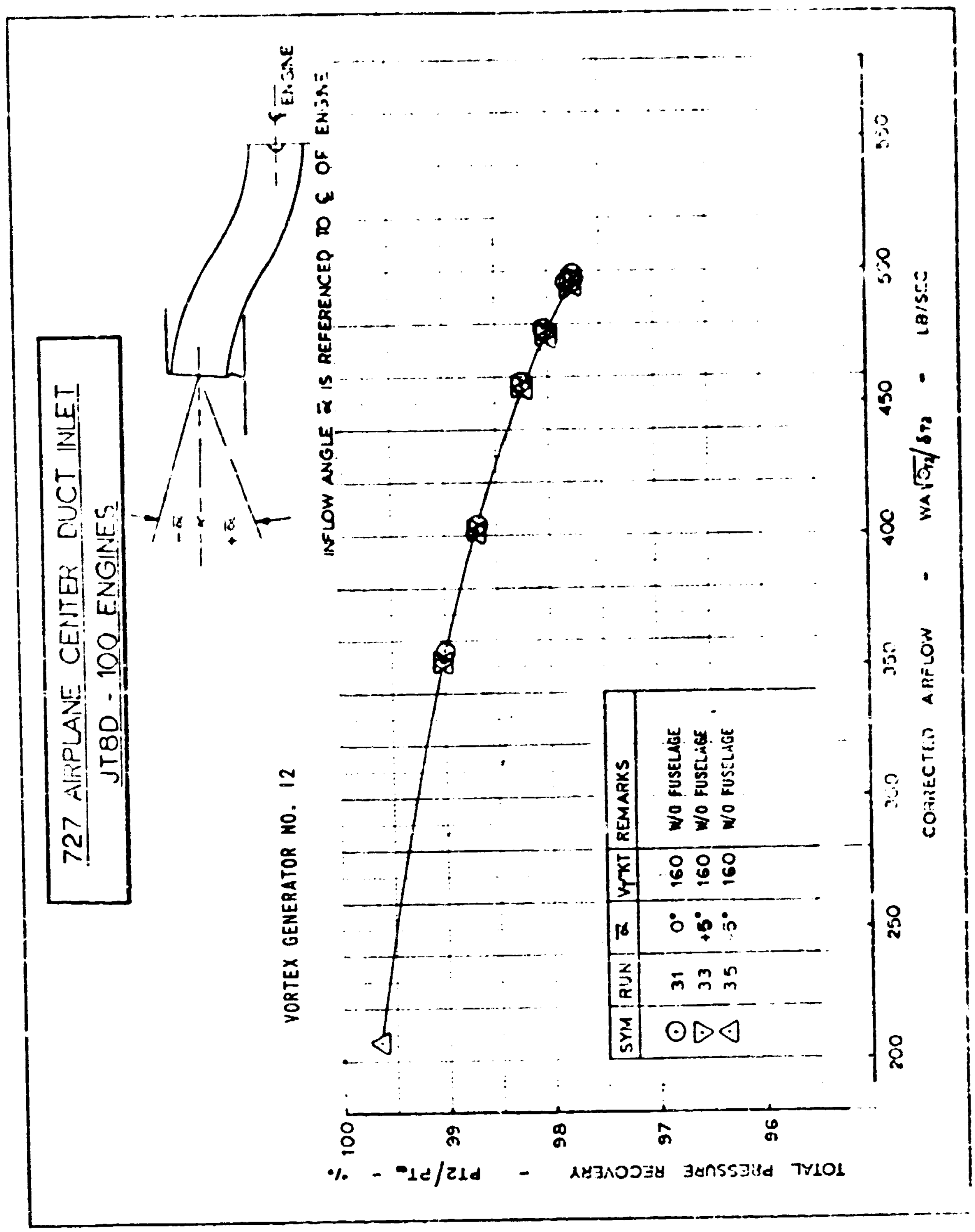

FIGURE 48. - PRESSURE RECOVERY VS. AIRFLOW, WITH VORTEX GENERATOR CONFIG. 12 EFFECT OF INLET INFLOW ANGLE

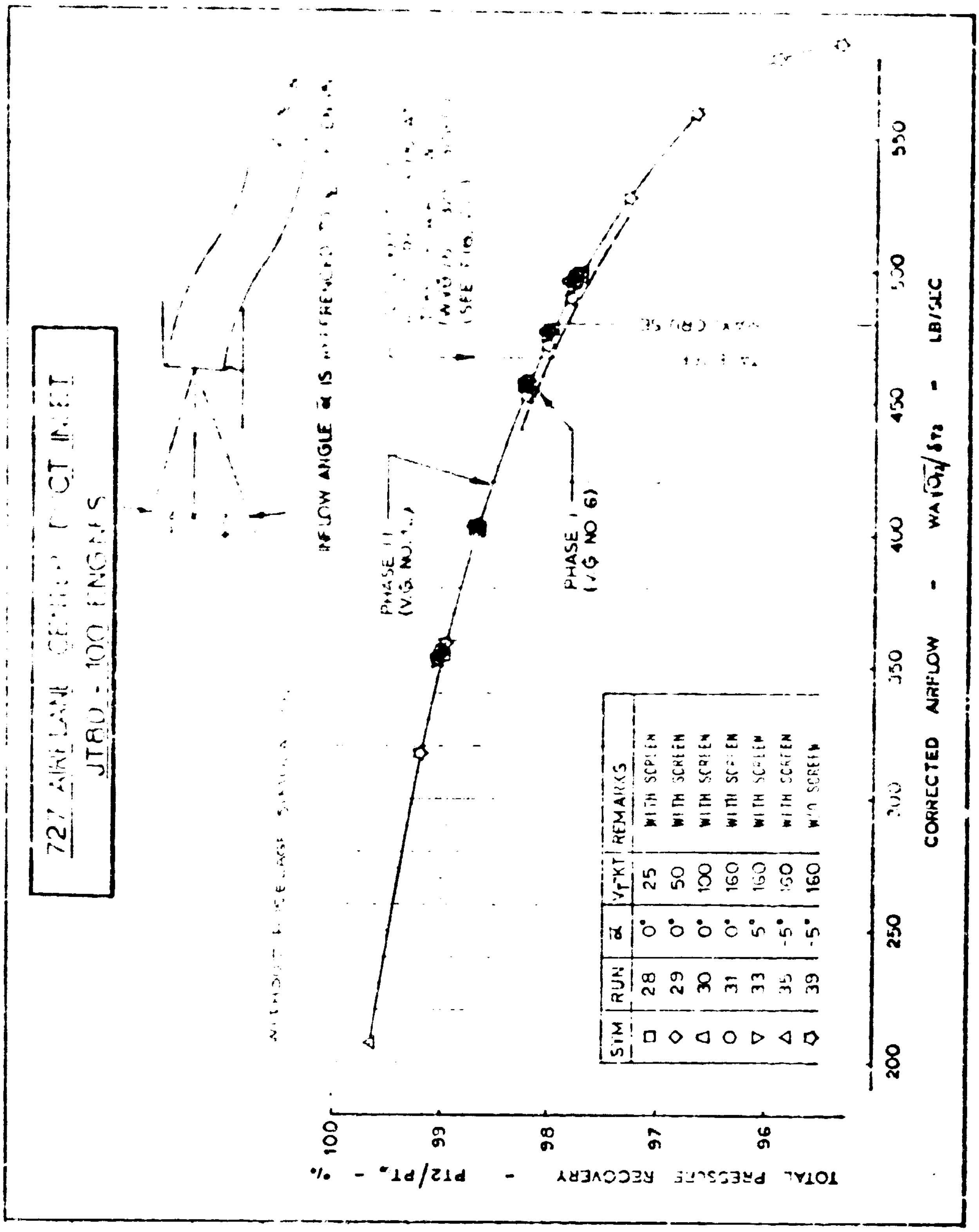

FIGURE 49. - TOTAL PRESSURE RECOVERY COMPARISON OF PHASE I, II AND 727-200

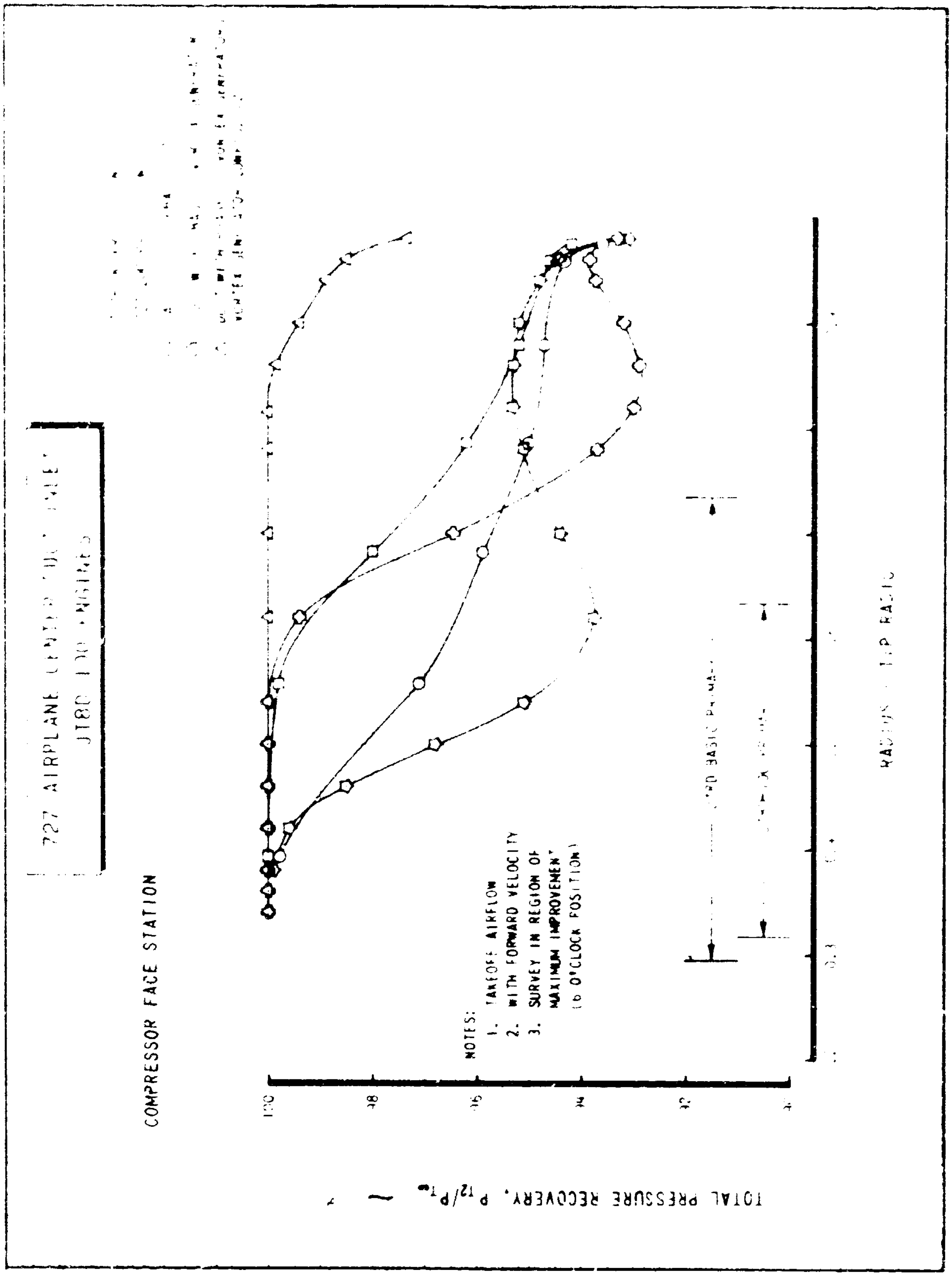

FIGURE 50. - PRESSURE RECOVERY PROFILES 727-100, -200, PHASE I AND II, AREA OF MAXIMUM IMPROVEMENT (6 O'CLOCK)

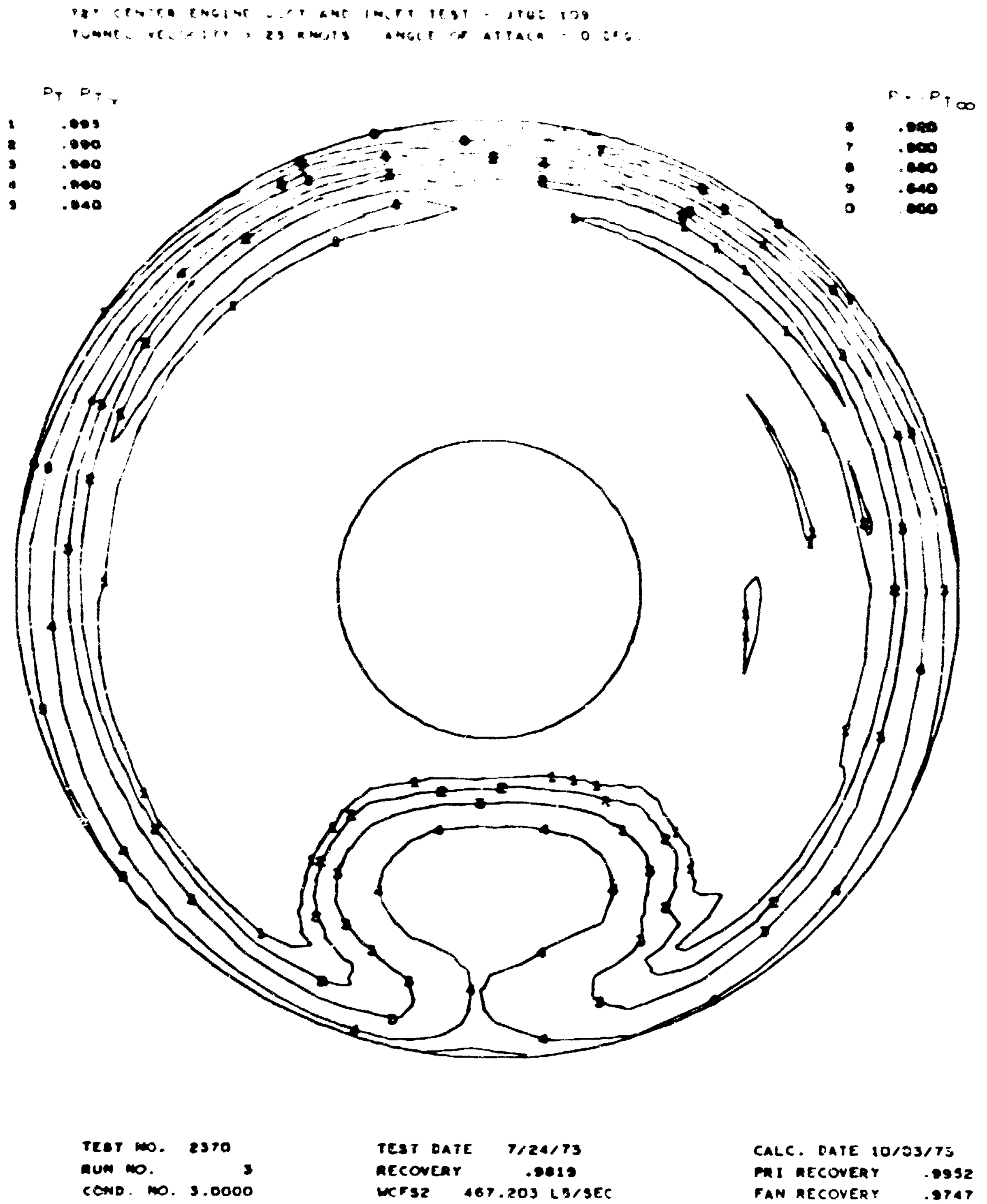

FIGURE 51. - 25-KNOT STEADY-STATE COMPRESSOR FACE PRESSURE RECOVERY MAP,
(WITHOUT FLOW CONTROL DEVICES)

727 CENTER ENGINE DUCT AND INLET TEST - JT8D-109
TUNNEL VELOCITY = 160 KNOTS ANGLE OF ATTACK = 0 DEG.

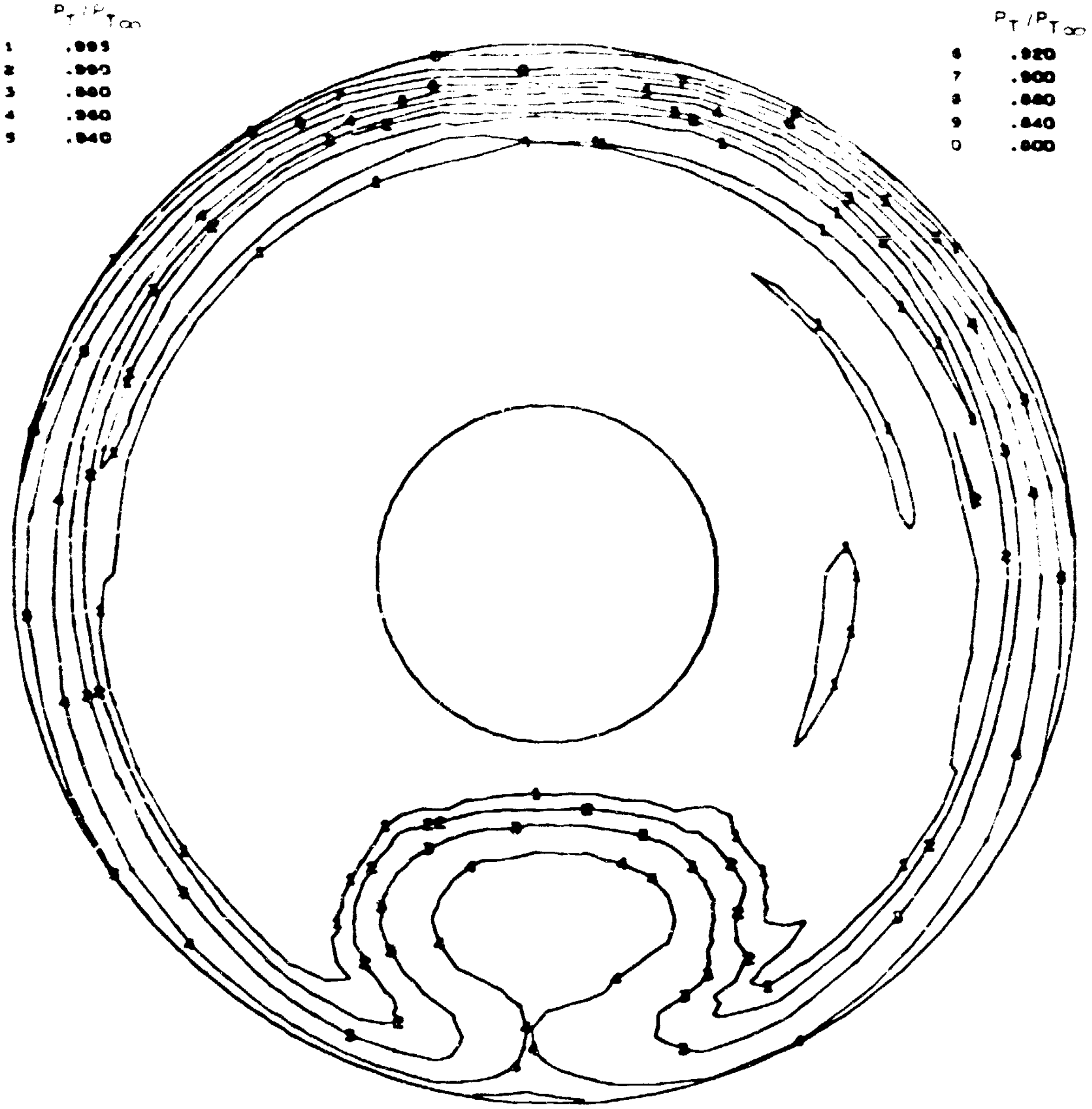

TEST NO. 2370	TEST DATE 7/25/73	CALC. DATE 10/03/73
RUN NO. 5	RECOVERY .9821	PRI RECOVERY .9957
COND. NO. 5.0000	WCFS2 470.211 LB/SEC	FAN RECOVERY .9747

FIGURE . - 160-KNOT STEADY-STATE COMPRESSOR FACE PRESSURE RECOVERY MAP,(WITHOUT FLOW CONTROL DEVICES)

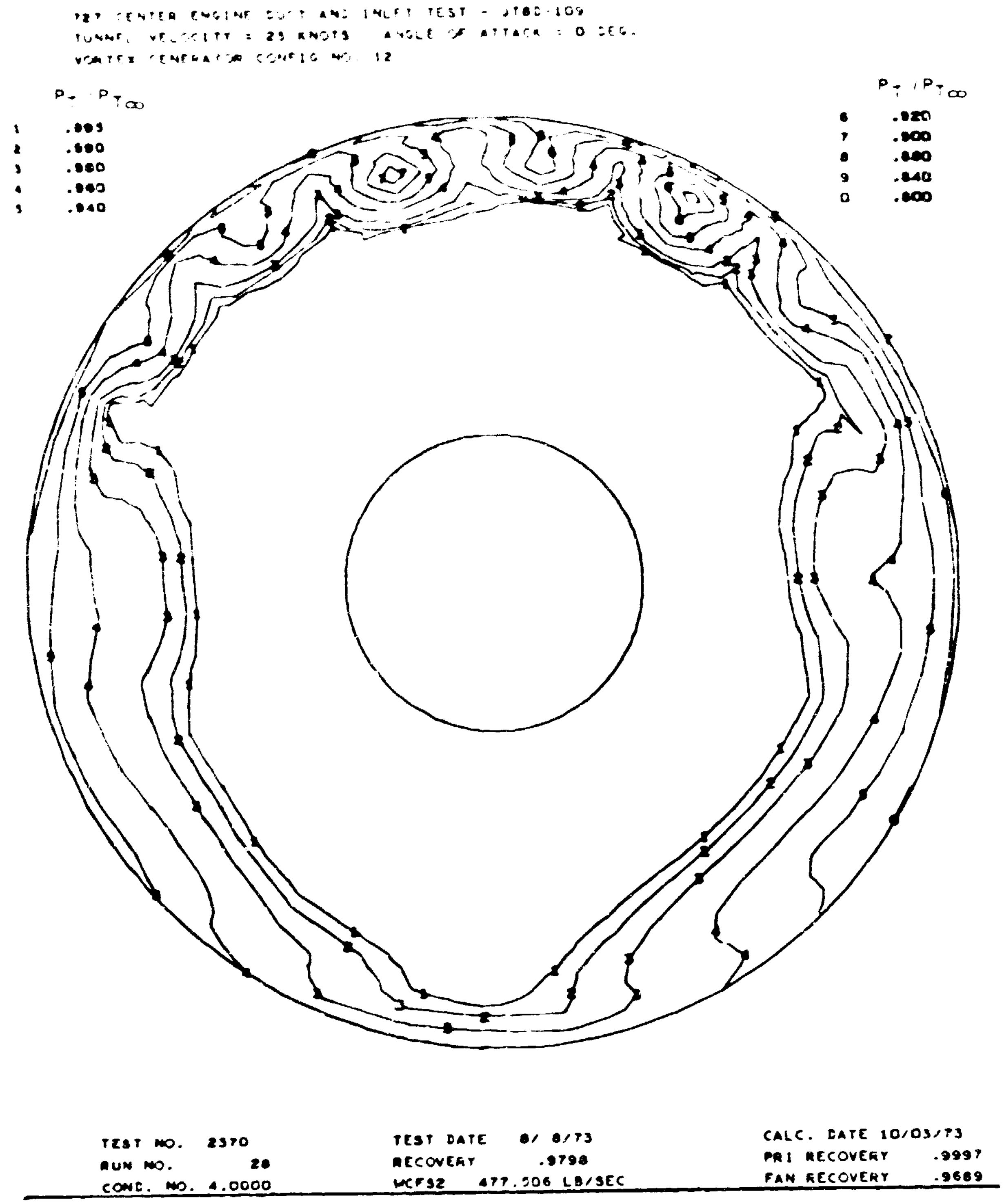

FIGURE 53. - 25-KNOT STEADY STATE COMPRESSOR FACE PRESSURE RECOVERY MAP, WITH VORTEX GENERATOR CONFIG. 12 ($\bar{\alpha}$ = 0°)

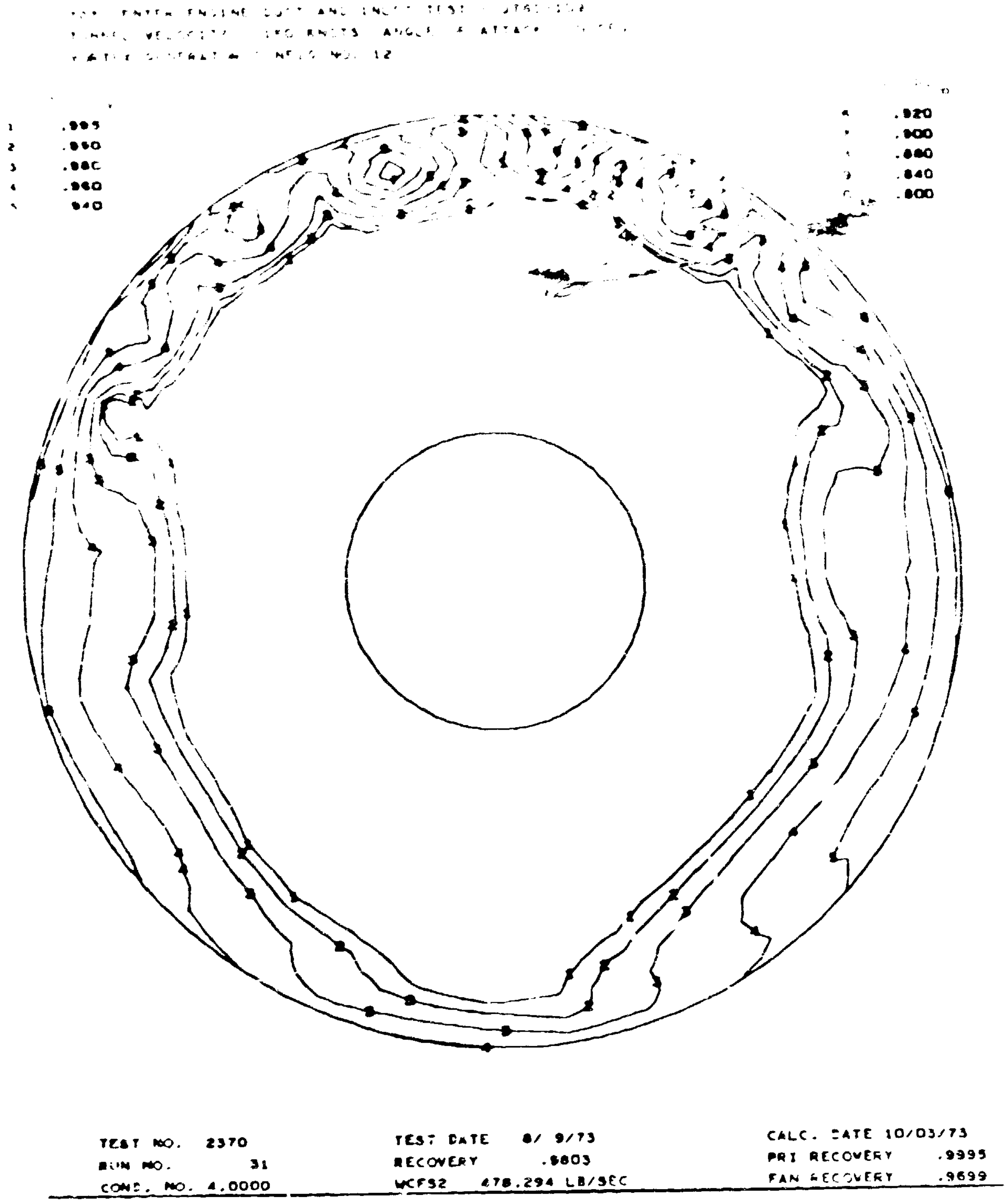

FIGURE 54. - 160-KNOT STEADY-STATE COMPRESSOR FACE PRESSURE RECOVERY MAP, WITH VORTEX GENERATOR CONFIG. 12 ($\bar{\alpha}$ = 0°)

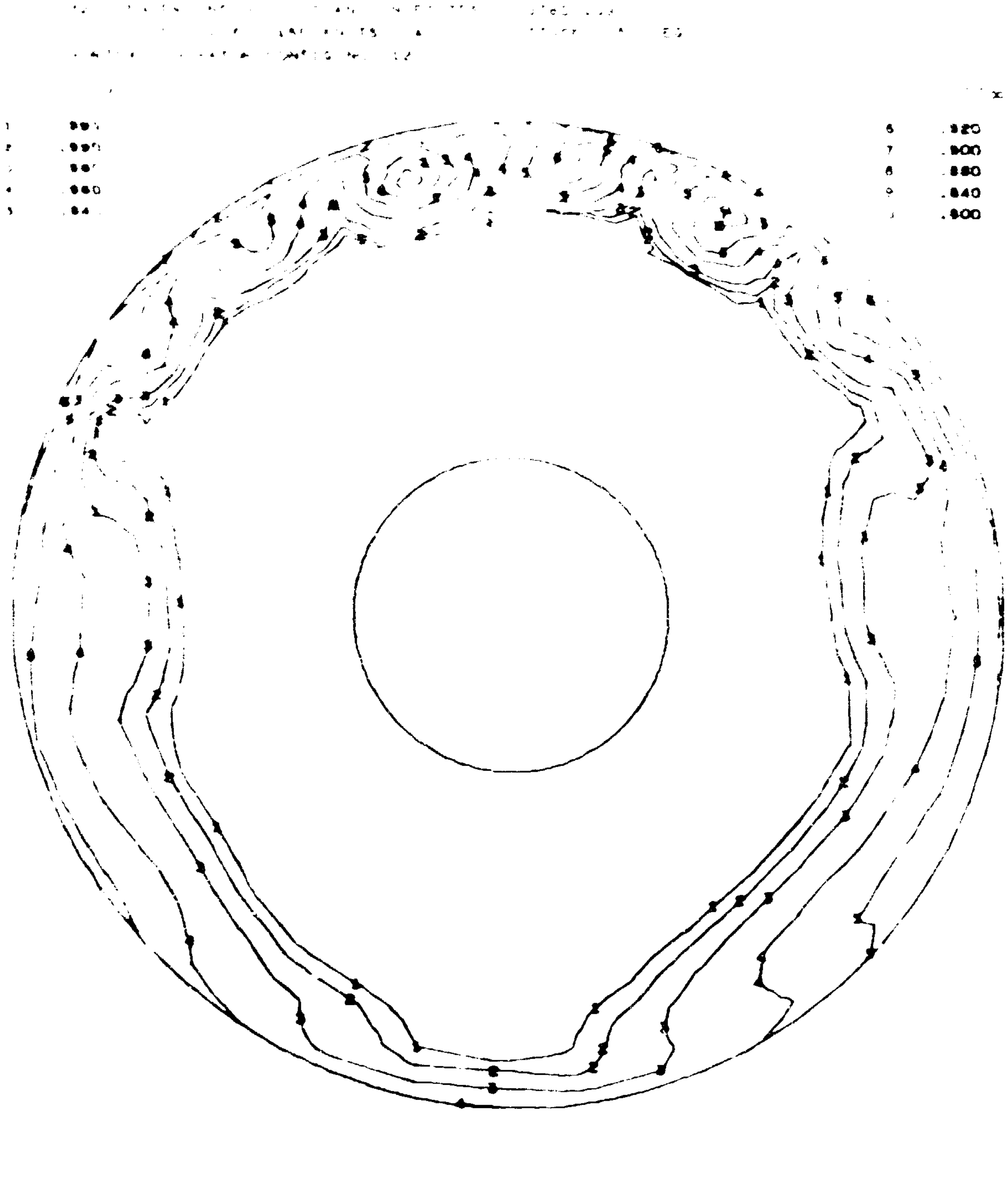

TEST NO. 2370	TEST DATE 8/10/73	CALC. DAT 10/03/73
RUN NO. 33	RECOVERY .9804	PRI RECOVERY .9995
CONF. NO. 4.0000	WCF52 475.900 LB/SEC	FAN RECOVERY .9700

FIGURE 55. - 160-KNOT STEADY-STATE COMPRESSOR FACE PRESSURE RECOVERY MAP, WITH VORTEX GENERATOR CONFIG. 12 ($\bar{\alpha}$ = 5°)

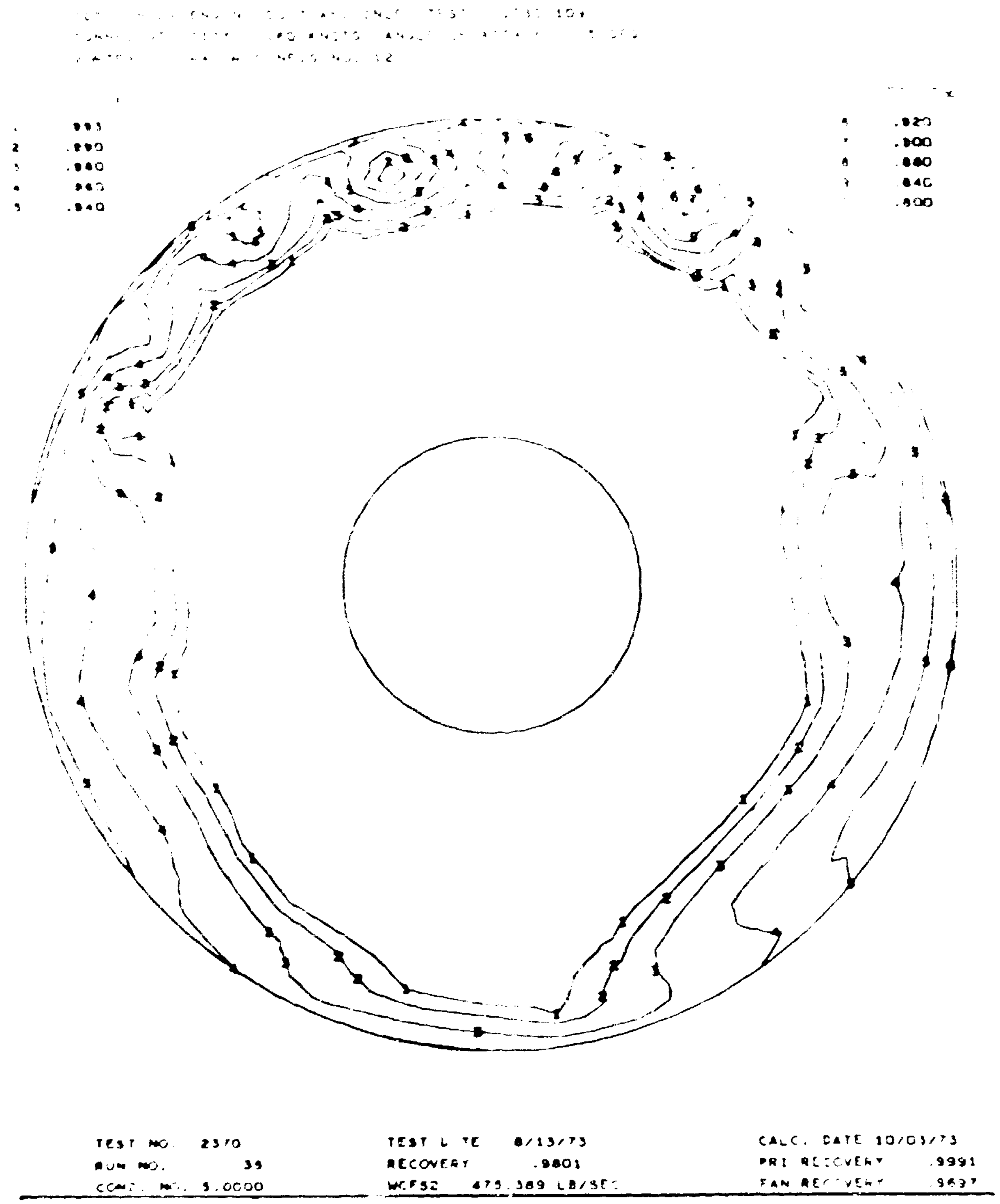

FIGURE 56. - 160-KNOT STEADY-STATE COMPRESSOR FACE PRESSURE RECOVERY MAP WITH VORTEX GENERATOR CONFIG. 12 ($\bar{\gamma}$ = -5°)

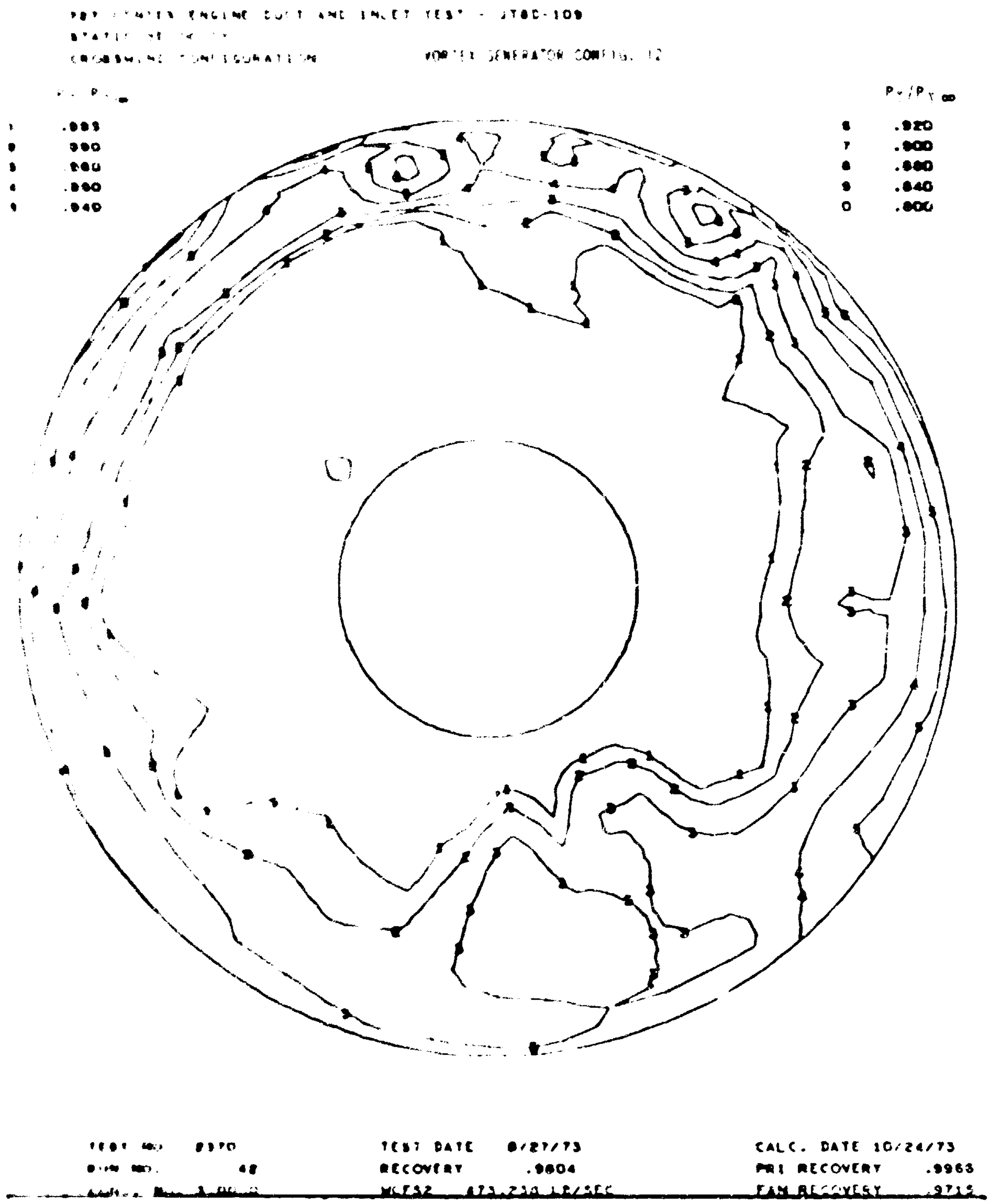

FIGURE 57. - 0-KNOT CROSSWIND STEADY-STATE COMPRESSOR FACE PRESSURE RECOVERY MAP, WITH FUSELAGE SIMULATION AND VORTEX GENERATOR CONFIG. 12 (β=90°)

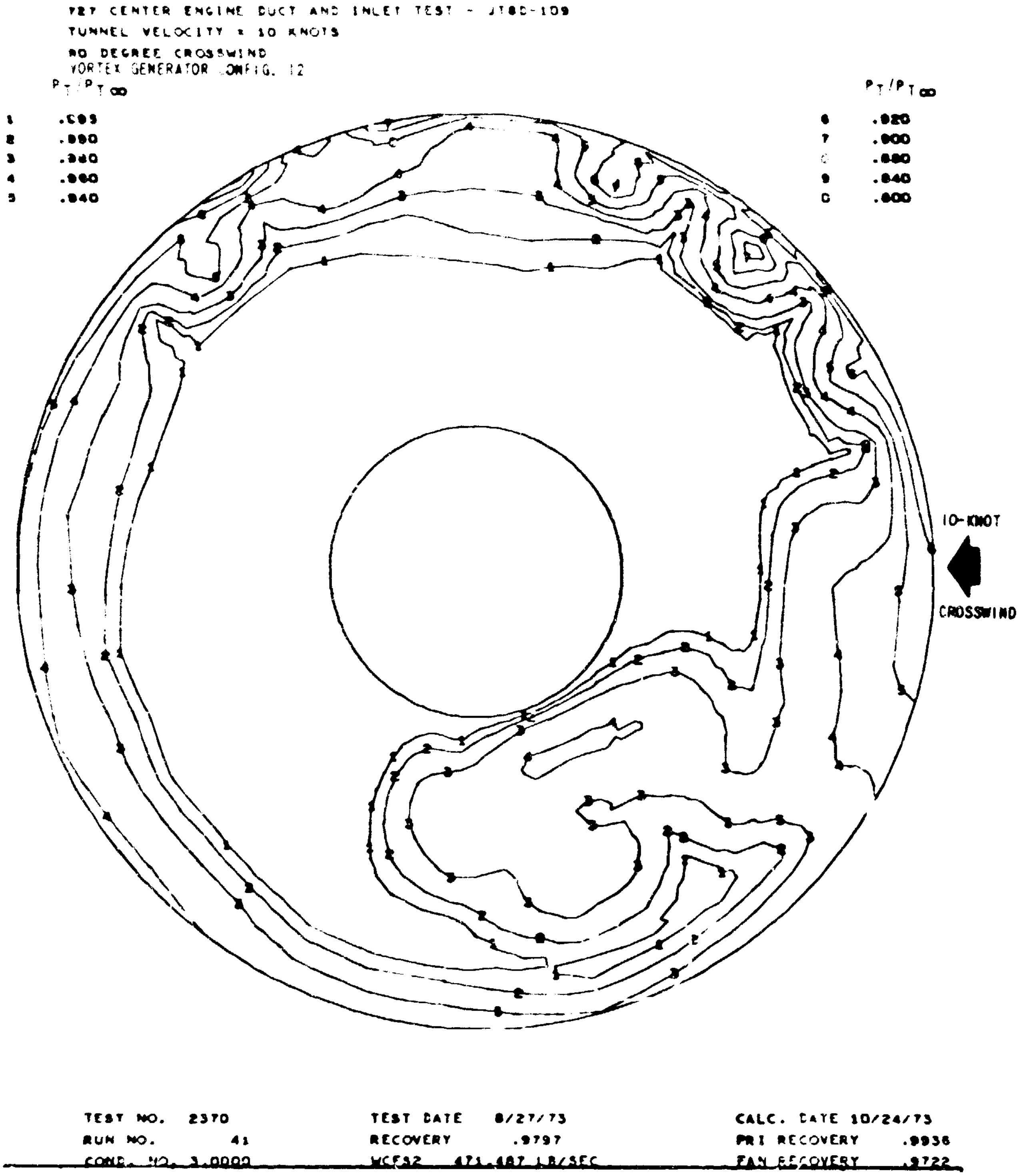

FIGURE 58. - 10-KNOT CROSSWIND STEADY-STATE COMPRESSOR FACE PRESSURE RECOVERY MAP, WITH FUSELAGE SIMULATION AND VORTEX GENERATOR CONFIG. 12 (β = 90°)

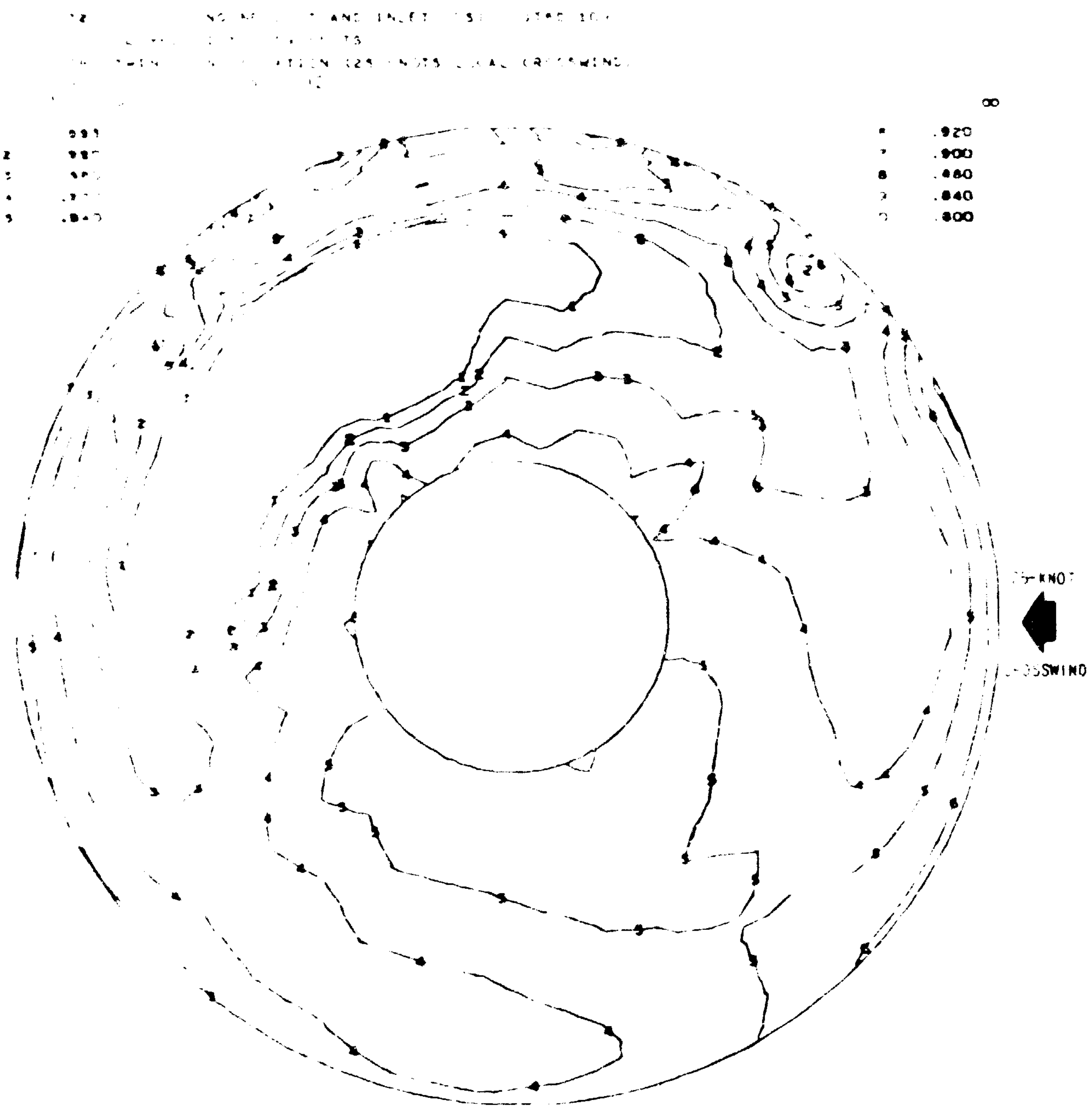

TEST DATE 8/28/73

CALC. DATE 10/24/73

RUN NO. 43

RECOVERY .9589

PRI RECOVERY .9601

470.983 LB/SEC

FIGURE 59. - 25-KNOT CROSSWIND STEADY-STATE COMPRESSOR FACE PRESSURE RECOVERY MAP, WITH FUSELAGE SIMULATION AND VORTEX GENERATOR CONFIG. 12 (β = 90°)

727 CENTER ENGINE DUCT AND INLET TEST - JT8D-109
TUNNEL VELOCITY = 28 KNOTS
CROSSWIND CONFIGURATION (35 KNOTS LOCAL CROSSWIND)

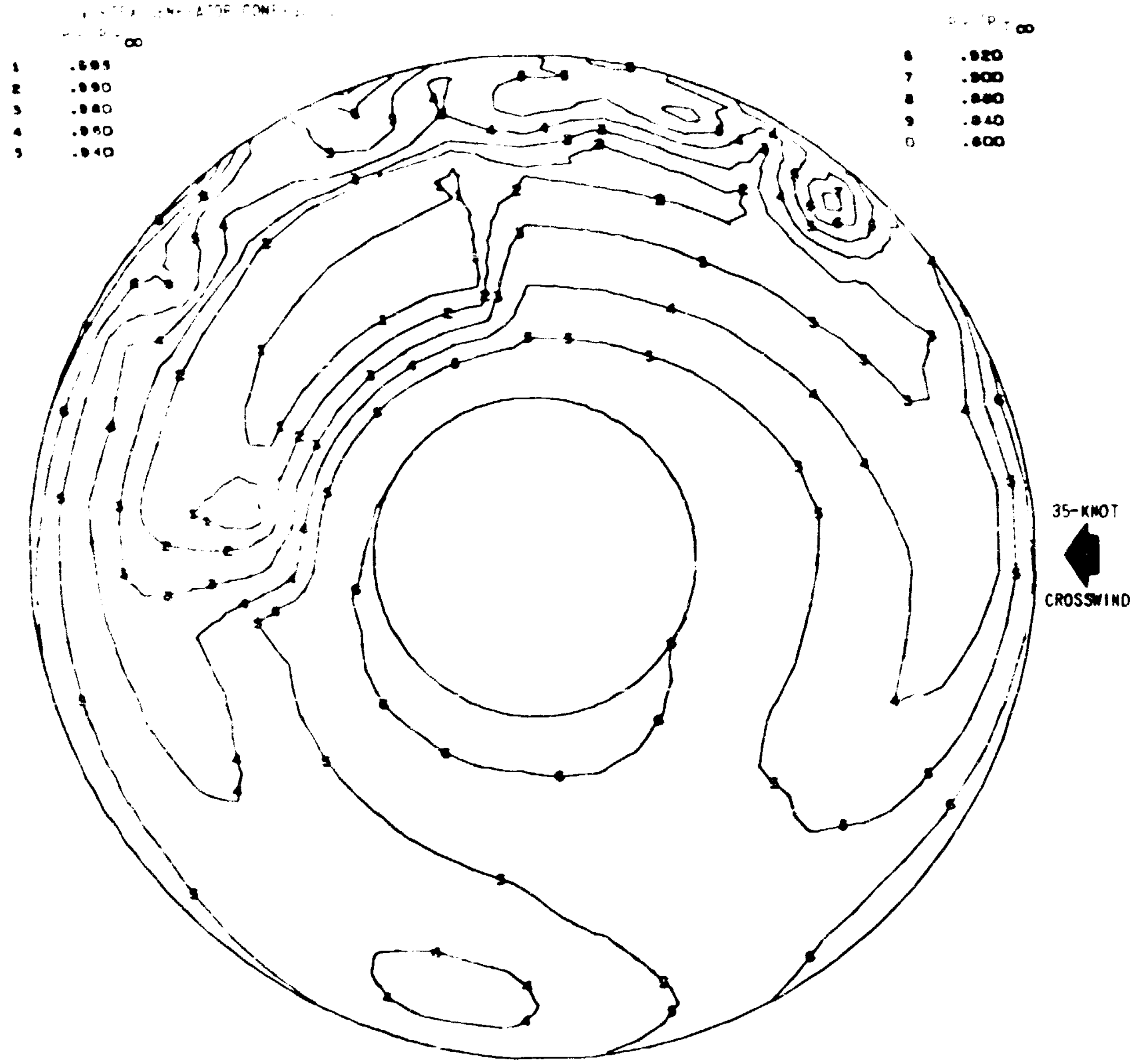

TEST NO. 2370	TEST DATE 8/28/73	CALC. DATE 10/24/73
RUN NO. 44	RECOVERY .9486	PRI RECOVERY .9438
CONF. NO. 3.0000	WCFS2 475.965 LB/SEC	FAN RECOVERY .9514

FIGURE 60. - 35-KNOT CROSSWIND STEADY-STATE COMPRESSOR FACE PRESSURE RECOVERY MAP, WITH FUSELAGE SIMULATION AND VORTEX GENERATOR CONFIG. 12 (β = 90°)

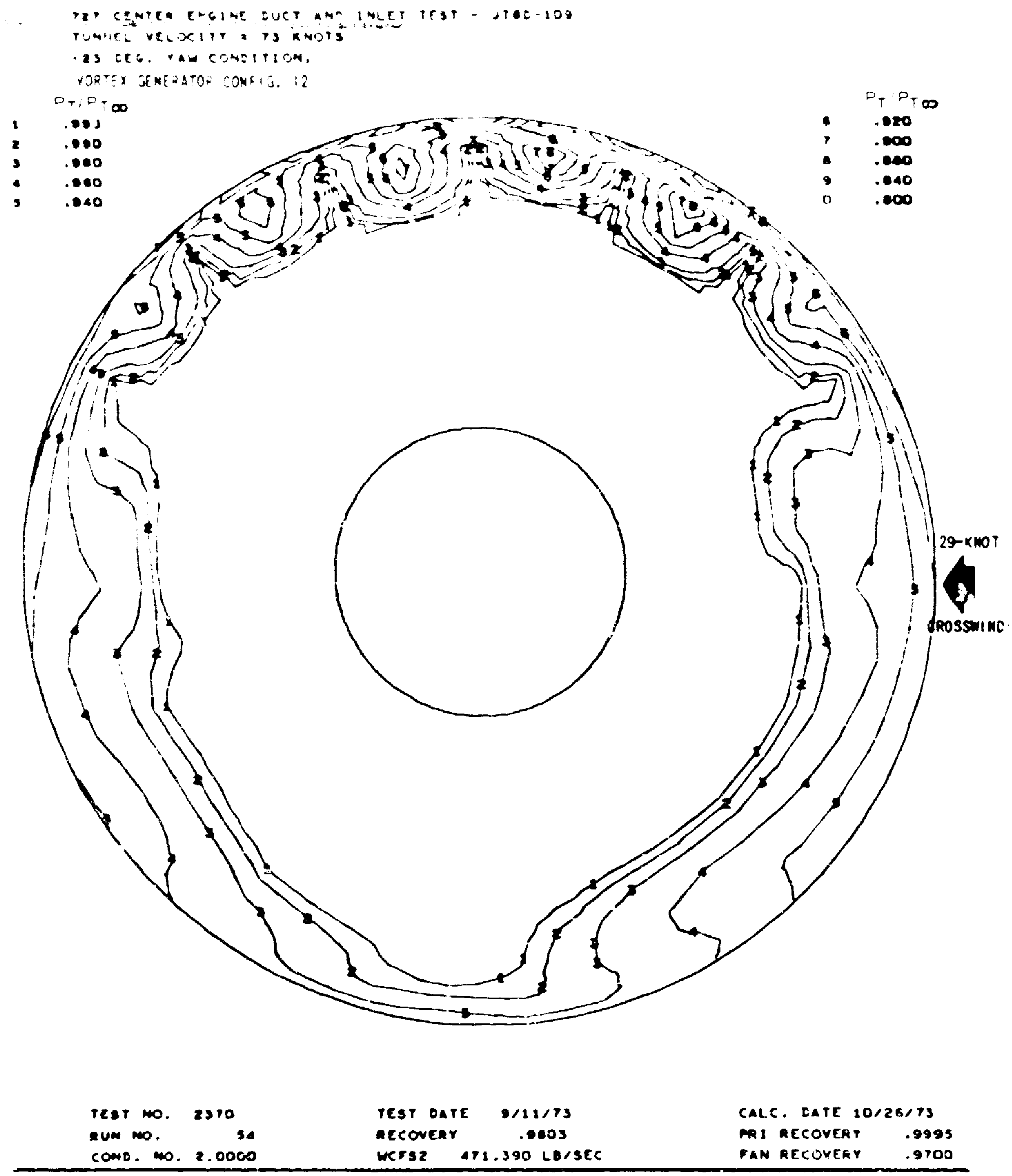

FIGURE 61. - 67-KNOT STEADY-STATE COMPRESSOR FACE PRESSURE RECOVERY MAP, WITH VORTEX GENERATOR CONFIG. 12 AT 23 DEGREE YAW

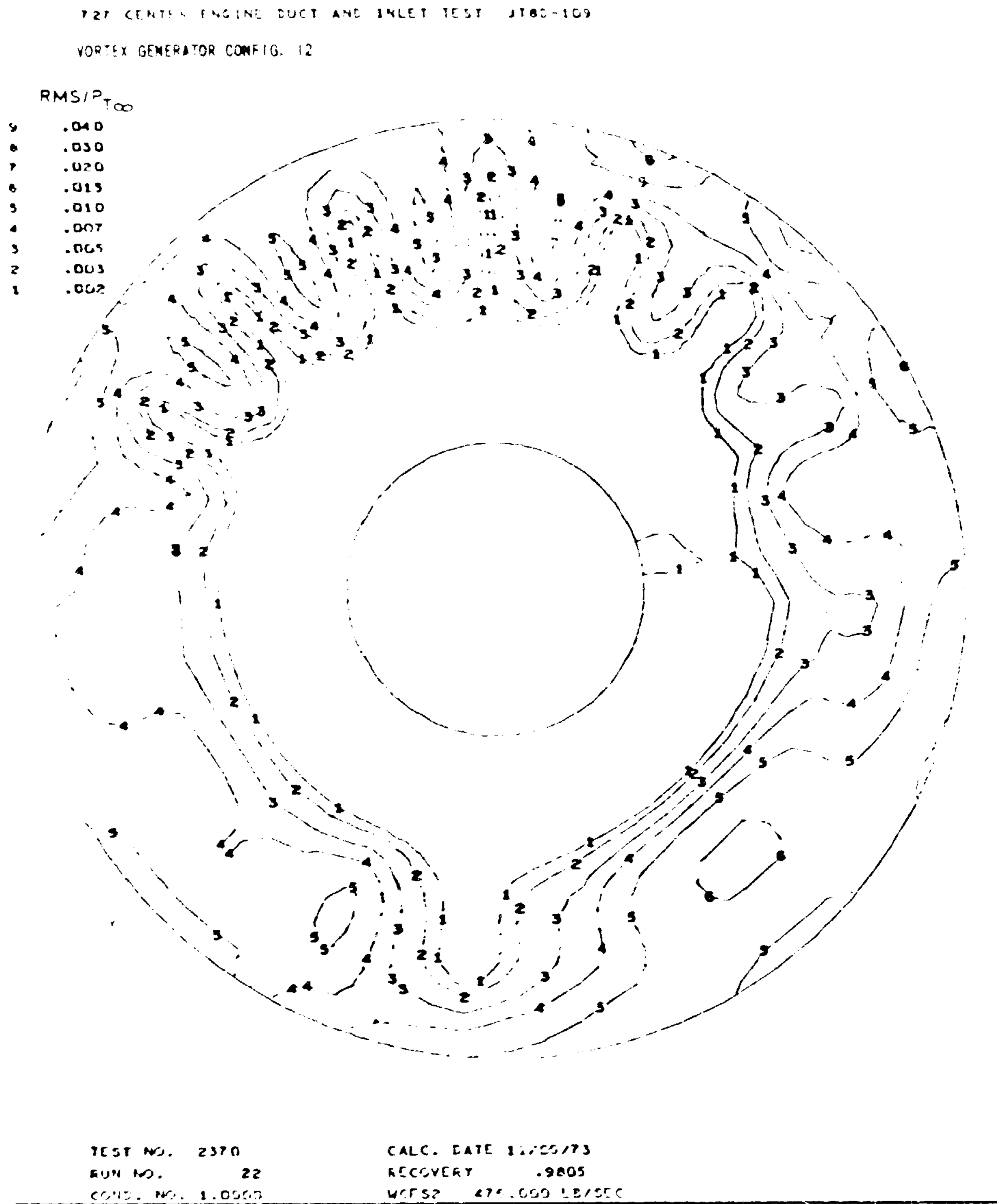

FIGURE 62. - 160-KNOT DYNAMIC (RMS/$P_{T\infty}$) COMPRESSOR FACE CONTOUR MAP, WITH VORTEX GENERATOR CONFIG. 12

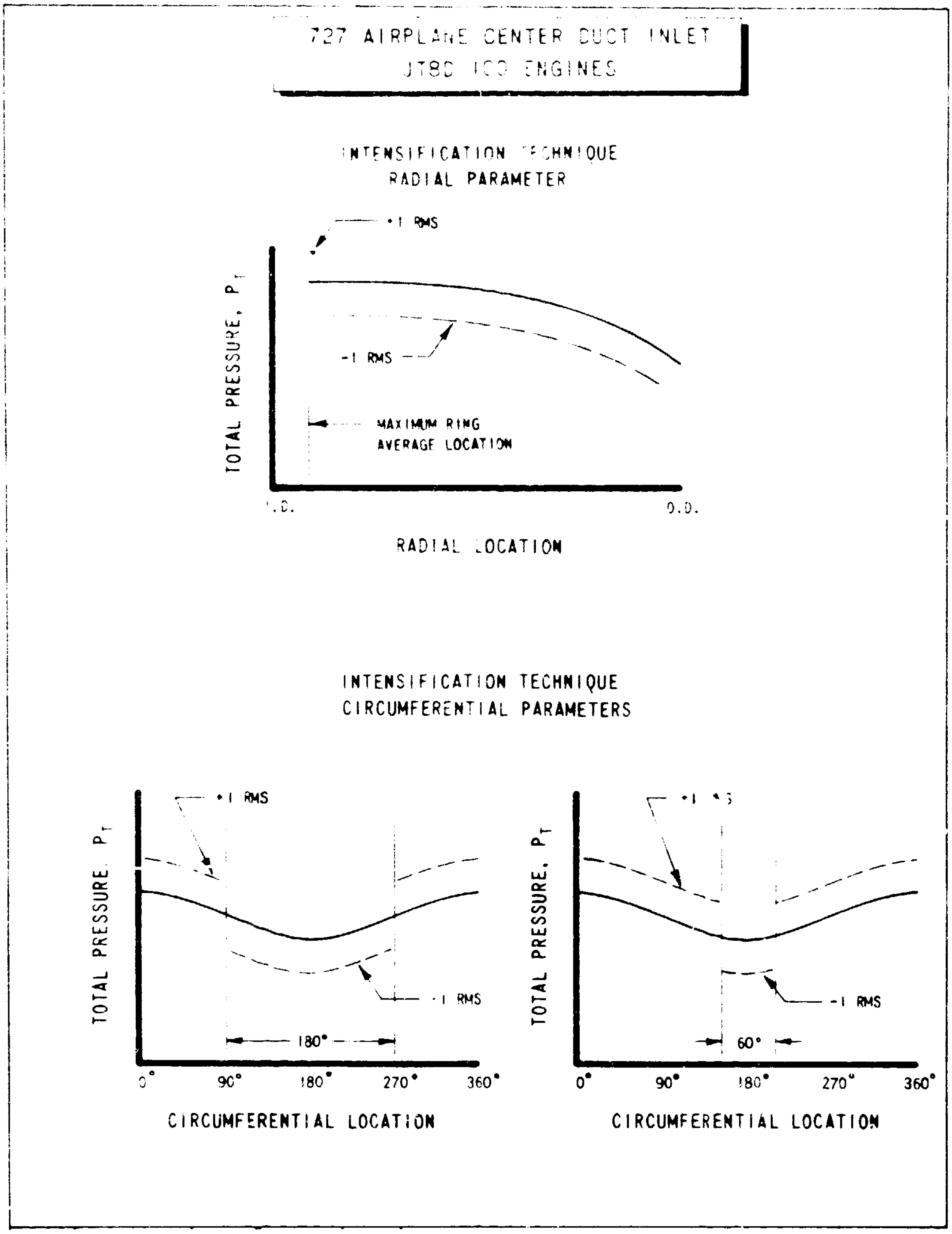

FIGURE 63. - RADIAL AND CIRCUMFERENTIAL PRESSURE DISTORTION INTENSIFICATION TECHNIQUE (P&WA METHOD)

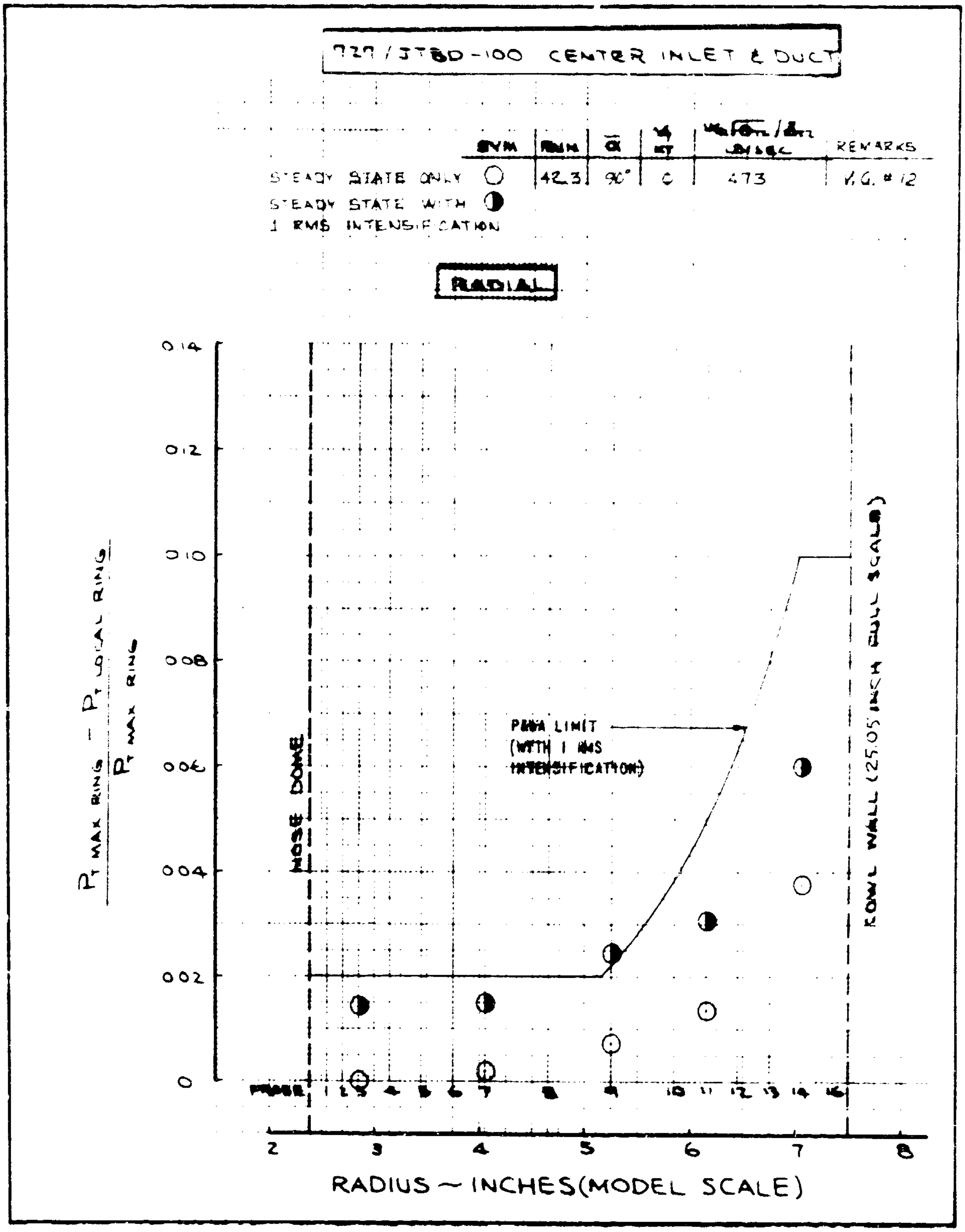

FIGURE 64. - 0-KNOT (P&WA METHOD) RADIAL PRESSURE DISTORTION WITH FUSELAGE SIMULATION AND VORTEX GENERATOR CONFIG. 12 (β = 90°)

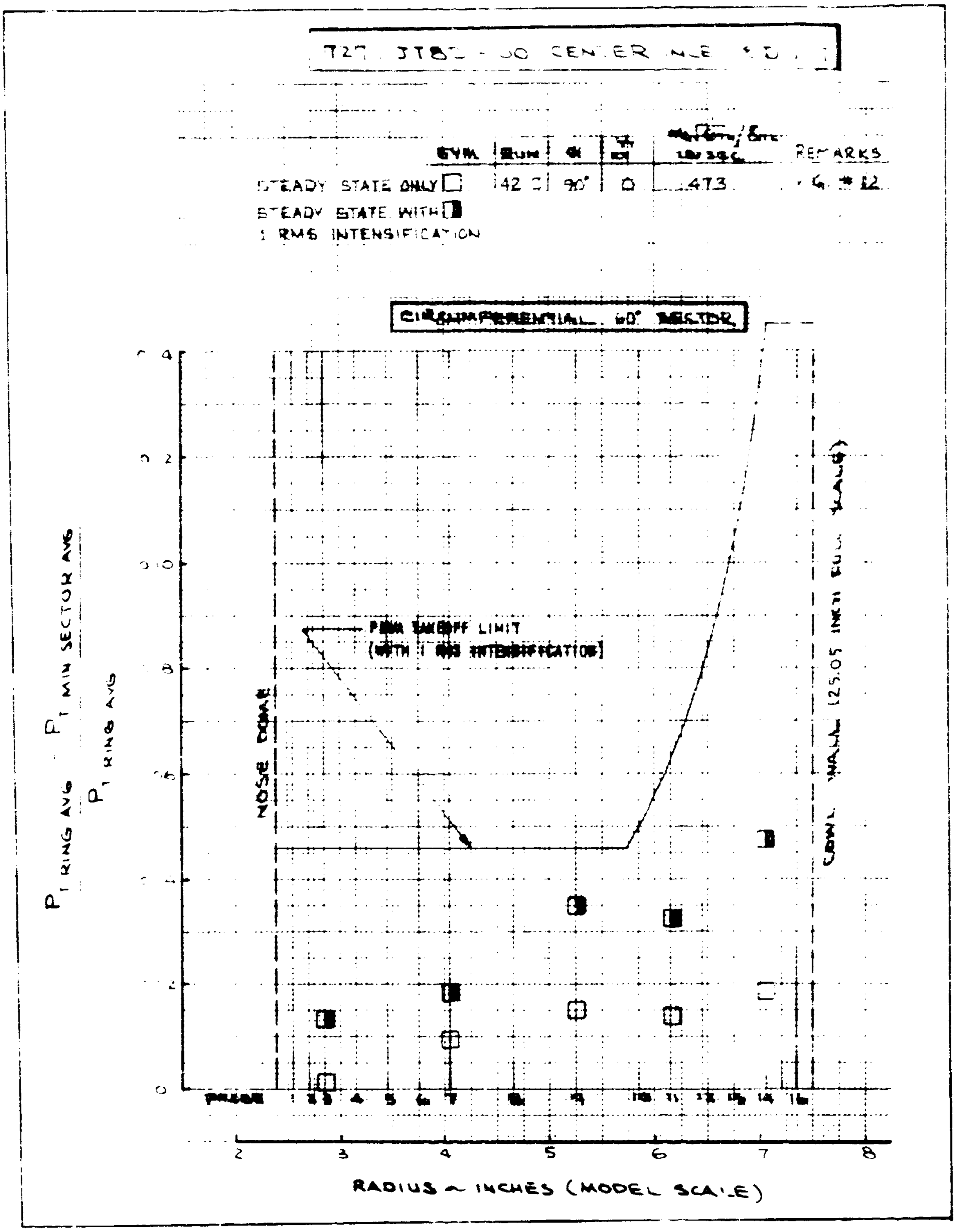

FIGURE 65. - 0-KNOT (P&WA METHOD) 60°-SECTOR CIRCUMFERENTIAL PRESSURE DISTORTION, WITH FUSELAGE SIMULATION AND VORTEX GENERATOR CONFIG. 12 (β = 90°)

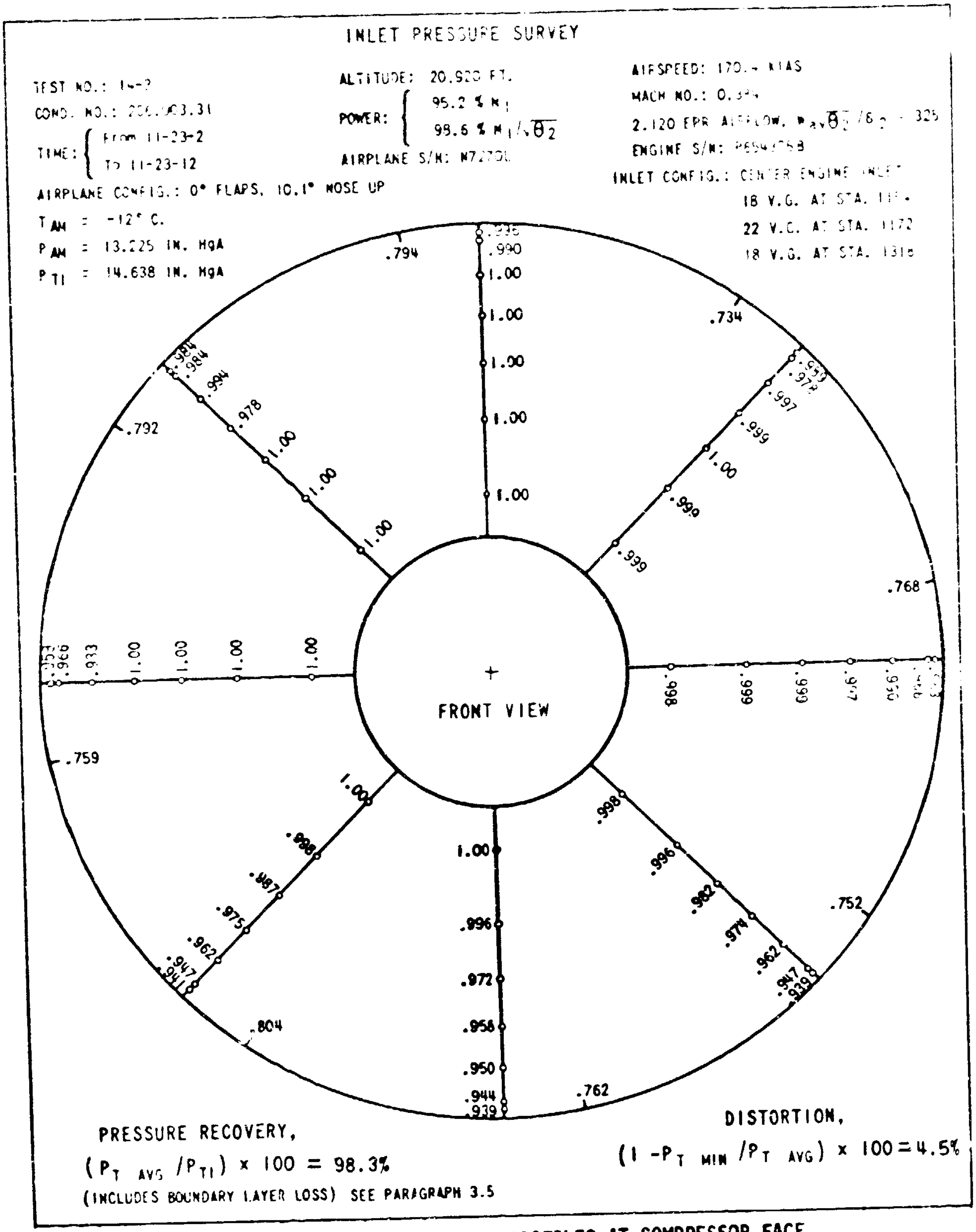

FIGURE 66. - TOTAL PRESSURE RECOVERY PROFILES AT COMPRESSOR FACE
727-200 FLIGHT TEST NO. 14-3

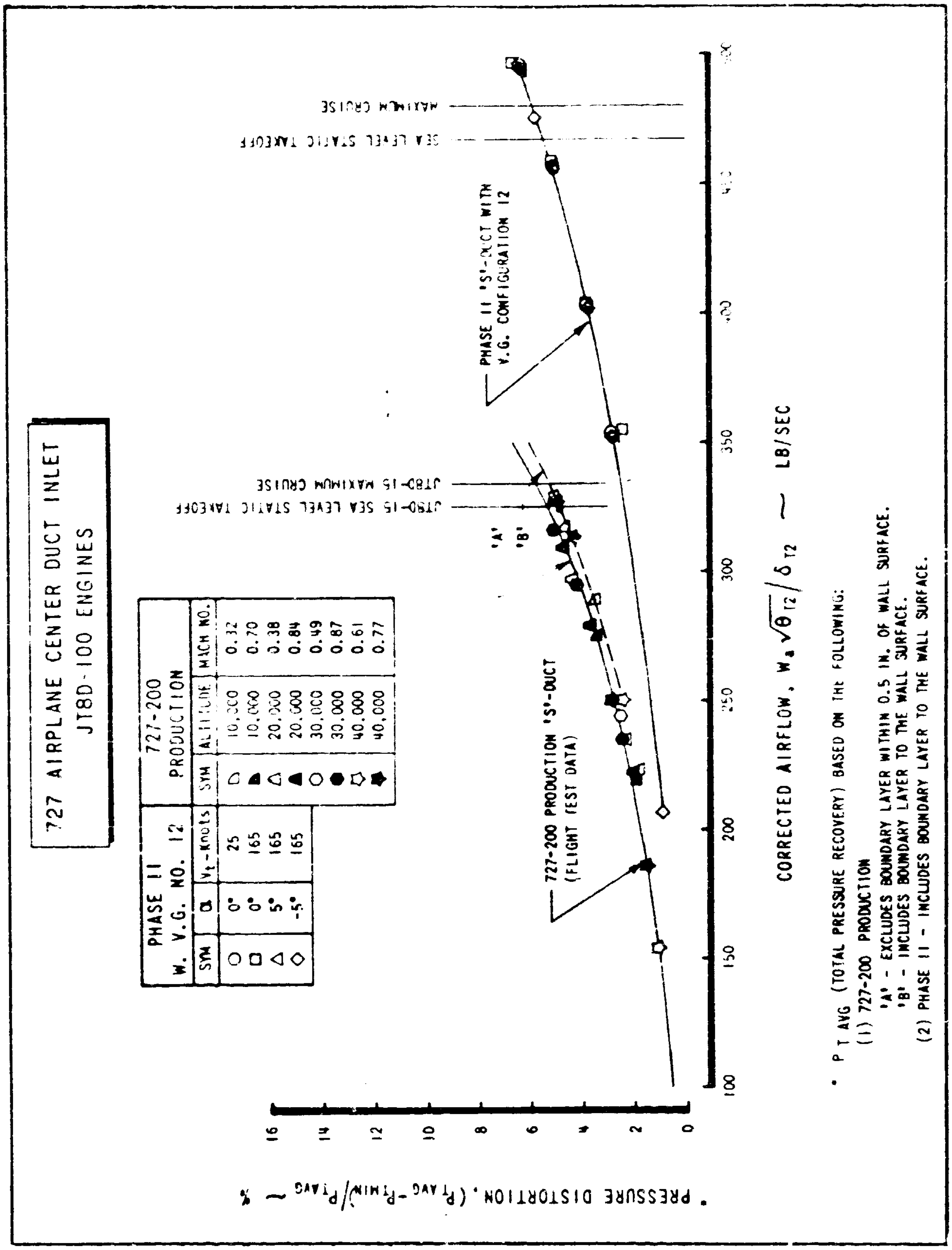

FIGURE 67. - STEADY-STATE PRESSURE DISTORTION VS. AIRFLOW AT FORWARD SPEEDS, FOR 727-200 AND PHASE II DUCT WITH VORTEX GENERATOR CONFIG. 12

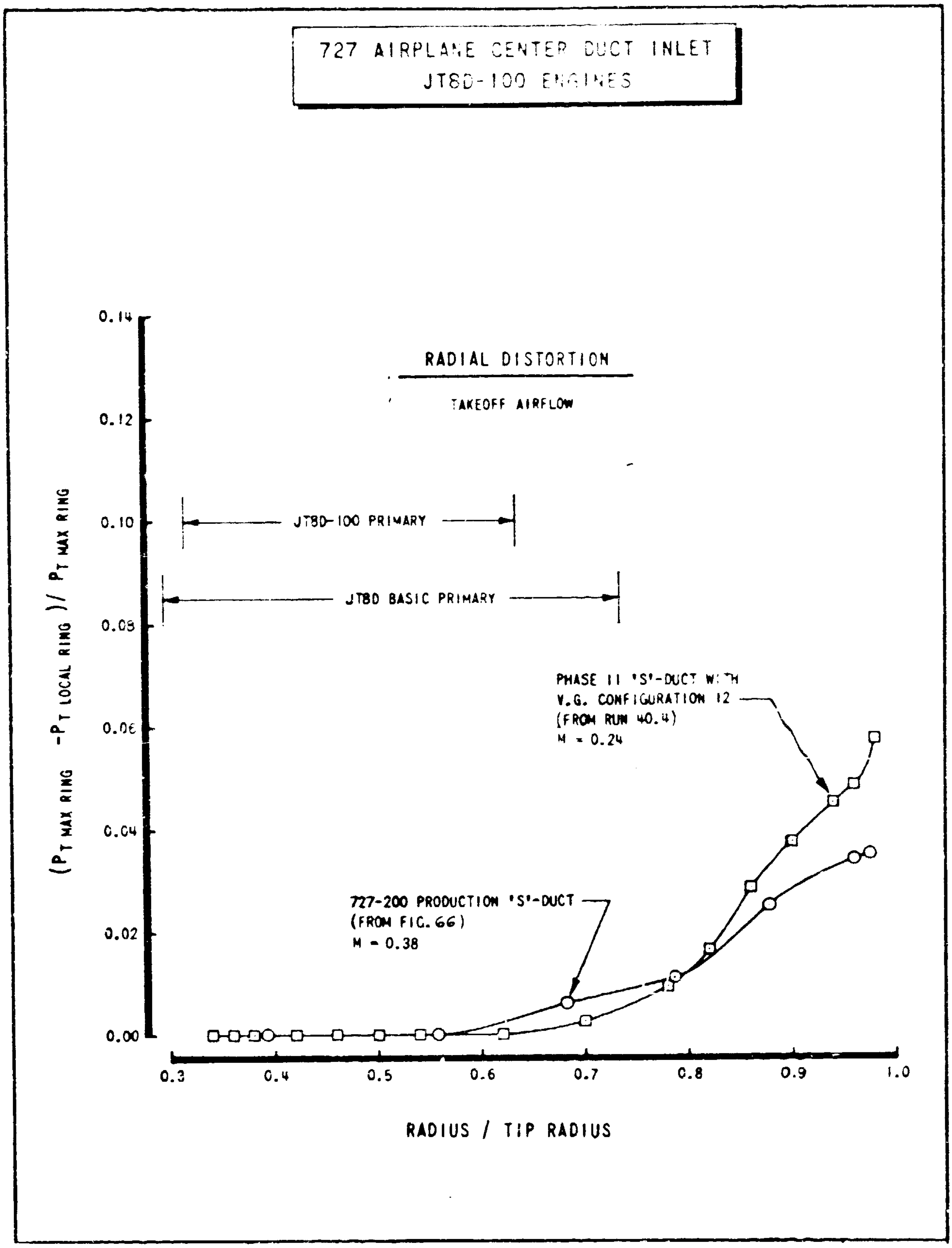

FIGURE 68. - STEADY-STATE RADIAL PRESSURE DISTORTIONS FOR 727-200 AND PHASE II DUCT, WITH VORTEX GENERATORS CONFIG. 12

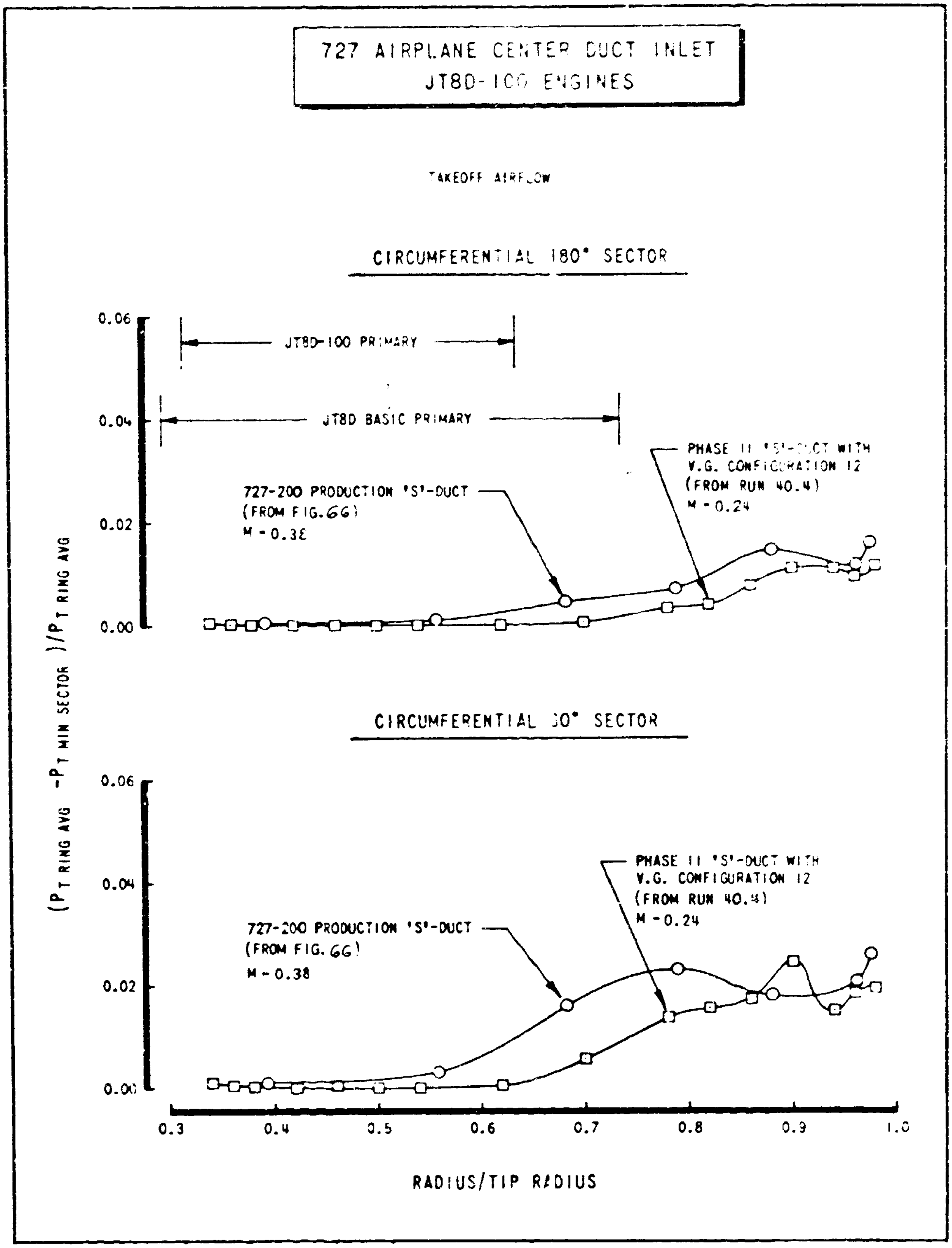

FIGURE 69. - STEADY-STATE CIRCUMFERENTIAL PRESSURE DISTORTIONS FOR 727-200 AND PHASE II DUCT, WITH VORTEX GENERATOR CONFIG. 12

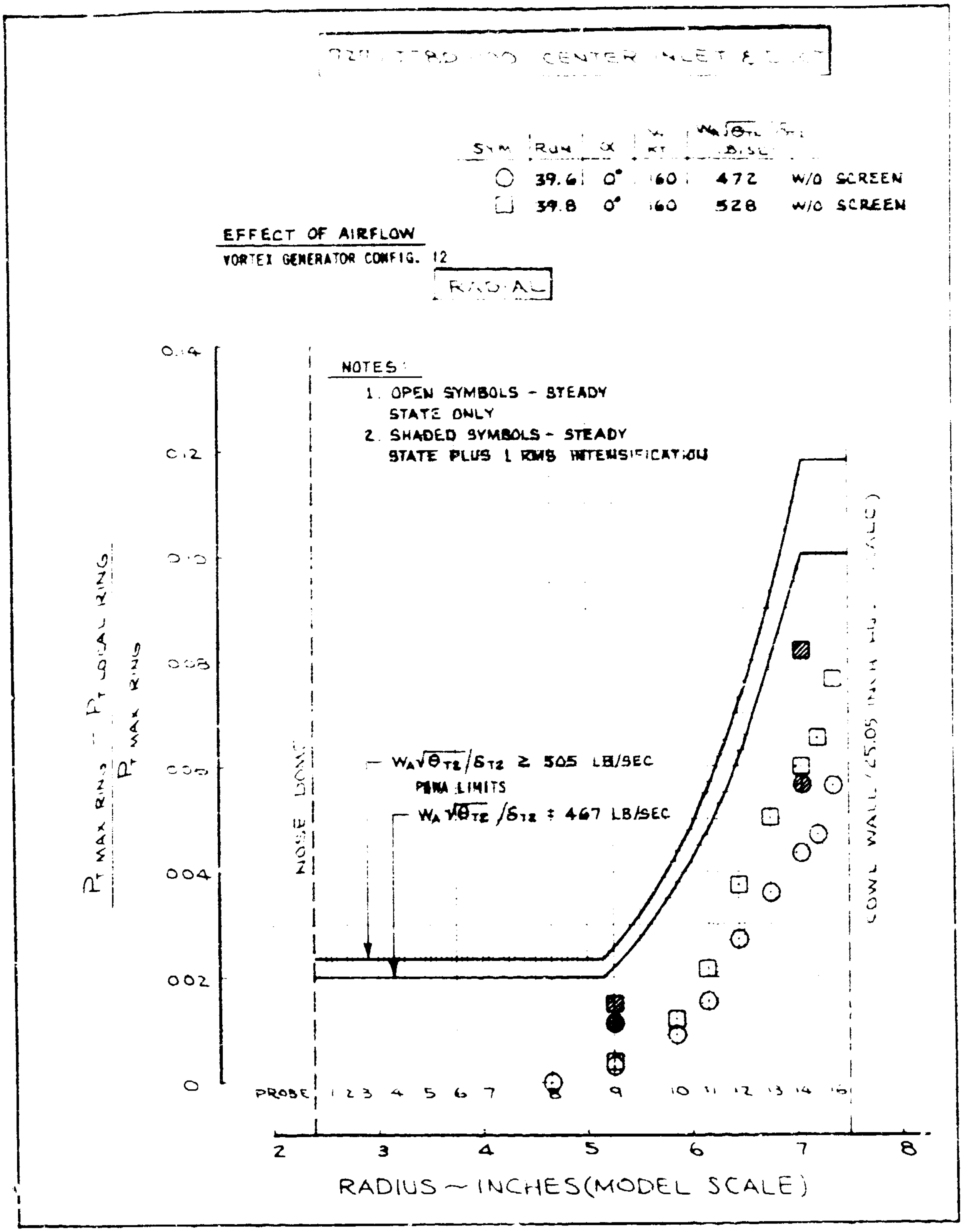

FIGURE 70. - 160-KNOT RADIAL PRESSURE DISTORTION AT 528 LB/SEC AIRFLOW, WITH VORTEX GENERATOR CONFIG. 12 ($\bar{\alpha}$ = 0°.

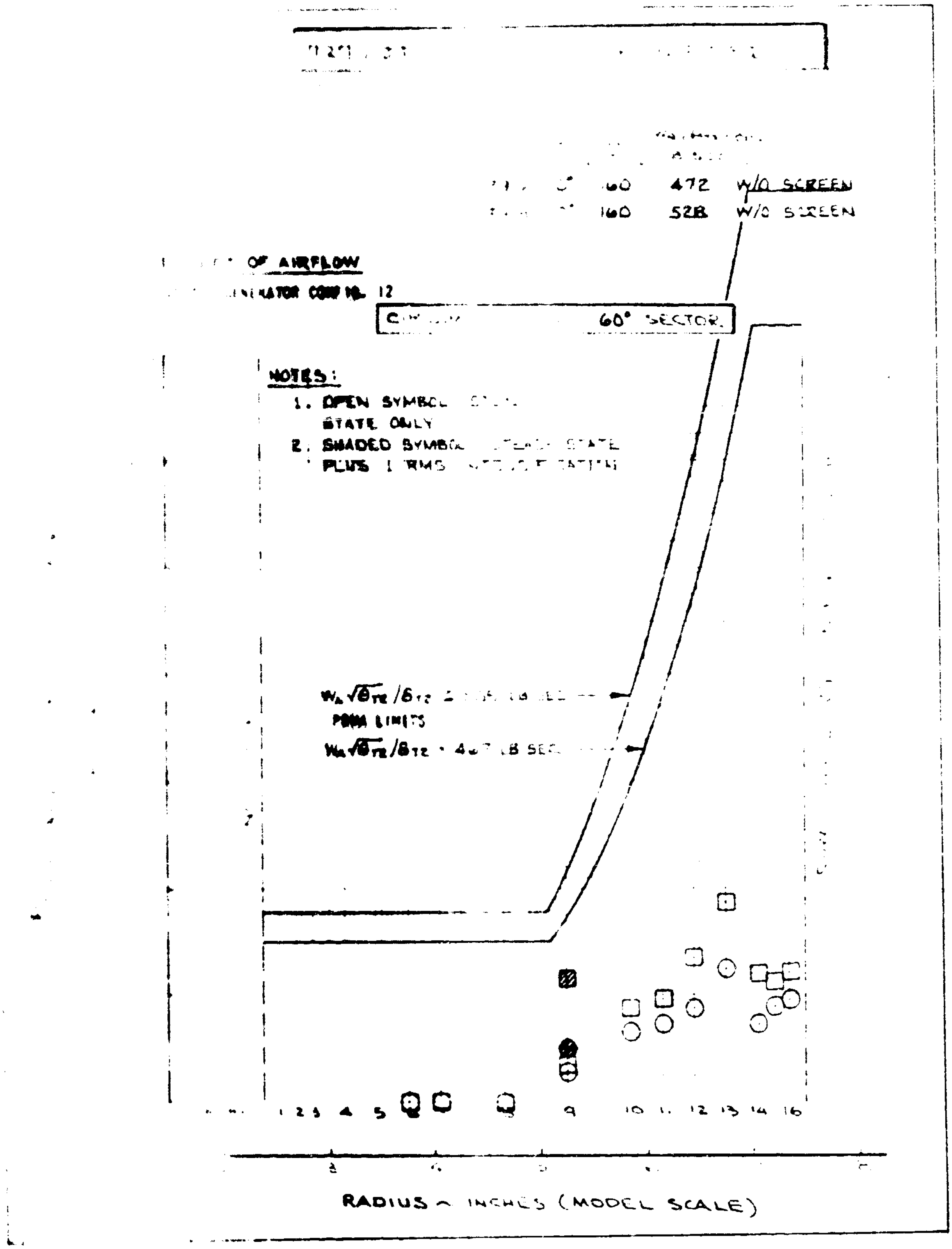

FIGURE 71. - 160-KNOT 60°-SECTOR CIRCUMFERENTIAL PRESSURE DISTORTION
AT 528 LB/SEC AIRFLOW, WITH VORTEX GENERATOR CONFIG 12 ($\bar{\imath}$ = 0°)

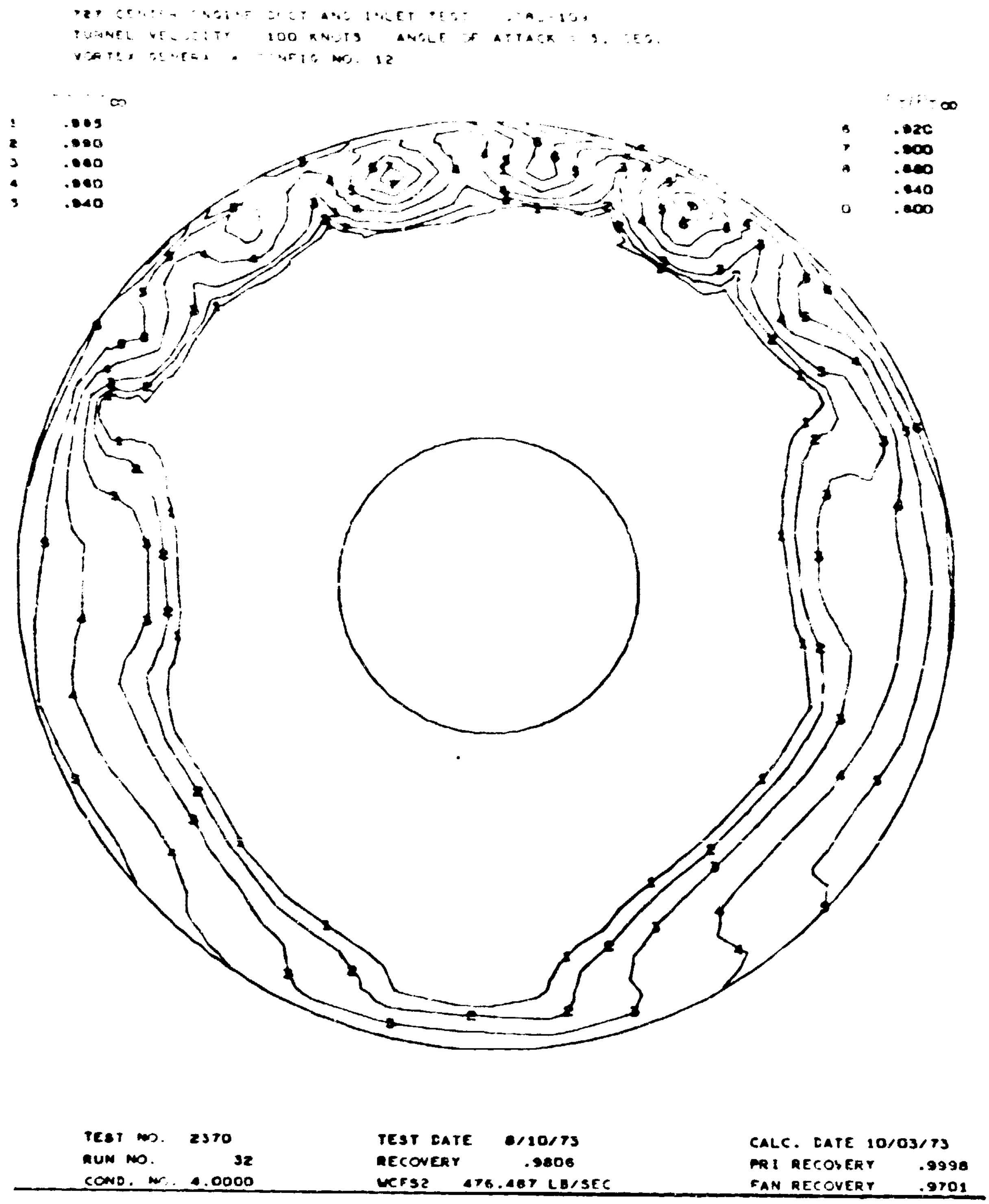

FIGURE 72. - 100-KNOT STEADY-STATE COMPRESSOR FACE PRESSURE RECOVERY MAP, WITH VORTEX GENERATOR CONFIG. 12 ($\bar{\alpha}$ = 5°)

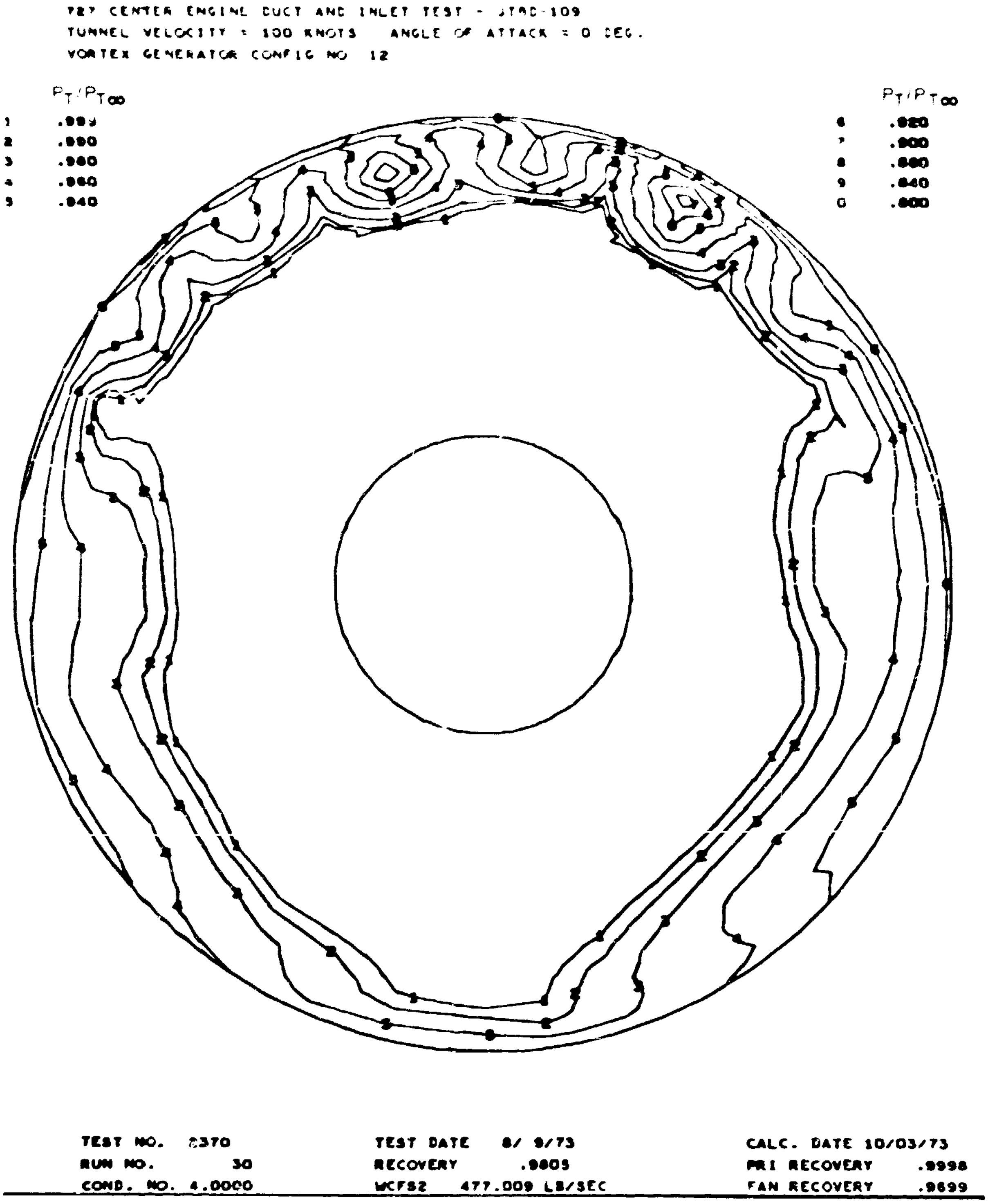

FIGURE 73. - 100-KNOT STEADY-STATE COMPRESSOR FACE PRESSURE RECOVERY MAP, WITH VORTEX GENERATOR CONFIG. 12 ($\bar{\alpha}$ = 0°)

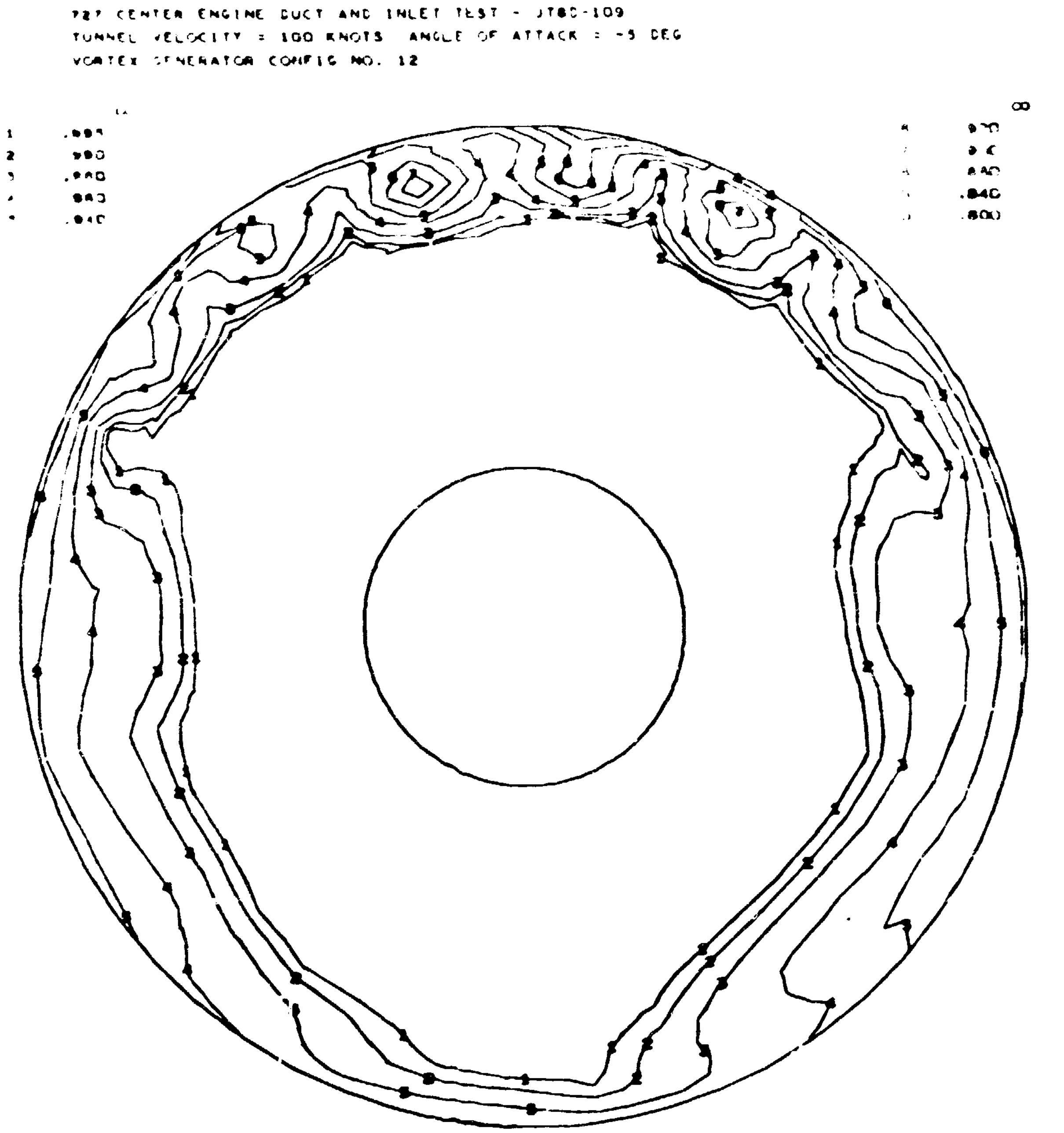

TEST NO.	2370	TEST DATE	8/13/73	CALC. DATE	10/03/73
RUN NO.	34	RECOVERY	.9805	PRI RECOVERY	.9997
COND. NO.	4.0000	WCFS2	476.823 LB/SEC	FAN RECOVERY	.9701

FIGURE 74. - 100-KNOT STEADY-STATE COMPRESSOR FACE PRESSURE RECOVERY MAP, WITH VORTEX-GENERATOR CONFIG. 12 ($\bar{\alpha}$ = 5°)

APPENDIX A

SYMBOLS

APPENDIX A

SYMBOLS

a	1/2 Major Axis of an Ellipse
A_{HI}	Highlight Area, Ft^2
A_{TH}	Throat Area, Ft^2
A_2	Compressor Face Area Ft^2
b	1/2 Minor Axis of an Ellipse
BWL	Body Water Line
CF	Compressor Face
D, d	Diameter, In, Ft
H	δ^*/θ, Shape Factor
Hz	Hertz
KT	Knots
L	Inlet Length, In, Ft
M	Mach Number
M_2	Compressor Face Mach Number
M_{TH}	Throat Mach Number
MCT	Max Continuous Thrust
MCR	Max Cruise Thrust
P_T	Local Total Pressure
PT_1	Highlight Total Pressure Taken as P_{T_∞}, PSIA

P_{T2}, $P_{T\ AVG}$	Compressor Face Average Total Pressure, PSIA
$P_{T\ MIN\ SECTOR\ AVG}$	Lowest average total pressure at a given radius in any 180-degree or 60-degree arc. (P&WA includes instantaneous values in their computation).
$P_{T\ LOCAL\ RING}$	Average total pressure over 360^{o} for a given radius
P_{TO}, $P_{T\infty}$	Freestream Total Pressure, PSIA
$P_{T\ MAX}$	Compressor Face Max Measured Total Pressure, PSIA
$P_{T\ MIN}$	Compressor Face Min Measured Total Pressure, PSIA
R	Radius, In, Ft
R_{HI}	Highlight Radius, In, Ft
RMS	Root Mean Square over frequency range noted (or standard deviation)
T_{T1}	Highlight Total Temperature, ^{o}R
T_{T2}	Total Temperature at Compressor Face, ^{o}R
u	Local Velocity in x direction, Ft/Sec
U	Velocity in x direction at Boundary Layer Edge, Ft/Sec
V_T	Tunnel Velocity, Knots
V.G.	Vortex Generator
Wa, W	Inlet Airflow, Lb/Sec
W_A, W_{COR}, $WCFS2 = W_A\ \theta_{T2}/\ T2$,	Corrected Inlet Airflow, Full Scale, Lb/Sec
w/o	Without

$\bar{\alpha}$	Inlet Inflow Angle, degrees
β	Yaw angle, degrees
ρ	Local density, Lb/Ft^3
ρ_e	Density at Boundary Layer Edge, Lb/Ft^3
δ_{T2}	$P_{T2}/14.7$
δ_{T1}	$P_{T1}/14.7$
δ^*	Displacement Thickness, In.
δ	Boundary Layer Thickness, In.
θ	Momentum Thickness, In.
θ_{T2}	$T_{T2}/518.7$
θ_{T1}	$T_{T1}/518.7$

REFERENCES

1. Boeing Commercial Airplane Company, "Program on Ground Test of Modified Quiet, Clean, JT3D and JT8D Turbofan Engines in Their Respective Nacelles", Phase I Final Report, NASA-CR-06-41244, dated September, 1973.

2. Boeing Commercial Company, "Low-Speed Wind Tunnel Flow Field Results for JT8D Refan Engines on the Boeing 727-200", NASA-CR-06- (to be released).

3. M. B. Sussman, G. W. N. Lampard, D. J. Hill, R. R. Bowen, et al "A Study of Inlet/Engine Interaction in a Transonic Propulsion Wind Tunnel", Boeing Document D6-60116, dated January, 1970.

4. H. D. Taylor, "Application of Vortex Generator Mixing Principle to Diffusers", Concluding Report, Air Force Contract W33-038 AC-21825, U.A.C. Rep. R-15064-5, United Aircraft Corporation, Res. Dept., dated Dec. 31, 1948.

5. E. F. Valentine and R. B. Carroll, "Effects of Several Arrangements of Rectangular Vortex Generators on the Static-Pressure Rise Through a Short 2:1 Diffuser", NACA RM L50L04, dated Feb., 1951.

6. E. F. Valentine and R. B. Carroll, "Effects of Some Primary Variables of Rectangular Vortex Generators on the Static-Pressure Rise Through A Short Diffuser", NACA RM L52B13, dated May, 1952.

7. H. H. Pearcy and C. M. Stuart, "Methods of Boundary-Layer Control for Postponing and Alleviating Buffeting and other Effects of Shock-Induced Separation:, Presented at the IAS National Summer Meeting, Los Angeles, Calif., dated June, 1959.

8. H. Sprenger, "Experimentelle Untersuchungen an Geraden und Gekrummten Diffusoren", Prom. Nr. 2803, 1959 - Dissertation, ETH Zurich.

9. Pratt & Whitney Aircraft, "Phase I Engine Definition and Characteristics of the JT8D-100 Turbofan Engine", PWA TM-4713, dated April 13, 1973.